Department of Civil and Environmental Engineering

Flow–plant–sediment interactions: Vegetative resistance modeling and cohesive sediment processes

Kaisa Västilä

Aalto University

DOCTORAL DISSERTATIONS

Aalto University publication series
DOCTORAL DISSERTATIONS 220/2015

Flow–plant–sediment interactions: Vegetative resistance modeling and cohesive sediment processes

Kaisa Västilä

A doctoral dissertation completed for the degree of Doctor of Science (Technology) to be defended, with the permission of the Aalto University School of Engineering, at a public examination held at the lecture hall R1 of the school on 15 January 2016 at 12.

Aalto University
School of Engineering
Department of Civil and Environmental Engineering
Water and Environmental Engineering Research Group

Supervising professor
Professor Harri Koivusalo

Thesis advisors
Dr. Juha Järvelä, Aalto University School of Engineering, Finland

Preliminary examiners
Dr.-Ing. Ingo Schnauder, gerstgraser - Ingenieurbüro für Renaturierung, Germany
Dr. Timo Huttula, Finnish Environment Institute, Finland

Opponent
Assistant Professor Anne Lightbody, University of New Hampshire, United States

Aalto University publication series
DOCTORAL DISSERTATIONS 220/2015

ISBN 978-952-60-6598-4 (printed)
ISBN 978-952-60-6597-7 (pdf)
ISSN-L 1799-4934
ISSN 1799-4934 (printed)
ISSN 1799-4942 (pdf)
http://urn.fi/URN:ISBN:978-952-60-6597-7

Unigrafia Oy
Helsinki 2015

Finland

441 697
Printed matter

Aalto University

Abstract

Aalto University, P.O. Box 11000, FI-00076 Aalto www.aalto.fi

Author
Kaisa Västilä

Name of the doctoral dissertation
Flow–plant–sediment interactions: Vegetative resistance modeling and cohesive sediment processes

Publisher School of Engineering

Unit Department of Civil and Environmental Engineering

Series Aalto University publication series DOCTORAL DISSERTATIONS 220/2015

Field of research Water and Environmental Engineering

Manuscript submitted 5 June 2015 **Date of the defence** 15 January 2016

Permission to publish granted (date) 16 November 2015 **Language** English

☐ **Monograph** ☒ **Article dissertation (summary + original articles)**

Abstract

Riparian vegetation growing on river banks and floodplains has pronounced impacts on the flow of water and the transport of substances, including fine sediment. These plant-mediated processes shape fluvial ecosystems and are essential in applications of environmental hydraulics, such as in compound channels with vegetated floodplains. The flow–plant–sediment interactions need to be estimated at different scales, but suitable parameterization of natural flexible vegetation for hydraulic analyses has been difficult.

The objective of this thesis was to provide new insight on flow resistance and cohesive sediment processes in compound channels with riparian vegetation. The cross-cutting aim was to improve the parameterization of natural, flexible, foliated plants. The drag forces and the flexibility-induced reconfiguration were examined for five woody species in a laboratory flume. The flow resistance, net deposition and the suspended sediment transport were quantified under differing floodplain vegetation conditions (bare, grassy, woody) in a cohesive agricultural compound channel. The experimental investigations were accompanied with the application of existing and new models.

The drag forces and reconfiguration of foliated woody plants were controlled by the leaf-area-to-stem-area-ratio, because both the foliage and the stem contributed notably to the plant-scale drag. The flow resistance of natural foliated vegetation was successfully modeled using a novel drag–density parameterization (Eqs. 18–23) that accommodates the reconfiguration and density separately for the foliage and the stem. The new parameterization improved the description of woody vegetation compared to the conventional approach of considering plants as rigid cylindrical elements. The flow resistance in the compound channel could be estimated by a two-layer model using the drag–density parameter and the vegetation height represented by the cross-sectional blockage factor. These same vegetation properties explained the net erosion and deposition of cohesive sediment on the floodplain, although deposition was supply-limited in long and dense plant stands. The timing and magnitude of cohesive sediment transport in the agricultural compound channel were governed by out-of-channel processes.

As a practical implication, the sediment load transported in compound channels can be managed by appropriately maintained floodplain vegetation. In conclusion, straightforward approaches accompanied with a physically-based vegetation parameterization can be successfully used to describe the effects of natural flexible riparian plants on flow resistance and sediment deposition.

Keywords drag force, flow resistance, riparian vegetation, foliage, cohesive sediment, sediment transport, compound channels, modeling

ISBN (printed) 978-952-60-6598-4 **ISBN (pdf)** 978-952-60-6597-7

ISSN-L 1799-4934 **ISSN (printed)** 1799-4934 **ISSN (pdf)** 1799-4942

Location of publisher Helsinki **Location of printing** Helsinki **Year** 2015

Pages 158 **urn** http://urn.fi/URN:ISBN:978-952-60-6597-7

A! Aalto-yliopisto

Tiivistelmä

Aalto-yliopisto, PL 11000, 00076 Aalto www.aalto.fi

Tekijä
Kaisa Västilä

Väitöskirjan nimi
Virtaus–kasvi–sedimentti-vuorovaikutukset: Kasvillisuuden virtausvastuksen mallintaminen ja koheesiivisen sedimentin prosessit

Julkaisija Insinööritieteiden korkeakoulu

Yksikkö Yhdyskunta- ja ympäristötekniikan laitos

Sarja Aalto University publication series DOCTORAL DISSERTATIONS 220/2015

Tutkimusala Vesi- ja ympäristötekniikka

Käsikirjoituksen pvm 05.06.2015 **Väitöspäivä** 15.01.2016

Julkaisuluvan myöntämispäivä 16.11.2015 **Kieli** Englanti

☐ **Monografia** ☒ **Yhdistelmäväitöskirja (yhteenveto-osa + erillisartikkelit)**

Tiivistelmä

Rantavyöhykkeen kasvillisuus luiskissa ja tulvatasanteilla vaikuttaa merkittävästi uomien virtausolosuhteisiin sekä hienojakoisen sedimentin ja muiden aineiden kulkeutumiseen. Nämä virtaus–kasvi–sedimentti-vuorovaikutukset muokkaavat virtavesien ekosysteemejä. Lisäksi niitä hyödynnetään luonnonmukaisen vesirakentamisen menetelmissä, kuten tulvatasanteellisissa kaksitasouomissa. Kasvillisuuden vaikutukset tulee voida arvioida eri skaaloilla, mutta taipuisan luonnonkasvillisuuden kuvailu hydraulisia analyysejä varten on ollut vaikeaa.

Väitöskirjan tavoitteena oli lisätä tietämystä virtausvastuksesta ja koheesiivisen sedimentin prosesseista tulvatasanteellisissa uomissa keskittyen erityisesti taipuisten, lehdellisten luonnonkasvien parametrisoinnin kehittämiseen. Vastusvoima ja taipuisuuden aikaansaama rekonfiguraatio määritettiin viidelle puulajille laboratoriovirtauskourussa. Virtausvastusta sekä sedimentin kasautumista ja kulkeutumista selvitettiin koheesiivisessa kaksitasoisessa maatalousuomassa, jossa oli eri tavoin kasvitettuja tulvatasannekoealoja (kasviton, ruohovartinen, puuvartinen). Kokeellisen tutkimuksen lisäksi sovellettiin olemassaolevia ja uusia malleja.

Lehdellisten puuvartisten kasvien vastusvoimaa ja rekonfiguraatiota sääteli lehtiala–varsiala-suhde, sillä sekä lehvästö että varsi vaikuttivat merkittävästi kokonaisvoimaan. Lehdellisen luonnonkasvuston virtausvastus mallinnettiin onnistuneesti käyttäen uutta vastuskertoimeen ja tiheyteen perustuvaa parametrisointia (yhtälöt 18–23), joka huomioi rekonfiguraation ja tiheyden erikseen lehvästölle ja varrelle. Uusi parametrisointi paransi puuvartisen kasvillisuuden kuvausta verrattuna tavanomaiseen tapaan esittää kasvit jäykkinä sylinterimäisinä kappaleina. Kaksitasouoman virtausvastus pystyttiin arvioimaan virtausmallilla, joka käyttää vastuskertoimen ja tiheyden lisäksi kasvillisuuden korkeutta ja sen perusteella määritettyä poikkileikkauksen peittävyyttä. Nämä kasviominaisuudet selittivät myös koheesiivisen sedimentin nettoeroosiota ja -kasautumista tulvatasanteella, vaikka pitkät tiheän kasvuston alueet rajoittivatkin kasautumista. Sedimenttikulkeuma ja sen ajoitus kaksitasoisessa maatalousuomassa määräytyivät uoman ulkopuolisten prosessien perusteella.

Käytännöllisenä näkökohtana havaittiin, että sopivasti hoidetulla tulvatasannekasvustolla voidaan säädellä sedimentin kulkeutumista alavirtaan kaksitasouomissa. Tutkimuksen johtopäätöksenä on, että suoraviivaisilla analyyseillä ja fysikaalisperusteisella kasvillisuuden parametrisoinnilla voidaan kuvata rantavyöhykkeen kasvuston vaikutusta virtausvastukseen ja hienon sedimentin kasautumiseen.

Avainsanat vastusvoima, virtausvastus, rantavyöhykkeen kasvillisuus, lehvästö, koheesiivinen sedimentti, sedimentin kulkeutuminen, kaksitasouomat, mallinnus

ISBN (painettu) 978-952-60-6598-4 **ISBN (pdf)** 978-952-60-6597-7

ISSN-L 1799-4934 **ISSN (painettu)** 1799-4934 **ISSN (pdf)** 1799-4942

Julkaisupaikka Helsinki **Painopaikka** Helsinki **Vuosi** 2015

Sivumäärä 158 **urn** http://urn.fi/URN:ISBN:978-952-60-6597-7

Acknowledgements

I have enjoyed conducting this doctoral research at the Water Engineering research group of Aalto University School of Engineering. I sincerely thank my instructor Dr. Juha Järvelä who has taught me how to conduct good research, shared his expertise and network on environmental hydraulics, and generally pushed me to strive for the best. I am very grateful to my supervisor Prof. Harri Koivusalo for his support and guidance throughout the thesis process and for his comments on the thesis. I gratefully acknowledge Prof. Timo Huttula and Dr.-Ing. Ingo Schnauder for pre-examining the thesis, and Assistant Prof. Anne Lightbody for accepting the invitation to act as the official opponent.

I am thankful to the people who have made my experimental flume research possible. Prof. Andreas Dittrich kindly accepted me to conduct flume experiments at the Leichtweiß-Institute for Hydraulic Engineering and Water Resources of the Technical University Braunschweig. Prof. Jochen Aberle importantly contributed on the design of the experiments and writing of the related articles. Dr. Thomas Schoneboom and the laboratory personnel at the Leichtweiß-Institute as well as Benjamin Rheiner helped with the flume measurements.

The field investigations at the Ritobäcken Brook would not have been possible without the help of many people. I warmly thank the laboratory and service personnel of the Aalto Water Engineering, particularly Matti Keto, Antti Louhio, Aino Peltola, Marina Sushko, Anne-Maj Seppälä and Ari Järvinen, as well as Pertti Hyvönen from Pythagoras Oy. I acknowledge Jyrki Nurminen, Tero Niemi, Johanna Jalonen, Regina Sopper and Anna-Maija Västilä for their contribution to the field measurements. Niina Siitonen, Suvi Kattainen and Janne Jurmu have focused on the field site in their candidate and master theses. I gratefully acknowledge Harri Aulaskari, Irmeli Ahtela and Kari Koppelmäki from the Uusimaa Centre for Economic Development, Transport and the Environment as well as Kirsti Lahti, Asko Särkelä and Pasi Valkama from the Water Protection Association of the River Vantaanjoki and Helsinki Region for cooperation. I also thank people from the Finnish Environment Institute, among others Jukka Jormola, Auri Sarvilinna and Dr. Petri Ekholm, for advice and connections to the practical applications. I'm grateful to the landowners at the Ritobäcken, particularly Henrik Lindström, for their patience and understanding.

The thesis work was conducted as part of projects funded by the Finnish

Academy (Grant No. 133113), Maa- ja vesitekniikan tuki ry, and the Ministry of Agriculture and Forestry. I am also happy to have been supported by personal grants from the following foundations: Maa- ja vesitekniikan tuki ry, Emil Aaltosen säätiö, Oskar Öflundin säätiö, VALUE doctoral school, Tekniikan edistämissäätiö and Sven Hallinin säätiö.

I thank my colleagues at the Aalto Water Engineering for making it such a nice place to work. I'm particularly thankful to Johanna Jalonen for collaboration and friendship, and to Marie Touvenot-Korppoo for her help at the early stages of the PhD process. I acknowledge all those teachers and professors who have, from the first year in the primary school to the last year at the university, supported me and inspired me to learn natural sciences, mathematics and engineering (special thanks to Prof. Emer. Pertti Vakkilainen, Prof. Olli Varis and Prof. Riku Vahala). I'm most grateful to Mum, Dad, Elina, Anna-Maija, Ritva, Hannu and friends for the various kinds of help and support they have offered. I express sincere thanks to my husband Henri whose understanding, help and good nerves have made it possible to complete the thesis within this timeframe. Finally, big thanks to our adorable son Otso whose lovely smiles and hugs have kept me distracted from work during my free time.

Helsinki, November 2015

Kaisa Västilä

List of Publications

This doctoral dissertation consists of a summary and of the following publications which are referred to in the text by their numerals. The numbering of the publications is organized from the smallest to the largest examined scale.

I. Västilä, Kaisa; Järvelä, Juha. 2014. Modeling the flow resistance of woody vegetation using physically-based properties of the foliage and stem. Water Resources Research, 50, 1, 229–245. doi: 10.1002/2013WR013819.

II. Västilä, Kaisa; Järvelä, Juha; Aberle, Jochen. 2013. Characteristic reference areas for estimating flow resistance of natural foliated vegetation. Journal of Hydrology, 492, 49–60. doi: 10.1016/j.jhydrol.2013.04.015.

III. Västilä, Kaisa; Järvelä, Juha; Koivusalo, Harri. 2015. Flow–vegetation–sediment interaction in a cohesive compound channel. Journal of Hydraulic Engineering, 10.1061/(ASCE)HY.1943-7900.0001058, 04015034.

IV. Västilä, Kaisa; Järvelä, Juha. 2011. Environmentally preferable two-stage drainage channels: considerations for cohesive sediments and conveyance. International Journal of River Basin Management, 9, 3–4, 171–180. doi: 10.1080/15715124.2011.572888.

Author's Contribution

Publication I: Modeling the flow resistance of woody vegetation using physically-based properties of the foliage and stem

The author was mainly responsible for designing the research based on the measurement system developed by the TU Braunschweig. The author was responsible for collecting the data and conducting the analyses. The author was mainly responsible for interpreting the results and writing of the paper. Dr. Järvelä participated in the design of the research, interpretation of the results and writing of the paper.

Publication II: Characteristic reference areas for estimating flow resistance of natural foliated vegetation

The author designed the research with Dr. Järvelä and Prof. Aberle based on the ideas emerging from their previous research. The author was responsible for collecting the data and conducting the analyses. The author was mainly responsible for interpreting the results and writing of the paper. Dr. Järvelä and Prof. Aberle participated in the interpretation of the results and writing of the paper. Prof. Aberle designed the measurement system.

Publication III: Flow–vegetation–sediment interaction in a cohesive compound channel

The author was mainly responsible for designing the research. The author was responsible for collecting the data and conducting the analyses. The author was mainly responsible for interpreting the results and writing of the paper. Dr. Järvelä participated in the design of the research, interpretation of the results and writing of the paper. Prof. Koivusalo participated in the writing of the paper.

Publication IV: Environmentally preferable two-stage drainage channels: considerations for cohesive sediments and conveyance

The author designed the research with Dr. Järvelä by further elaborating the original idea of Dr. Järvelä. The author was responsible for collecting the data and conducting the analyses. The author was mainly responsible for interpreting the results and writing of the paper. Dr. Järvelä participated in the interpretation of the results and writing of the paper.

Contents

List of Abbreviations and Symbols

ν	kinematic viscosity of the fluid (L^2T^{-1})
ρ	density of the fluid ($M\,L^{-3}$)
τ	total stress ($M\,L^{-1}T^{-2}$)
τ'	bed shear stress ($M\,L^{-1}T^{-2}$)
τ''	vegetative stress ($M\,L^{-1}T^{-2}$)
χ	reconfiguration parameter (-)
χ_F	reconfiguration parameter of the foliage (-)
χ_S	reconfiguration parameter of the stem (-)
χ_{tot}	reconfiguration parameter of foliated plants (-)
a	frontal area per unit volume (L^2L^{-3})
aH	frontal area index ($L^{-3}L^{-3}$)
A_W	wetted cross-sectional area of the channel (L^2)
$A_{O,tot}$	frontal projected area of a foliated plant in still air (L^2)
A_B	unit bed area (L^2)
A_C	characteristic reference area (L^2)
A_L	one-sided leaf area (L^2)
A_L/A_S	leaf-area-to-stem-area ratio (L^2L^{-2})
$A_{P,F}$	frontal projected area of the foliage under flow (L^2)
$A_{P,tot}$	frontal projected area of a foliated plant under flow (L^2)
A_S	frontal projected stem area (L^2)
$A_{S,lat}$	lateral projected stem area (L^2)
A_V	cross-sectional area of the channel covered by vegetation (L^2)
ANOVA	analysis of variance
B_X	cross-sectional vegetative blockage factor (L^2L^{-2})
c_v	coefficient of variation (-)
C	Chézy coefficient ($M^{1/2}T^{-1}$)
C^*	bulk drag coefficient lumping the bed and interfacial shear (-)
C_D	drag coefficient (-)

$C_{D\chi,\mathrm{tot}}$	drag coefficient of foliated plants at the reference velocity u_χ (-)
$C_{D\chi,F}$	foliage drag coefficient at the reference velocity $u_{\chi,F}$ (-)
$C_{D\chi,S}$	stem drag coefficient at the reference velocity $u_{\chi,S}$ (-)
$C_{D,F}$	foliage drag coefficient (-)
$C_{D,S}$	stem drag coefficient (-)
C_f	drag coefficient of the bed (-)
C_v	drag coefficient at the interface between vegetation and open water (-)
$C_D a$	drag–density parameter (L^2L^{-3})
$C_D aH$	drag–area parameter ($L^{-3}L^{-3}$)
D	floc diameter (L)
D_S	stem diameter (L)
f	friction factor (-)
f'	friction factor of bed (-)
f''_{tot}	friction factor of vegetation (-)
F	drag force ($M\,L\,T^{-2}$)
F_F	foliage drag force ($M\,L\,T^{-2}$)
F_S	stem drag force ($M\,L\,T^{-2}$)
F_{tot}	total drag force of a foliated plant ($M\,L\,T^{-2}$)
g	gravitational acceleration ($L\,T^{-2}$)
h	water depth [floodplain water depth for compound channels] (L)
h/H	relative submergence ($L\,L^{-1}$)
H	vegetation height (L)
K	constant of Eq. 1 ($L^{1/3}T^{-1}$)
L_b	total length of the interface between bed and open water (L)
l_C	characteristic length scale (L)
L_v	total length of the interface between vegetation and open water (L)
LES	large eddy simulation
m	number of plants per bed area (L^{-2})
m_D	dry mass of grassy plants per unit bed area ($M\,L^{-2}$)
m_W	wet mass of grassy plants per unit bed area ($M\,L^{-2}$)
$m_{F,D}$	foliage dry mass of woody plants (M)
$m_{F,W}$	foliage wet mass of woody plants (M)
$m_{S,D}$	stem dry mass of woody plants (M)
$m_{S,W}$	stem wet mass of woody plants (M)
n_{base}	Manning's resistance coefficient of the two-stage channel having a bare floodplain (-)

n_{mc}	Manning's resistance coefficient at bankful flows (-)
n_{tot}	Manning's resistance coefficient at overbank flows (-)
n_{veg}	Manning's resistance coefficient of the floodplain vegetation (-)
N	number of specimens (-)
P	wetted perimeter (L)
Q	discharge (L^3T^{-1})
Q_S	suspended sediment load ($M\,T^{-1}$)
R	hydraulic radius (L)
Re	Reynolds number
S	energy slope ($L\,L^{-1}$)
SS	suspended sediment
SSC	suspended sediment concentration ($M\,L^{-3}$)
T	turbidity (NTU)
u_χ	reference velocity of Eq. 10 ($L\,T^{-1}$)
$u_{\chi,F}$	reference velocity of the foliage drag in Eqs. 16–23 ($L\,T^{-1}$)
$u_{\chi,S}$	reference velocity of the stem drag in Eqs. 16–23 ($L\,T^{-1}$)
u_C	characteristic approach velocity ($L\,T^{-1}$)
u_m	cross-sectional mean flow velocity ($L\,T^{-1}$)
u_v	mean flow velocity within vegetation ($L\,T^{-1}$)
u^*_v	dimensionless mean flow velocity within vegetation (-)
u_o	mean flow velocity in the unvegetated segment of the cross-section ($L\,T^{-1}$)
u^*_o	dimensionless mean flow velocity in the unvegetated segment of the cross-section (-)
x_a	advection length scale (L)
w_s	particle settling velocity ($L\,T^{-1}$)
z	thickness of a vertical layer (L)
Z	vertical coordinate (L)

1. Introduction

1.1 Background

Vegetation is an essential part of not only permanently submerged aquatic ecosystems but also of riparian ecosystems that are situated above the low water marks of channels. Riparian areas are occasionally submerged or at least affected by the elevated water tables, as defined by Naiman et al. (1993). Aquatic and riparian vegetation provides habitat, reproduction and rearing sites, shelter, and nourishment for biological communities including macroinvertebrates (e.g., Rantala et al. 2004; Naiman et al. 2005; Demars et al. 2012) and fish (e.g., Gregory et al. 1991; Dibble et al. 1997). The various types of plants and plant parts serve as functional habitats, or biotopes, for specific assemblages of species from different taxa (e.g., Kemp et al. 2000).

Aquatic and riparian plant stands importantly modify the physical and chemical environment by influencing the transport of water, energy and substances. Vegetation traps sediment and particulate matter and takes up dissolved nutrients while releasing other substances, such as dissolved organic carbon (e.g., Gregory et al. 1991; Tabacchi et al. 1998; Clarke 2002). Vegetation also reinforces the soil against erosion (e.g., Wynn and Mostaghimi 2006a). On annual and longer time scales, areas growing aquatic or riparian plants can act as a source or sink of matter depending on the examined compound, the seasonal phenology of the plant species, the processes in the underlying sediment, and the water level (e.g., Carpenter and Lodge 1986; Naiman and Décamps 1997). Vegetation controls light extinction and water temperature (e.g., Carpenter and Lodge 1986; Tabacchi et al. 1998), and affects the sediment chemistry (e.g., Clarke 2002) and composition (e.g., Cotton et al. 2006) both within and near the plant stands. On the other hand, these same factors and processes that are influenced by plants also control the establishment and colonization of plant stands (e.g., Franklin et al. 2008). Marion et al. (2014) note that many of these important biophysical processes take place at the water–plant and water–sediment interfaces.

The interactions between plants, flow hydraulics and physical sediment processes are complex and interconnected. The presence of vegetation induces additional drag forces and alters the flow field, affecting e.g. the vertical velocity profiles and turbulence characteristics (e.g., Stephan and Gutknecht 2002; Righetti 2008; Nepf, 2012a; Siniscalchi et al., 2012; Sukhodolov and Sukhodolova 2012; Nikora et al. 2013). Similar modifications are caused on

wind flow by the drag exerted by terrestrial vegetation, such as forest stands (e.g., de Langre 2008). The vegetative drag forces increase the flow resistance, thus decreasing mean flow velocities and raising water levels (e.g., Nikora et al. 2008; Nepf 2012b; Aberle and Järvelä 2013). Further, vegetation notably influences the bed shear stress as well as the near-bed velocity and turbulence within and outside of plant stands (e.g., McBride et al. 2007; Ortiz et al. 2013). Therefore, vegetation affects the net sediment transport (e.g., Manners et al. 2015) and the spatial patterns of erosion and deposition of both coarse and fine sediment (e.g., Abt et al. 1994; Bos et al. 2007; Bouma et al. 2009; Heppell et al. 2009; Zong and Nepf 2011).

Vegetation-induced effects on the physical sediment processes modify the morphodynamics and morphology of channels, deltas and tidal areas at different spatial scales (e.g., Temmerman et al. 2007; Zinke et al. 2011; Camporeale et al. 2013; Curran and Hession 2013). For instance, vegetation has been found to control local-scale bank retreat (Pizzuto et al. 2010), reach-scale channel width and depth (e.g., Huang and Nanson 1997; McBride et al. 2010), and the planform-scale properties of braiding rivers (Bertoldi et al. 2011). The presence of plants can even affect the planform type of rivers, with vegetation establishment on banks and bars observed to transform a braiding laboratory channel to a meandering one (e.g., Tal and Paola 2007). Ultimately, the establishment of plant stands has been found to concentrate the flow on bare surfaces, which leads to formation of channels (Temmerman et al. 2007) and entire channel networks (Vandenbruwaene et al. 2013) in tidal areas. Because of these profound influences on the sediment processes and fluvial geomorphology, some aquatic and riparian plant species can transform bare substrate into a suitable habitat for themselves (e.g., Gurnell 2014). Those species that are capable of creating habitat and modifying the availability of resources to other species as well, and that thus shape the structure of aquatic and riparian ecosystems, are referred to as “ecosystem engineers” (sensu Jones et al. 1994).

Not only does the biota affect the sediment and geomorphological processes, but it is also affected by these same processes. The study of these two-way interactions is referred to as biogeomorphology (e.g., Baptist 2005). In water environment, biogeomorphological research topics include the spatial self-organization of plant communities through scale-dependent positive and negative feedbacks that affect the survival of the individual specimens (e.g., Bouma et al. 2009; Schoelynck et al. 2012). The two-way interactions have been modeled by assuming that plants colonize those new deposits that are dry during the season of low discharge (Crosato and Saleh 2011) and by allowing plant removal and erosion in areas experiencing high flow velocities (Nicholas 2013). For biogeomorphological models to be fully coupled, ecological processes including seed dispersal, plant growth and succession should be incorporated (e.g., Solari et al. 2015).

Technical issues associated with physical sediment processes and morphodynamics include channel aggradation and degradation, bank stability, bed armoring and siltation, sedimentation in harbors and estuaries, and scouring of hydraulic structures (e.g., García 2008a). Sediment transport is a natu-

ral and integral part of healthy fluvial, estuarine and coastal ecosystems. However, the impacts of human actions on the quantity and quality of fine sediment constitute severe environmental concerns (e.g., Owens et al. 2005). Fine sediment increases turbidity and decreases the penetration of light into the water column, while the cohesive fraction formed of primary particles smaller than 60 μm conveys heavy metals, nutrients, pesticides and other sorbed substances (e.g., Bilotta and Brazier 2008). Excessive amount of fine sediment affects negatively the aquatic biota (e.g., Wood and Armitage 1997; Bilotta and Brazier 2008), reducing the species richness of macroinvertebrates (e.g., Larsen et al. 2009) and impacting the physiology, habitat and behavior of fish (e.g., Kemp et al. 2011). The amount and timing of fine sediment transport could potentially be managed by making use of the controls vegetation exerts on the sediment processes.

Because of its physical, biological and chemical benefits, vegetation is a key factor in applications of environmental hydraulics in fluvial, coastal and estuarine areas. There is a growing interest towards such environmentally preferable approaches (e.g., Hey 2009; Temmerman et al. 2013; de Vriend et al. 2014) because many adverse environmental impacts are associated with conventional hard hydraulic structures and engineering practices. Conventional measures, such as channelization, dikes and the modification of catchment-scale hydrological regimes by drainage, have had particularly negative effects on the environment in agricultural channels (e.g., Blann et al. 2009) and riverine floodplains (e.g., Brinson and Malvarez 2002; Tockner and Stanford 2002). In addition, hard engineering approaches do not necessarily provide a long-term solution because they typically require continual, expensive maintenance. On the other hand, approaches aimed at mitigating the environmental impacts are not successful unless proven so. For instance, Shields (2009) reported that bank stabilization and grade control by weirs did not have the intended decreasing impact on the catchment-scale sediment loads in six streams, which underlines that a strong scientific basis is needed in projects designed to decrease harmful environmental impacts. For advancing the understanding of the fundamental processes relevant to environmental hydraulics, field-based research is considered particularly important (e.g., Sukhodolov 2015).

Many research and engineering purposes require reliable estimates of the vegetative drag forces, flow resistance and effects on the transport processes, including erosion and sediment deposition. This necessitates describing the natural plants with suitable vegetative parameters e.g. in hydraulic models and analyses. The parameterization of the vegetation should preferably be based on physically sound and readily measurable properties of the plants, which is a cross-cutting topic of this thesis. Within the research field of flow–plant–sediment interactions, the thesis specifically focuses on resistance modeling and cohesive sediment processes in flows with natural riparian vegetation.

1.2 Scope and context

The interactions between vegetation and flow, and vegetation and sediment transport, have spurred a vast body of research. Because of the large variety in the types and properties of natural plants and plant stands, and the inherent complexity of natural vegetation from the viewpoint of hydrodynamics and sediment transport (e.g., Nepf 2012a; Aberle and Järvelä 2015), the thesis intentionally focuses on certain vegetation types, flow conditions, and sediment transport modes. Section 1.2.1 describes and justifies the selected focus on natural riparian vegetation typical of compound channels while Section 1.2.2 describes environmental compound (two-stage) channels, a related engineering approach that serves as the hydraulic context of the thesis.

1.2.1 Focus on natural flexible riparian vegetation

Riparian areas, including floodplains and river banks, grow both grassy and woody vegetation. Grassy plants are herein considered in a wide sense to represent all those riparian species that are not woody. Grasses typically have flexible stems and often foliage and flowers. Woody bushes, shrubs, and trees have a more complex structure, with the foliage considered herein to comprise the relatively flexible leaves and petioles while the term stem encompasses all the less flexible woody parts of the trunk, branches and terminal twigs. For both grassy and woody plants, the flexibility leads to various changes in the shape, frontal projected area, and hydraulic behavior under flow. These changes are often considered as a whole and referred to as reconfiguration (e.g., Vogel 1994; de Langre 2008). Grassy stems obtain a more streamlined orientation by bending towards downstream, and submerged stands can experience a progressive waving of the grass blades called monami (e.g., Grizzle et al. 1996; Nepf 2012a). For woody plants, photographs taken under flow reveal that the frontal projected area is reduced as the flow velocity increases, mainly because the leaves and leaf clusters obtain a more parallel orientation to the main flow direction (e.g., Vogel 1989; Vollsinger et al. 2005), and to a minor degree because the main stem and branches bend into the main flow direction (e.g., Rudnicki et al. 2004; Xavier 2009; Stone et al. 2013). This reconfiguration typically reduces the drag forces encountered by the organisms (e.g., Vogel 1994), which is important for preventing potential damage to the specimens by water flow or wind.

Earlier investigations on the hydraulic effects of natural plants have been conducted e.g. with aquatic macrophytes (e.g., Green 2005; Sand-Jensen et al. 2008; Sukhodolov and Sukhodolova 2010; Sukhodolov and Sukhodolova 2012; Siniscalchi and Nikora 2013), semi-aquatic species (e.g., Albayrak et al. 2014), seaweeds (e.g., Boller and Carrington 2006; 2007), grasses and sedges (e.g., Järvelä 2002a; Wilson and Horritt 2002; Rhee et al. 2008), cereal crops (e.g., Yue et al. 2007), and deciduous and coniferous shrubs and trees (e.g., Oplatka 1998; Freeman et al. 2000; Järvelä 2002a, Koizumi et al. 2010; Wunder et al. 2011; Dittrich et al. 2012; Jalonen and Järvelä 2014). Most of these studies are targeted on examining the velocity profiles, turbulence char-

acteristics or the hydraulic behavior of single plants, but not on the parameterization of the vegetative drag and flow resistance.

Modeling of the influence of natural plants on the bed-material and suspended sediment transport has received little attention, as noted by Vargas-Luna et al. (2015). Although fluvial sediment loads have been intensively studied, the role and characteristics of vegetation in causing sediment deposition are little studied (e.g., Osterkamp et al. 2012). As an example, deposition on floodplains has been measured e.g. by Walling (1999) and Kronvang et al. (2009), and simulated e.g. by Walling and He (1997) and Asselman and van Wijngaarden (2002), but these studies do not provide a description of the floodplain vegetation. Even many studies aimed at investigating the effects of real vegetation on sediment processes (e.g., Abt et al. 1994; Cotton et al. 2006; Wharton et al. 2006; Heppell et al. 2009) do not report those physical properties of the plants that are the key factors affecting flow characteristics and that can thus be expected to influence sediment processes (e.g., Curran and Hession 2013; Aberle and Järvelä 2015). Thus, generalizing the findings has been difficult. In fact, the study conducted by Corenblit et al. (2009) in a gravel-bed river is one of the few fluvial studies that have examined the relationship between natural riparian vegetation and annual net erosion and deposition using measurable, physically-based properties of the plant stands. The scarce flume studies that provide sufficient characterization of the investigated natural plants can focus on only a selected hydraulic context and sediment transport mode (e.g., Thornton et al. 1997; Rominger et al. 2010; Manners et al. 2015).

In an effort to overcome the complicated structure and flexibility of natural plants and plant stands, many studies on the flow–vegetation–sediment interaction have simulated plants with rigid cylindrical elements (e.g., Li and Shen 1973; Jordanova and James 2003; Bennett et al. 2008; Kothyari et al. 2009a; Zong and Nepf 2010; Gorrick and Rodríguez 2012). Vegetation is also commonly idealized as rigid cylinders in studies aiming to characterize the effects of plants on flow resistance and turbulent flow structures. Such studies range from flume experiments (e.g., Nepf 1999; Kothyari et al. 2009b; Ricardo et al. 2014) to the development of hydraulic models (e.g., Petryk and Bosmajian 1975; Pasche and Rouvé 1985; Huthoff et al. 2007; Konings et al. 2012; Battiato and Rubol 2014) and to the application of large eddy simulation (LES) approaches (e.g., Stoesser et al. 2009; Stoesser et al. 2010). However, the hydrodynamic behavior of objects is markedly affected by their flexibility, and simplifying natural vegetation as rigid cylinders is not necessarily justified, particularly when the plants are not simple-shaped and relatively rigid (see e.g., Nikora 2010; Aberle and Järvelä 2013; Chapman et al. 2015; Whittaker et al. 2015). Recently, vegetation has been increasingly simulated with artificial plants (e.g., Baptist 2005; Schoneboom 2011) and flexible strips or beams (e.g., Luhar and Nepf 2011; Ortiz et al. 2013; Marjoribanks et al. 2014a).

The importance of improving the parameterization of flexible, foliated natural vegetation is evident from recent articles that review the existing models and approaches for describing the effects of plants on flow hydraulics and sed-

iment transport (e.g., Nepf 2012b; Curran and Hession 2013; Marjoribanks et al. 2014b; Vargas-Luna et al. 2015; Aberle and Järvelä 2015). Reviewing the performance of eleven models, Vargas-Luna et al. (2015) concluded that flow resistance estimators that could take into account the complex structure and flexibility of natural vegetation are still lacking. Although certain models (e.g., Baptist 2005) performed reasonably for both artificial and natural plants, the prediction of flow resistance for grasses and foliated woody plants was uncertain in comparison to aquatic plants and leafless woody vegetation (Vargas-Luna et al. 2015). Thus, there is a need to improve the parameterization of natural plants by including the foliage and the effect of flexibility and reconfiguration, as concluded by Marjoribanks et al. (2014b) who reviewed current methods for estimating the influence of vegetation on flow hydraulics. Similarly, Curran and Hession (2013) state that species-specific variables including flexibility, structure, and life cycle, cause difficulties for modeling the vegetative impacts on fluvial hydraulics and sediment processes. Regarding the modeling of geomorphological processes, Zinke et al. (2011) found that the parameterization of the riparian vegetation was one of the most important factors causing uncertainty. Finally, Nepf (2012b) recommends that new research is needed to address the reconfiguration of plants that have a complex structure, such as branches and leaves differing in biomechanical properties.

1.2.2 Morphological and biomechanical properties of plants

From an engineering viewpoint, plants can be defined as composite, anisotropic, viscoelastic, highly heterogeneous structures onto which the flow of fluid exerts complex loads via tension, compression, bending, torsion and shear (Nikora 2010). The reaction of plants to flow depends on three types of plant characteristics (e.g., Nikora 2010; Aberle and Järvelä 2015): biomechanical characteristics, morphological characteristics (including linear, areal, volumetric and density characteristics) and plant–flow interaction characteristics. The latter two types are discussed in more detail in Section 1.3 with a view on the hydraulic parameterization of plants. The biomechanical characteristics mainly refer to the material properties of various plant tissues. One of the most important characteristics is the Young's modulus of bending that characterizes the flexibility of a plant part by relating the stress applied orthogonally to the plant part and the resulting strain. The effects of size and morphology on the flexibility are described by the second moment of the cross-sectional area. The product of the Young's modulus of bending and the second moment of the cross-sectional area is referred to as the flexural rigidity.

According to their biomechanical properties, plants can be grouped into two broad categories: bending plants of a relatively high flexural rigidity and tensile plants of a very low flexural rigidity (sensu Nikora 2010). Bending plants, such as riparian species, remain fairly erect in flow and experience mainly form drag. Form drag arises from differences in the pressure between the upstream and downstream sides of plant surfaces, and dominates for plant parts that are situated at a notable angle in relation to the main flow direction. By contrast, tensile plants, including many macrophytes, follow the flow, and

their flow resistance is thus mainly generated by viscous drag (e.g., Miler et al. 2012). Viscous drag results from skin friction and dominates for plant surfaces having close to a parallel orientation with respect to the main flow direction. For tensile plants, important biomechanical properties include the Young's modulus of tension as well as the maximum tensile stress and strain (e.g., Usherwood et al. 1997; Bociag et al. 2009; Miler et al. 2012, 2014).

The morphological and biomechanical properties of plants and plant parts show both inter-specific and intra-specific variation. Such variation has been observed for aquatic species because of adaptation to specific types of habitats (Miler et al. 2014). For trees, Niklas (1997) found that the flexural rigidity of woody parts varies as a function of the vertical location, indicating that younger branches are more flexible than older branches. For woody saplings, partly contradictory results have been obtained, with the flexural rigidity of the main stem reported to increase with the increasing height (Jalonen and Järvelä 2014) but to decrease with the increasing basal diameter (e.g., Sutili et al. 2012). Biomechanical scaling relationships have been developed e.g. between the flexural rigidity of the petioles and the load of the leaf lamina for different shapes of leaves (Niklas 1999).

The morphological characteristics of woody plants vary according to season, size and successional stage. For instance, the crown area and leaf coverage are the greatest in tall canopy trees, intermediate in sub-canopy trees, and the smallest in low understory plants (e.g., Yang et al. 2015). In addition, Yang et al. (2015) observed the crown area, leaf coverage and the proportion of leaned branches to decrease from climax forests of a late-successional stage to secondary shrubs of early-successional stage. For deciduous species, the abundance of the foliage in relation to the stem (which can be characterized e.g. by the leaf-area-to-stem-area ratio A_L/A_S) varies seasonally because of leaf flushing and shedding. Although the leaf-area-to-stem-area ratio is widely variable between specimens and stands, it appears to decrease with the increasing plant size, with A_L/A_S=6–26 recorded for saplings (Dittrich et al. 2012; Jalonen and Järvelä 2014) and A_L/A_S≈1–13 for mature trees (Cutini et al. 1998; Bréda 2003; Barclay et al. 2010). The effect of size on the morphological properties can be described with allometric scaling relationships. As an example, Weissteiner et al. (2015) reported that the basal diameter of tree saplings could be used to estimate their total one-sided stem area. However, the basal diameter was not able to predict the vertical variation that is important for considering flood events of different water levels.

The morphological and biomechanical variation at the intra- and inter-specific level complicates the prediction of the drag and flow resistance of natural vegetation. Each plant has a unique response to flow, to the extent that Schoneboom (2011) observed the drag and reconfiguration to differ between individual artificial plastic plants despite their identical morphological and biomechanical properties. This background motivates seeking such physically-based plant properties that could be incorporated into the modeling of the vegetative drag. A suitable parameterization of the vegetation may allow flow resistance predictions for riparian plants of different sizes and foliation condi-

tions. The next section briefly describes the current knowledge on the ecology and hydraulics of natural and man-made compound channels that form a typical environmental context for riparian plants.

1.2.3 Environmental compound channels

Compound channels consisting of a main channel and an occasionally inundated floodplain naturally develop in all geographic regions (e.g., Tockner and Stanford 2002), but they are also artificially constructed for hydraulic engineering purposes. Floodplain can be defined for instance based on channel morphology, vegetation types, or the frequency of inundation (see e.g. Curran and Hession 2013). Following the tradition in hydraulic engineering and fluvial geomorphology, this thesis considers a floodplain to consist of those areas that are situated above the bankfull level of the main channel at which the width-to-depth ratio is at its lowest. However, determination of the bankfull level is not always straightforward. Floodplains can be inundated by moderate to high flow events, rainfall, and lateral overland and sub-surface flow from the surrounding catchment (e.g., Junk 1989; Tocker and Stanford 2002). Floodplains are found along all sizes of channels, so that the average floodplain width ranges from few to thousands of meters depending on the size of the main channel (e.g., Tockner and Stanford 2002).

Flooding has ecological significance, which is recognized for instance in the flood pulse concept developed for periodically-flooded tropical rivers by Junk (1989). He notes that the variation of the dry and submerged conditions results in a physico-chemical environment that causes the biological communities to respond e.g. by morphological, physiological, and phenological adaptations. The flood pulse concept was extended to temperate, commonly engineered river systems by Tockner et al. (2000), who stress that also lower, non-periodic flow events that cause expansion and contraction are ecologically important. In short, natural floodplains comprise high biodiversity, and they are among the most biologically productive ecosystems on the earth (e.g., Tockner and Stanford 2002). Natural channels with surrounding floodplains are also geomorphologically relatively stable as they are typically closer to a state of dynamic equilibrium (as defined by e.g. Shields et al. 2003) than constructed trapezoidal channels.

Man-made compound channels (also called two-stage channels) have been recently proposed as an environmentally preferable engineering alternative to over-wide trapezoidal cross-sections (e.g., Powell et al. 2007; USDA 2007; Jormola et al. 2008). Conventionally, engineered rivers, brooks, and ditches are channelized and dredged to enhance the flow conveyance, but they often require frequent re-dredging because of excessive sediment deposition. In two-stage designs, a narrow main channel is bordered on one or both sides by a constructed, confined floodplain on which vegetation is sown, planted, or allowed to naturally develop (Figure 1). Depending on the designed level, the floodplain can be annually inundated from weeks to months. Two-stage channels can be aimed at bringing the sediment processes to a state of dynamic equilibrium or at improving the downstream water quality through the deposi-

tion of suspended sediment on the vegetated floodplain. Compared to over-wide trapezoidal designs, the compound cross-section is expected to decrease siltation in the main channel by keeping the low-flow velocities high enough, which can decrease the need for channel maintenance (Powell et al. 2007; USDA 2007). In addition, two-stage designs could potentially provide ecological benefits, including limited floodplain connectivity and ecological corridors for fauna. Under suitable conditions, even agricultural ditches are capable of supporting diverse fauna and flora (Needelman et al. 2007).

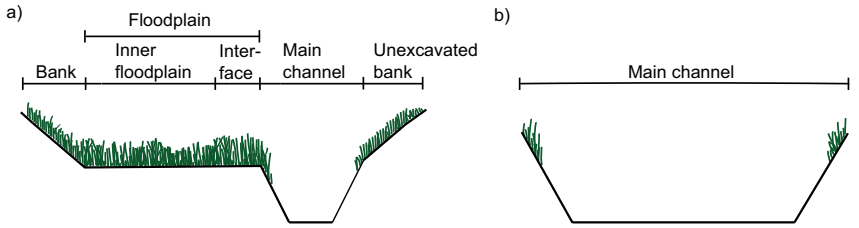

Figure 1. A two-stage channel with a vegetated floodplain on one side of the main channel (a), and a trapezoidal channel with bank vegetation (b).

The two-stage design has been adopted e.g. in agricultural drainage (e.g., Powell et al. 2007) and flood management (Sellin et al. 1990; Geerling et al. 2008) in an attempt to improve the conveyance of high flows while providing environmental benefits. Two-stage channels have been constructed also in Finland (e.g., Helmiö and Järvelä 2004; Jormola et al. 2008). In agricultural areas, there is a demand for such environmentally preferable solutions because of the requirements to improve water quality and biodiversity (see e.g., Puustinen et al. 2007; Aakkula et al. 2012). In addition, one-third of the formerly channelized agricultural brooks in Finland are currently in need of maintenance since they do not provide the required drainage performance (Pajula and Järvenpää 2007). While the operational needs are evident, published research on the performance of man-made two-stage channels is scarce.

The design and management of compound channels require reliable estimation of how the natural vegetation influences the flow and sediment transport. Making such estimates is particularly difficult for small channels where individual roughness elements, such as single bushes or large woody debris, have a large impact on the total flow resistance. Field studies in two-stage reaches often provide only a cursory description of the vegetation properties (e.g., Sellin et al. 1990; Myers and Lyness 1994; Helmiö and Järvelä 2004) and cannot therefore serve as a reliable reference for further designs.

Compound channels are hydraulically complex because of the interaction between the higher flow velocity of the main channel and the lower flow velocity of the floodplain (Figure 2). Such velocity differences result in the formation of a vertically-oriented shear layer with high Reynolds stresses at the interface between the main channel and floodplain (e.g., Knight and Shiono 1996). This shear layer produces strong vortices with vertical axes (see Figure 2), as recognized already in the first research on compound channels (e.g., Sellin 1964). The interface vortices exchange momentum and substances between the main

channel and floodplain. Because of the momentum exchange, the flow velocity is typically decreased in the main channel and increased on the floodplain while the total discharge capacity is decreased. For unvegetated floodplains, laboratory flume studies (e.g., Shiono and Knight 1991; Knight and Shiono 1996) have shown that the width of the shear layer increases as the relative depth (the water depth on the floodplain divided by the total water depth) decreases. Further, the measured values of bed shear stress have been found higher than those computed based on local depth and bed slope (Knight and Shiono 1996). On bare floodplains, the bed shear stress is affected by channel geometry, including the relative depth, floodplain width, main channel side slope, and symmetry (e.g., Shiono and Knight 1991; Knight and Shiono 1996). The shearing mechanisms are even more complex for meandering compound channels where the floodplain flow crosses over to the main channel in the bends (e.g., Shiono and Muto 1998). As illustrated in Figure 2 for overbank flows, there is typically an upward secondary flow near the edge of the floodplain towards the main channel and a downward secondary flow towards the corner of the main channel (e.g., Shiono and Knight 1991).

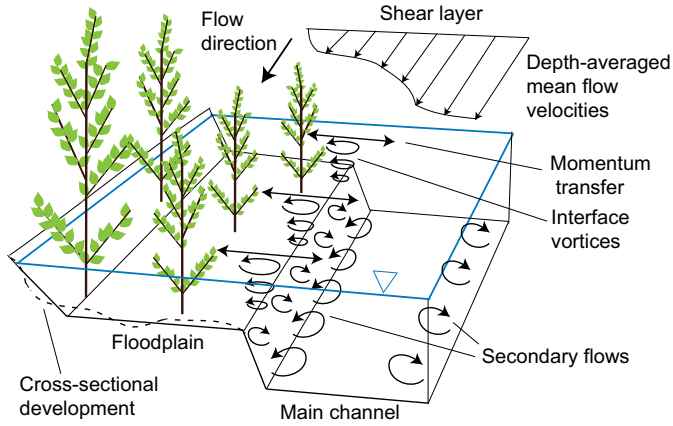

Figure 2. Hydraulics of compound channels at overbank flows (modified from Shiono and Knight 1991).

The presence of vegetation on the floodplain generally increases the streamwise flow velocity in the main channel and decreases that on the floodplain (e.g., Yang et al. 2007). As a result, floodplain vegetation increases the apparent shear stress and the turbulence intensity relative to the cross-sectional mean flow velocity at the interface region (Yang et al. 2007). Hopkinson and Wynn (2009) report similar findings for the interface region between an unvegetated main channel and a channel bank that was compared in bare and vegetated conditions. In their study, sparse trees had the least effect on turbulence, dense shrubs produced the highest interface turbulence, and folding grasses suppressed the near-bed turbulence most efficiently. McBride et al. (2007) found that simulated woody floodplain vegetation decreased the near-bed turbulence and boundary shear stress on the floodplain but increased them on the interface and in the main channel.

The understanding on the momentum transfer in compound channels has been gained in idealized laboratory conditions, and it remains to be investigated how efficiently interface vortices can supply fine sediment to vegetated floodplains in natural conditions. Flume studies show that the deposition of fine sediment within vegetation can be limited by both lateral and longitudinal supply (e.g., Sharpe and James 2006; Zong and Nepf 2011). In wide, densely vegetated areas, longitudinal advection is expected to be the main mechanism of suspended sediment (SS) supply, but deposition reduces the SS concentration in the downstream direction as the distance from the SS replenishment point increases (e.g., Zong and Nepf 2011).

The most straightforward, one-dimensional (1D) hydraulic analyses applied to compound channels quantify the total flow resistance using various equations based on partitioning the cross-section (e.g., Yen 2002). However, the resistance coefficient of the floodplain vegetation is typically calibrated against observed water levels or estimated from reference photographs (e.g., DEFRA 2004; Yang et al. 2014). The difficulties associated with the suitable parameterization of flexible, foliated plants (see Section 1.2.1) complicate the usage of sophisticated hydraulic models for naturally vegetated compound channels. For instance, Rameshwaran et al. (2013) validated four 3D models using laboratory data on compound meandering flows with bare floodplains, but the reliability of the models for real channels remains to be evaluated. As stated by Luhar and Nepf (2013), little of the understanding on the flow–vegetation interaction at the stand scale has been applied to reach-scale analyses. Considering practical channel design, there is a motivation to develop and promote straightforward hydraulic approaches that use physically-based vegetative properties. The state-of-the-art of parameterizing natural riparian vegetation for hydraulic analyses is reviewed in the next section.

1.3 Parameterizing natural vegetation for hydraulic analyses

The vegetative drag and flow resistance can be considered at different scales (e.g., Nikora et al. 2012; Luhar and Nepf 2013; Aberle and Järvelä 2015), ranging from the leaf scale (Vogel 1989; Albayrak et al. 2012) to foliage (e.g., Wilson et al. 2008; Xavier 2009), plant (e.g., Vollsinger et al. 2005; Butler et al. 2012), patch (e.g., Siniscalchi et al. 2012; Sukhodolova and Sukhodolov 2012), stand (e.g., Järvelä 2002a), and reach scales (e.g., Helmiö and Järvelä 2004; Green 2006; Nikora et al. 2008). Herein, the foliage scale refers to experiments where the leaves are naturally attached to the stem, thus exhibiting a range of orientations with respect to the main flow direction. By contrast, the leaf scale signifies single leaves examined in a downstream orientation. Because both the behavior of vegetation and the flow structure are affected by the ratio between the water depth (h) and the vegetation height (H), the relative submergence (h/H) is a key property to be considered in vegetated flows (e.g., Nepf 2012a; Aberle and Järvelä 2015). Emergent vegetation with $h/H<1.0$ protrudes through the water surface while submerged vegetation with $h/H>1.0$ remains completely below the surface.

In vegetated flows, the total flow resistance can be expressed in the form of three resistance coefficients: the Darcy–Weisbach friction factor (f), the Manning coefficient (n), or the Chézy coefficient (C). Although the coefficients are empirical, they are still widely used in practical engineering applications, particularly in the design of small channels. The three coefficients are related as

$$f = \frac{8gRS}{u_m{}^2} = \frac{8gn^2}{K^2R^{1/3}} = \frac{8g}{C^2} \tag{1}$$

where g is the gravitational acceleration, R is the hydraulic radius of the channel (the wetted cross-sectional area A_W divided by the wetted perimeter P), S is the energy slope, u_m is the cross-sectional mean flow velocity, and K is a constant (1 $m^{1/3}/s$). Starting from Chow (1959), there are several reference books reporting the coefficients for different types of channel linings and vegetation types.

The first attempt towards formally describing the total flow resistance of channels with submerged vegetation was based on the notion that Manning's n could be expressed as a function of the product of the mean flow velocity and the hydraulic radius, n=f(u_mR), as summarized by USDA (1954). In fact, the n–u_mR relationship describes the functional dependence of the flow resistance on the Reynolds number of the flow (for channel flow, Re=u_mR/ν, where ν is the kinematic viscosity of the fluid). USDA (1954) published empirically determined n–u_mR design curves for five vegetative retardance classes which were formed by categorizing the examined grassy species into five height classes and two density classes. As a practical aid for channel design, empirical n–u_mR curves have been obtained for grassy vegetation of different species, heights and densities (e.g., Kouwen 1992; Kirby et al. 2005; Rhee et al. 2008). However, the current state of the art of hydraulics prefers physically-based models that quantitatively incorporate the plant properties.

Physically-based approaches commonly employ the drag force (F) exerted by a plant or plant part in a flow. According to the standard fluid dynamics theory (e.g., Schlichting and Gersten 2000), F is related to the characteristic approach velocity (u_C), commonly taken as the mean flow velocity of the vegetated layer, yielding

$$F = \frac{1}{2}\rho C_D A_C u_C{}^2 \tag{2}$$

where ρ is the density of the fluid, C_D is the drag coefficient of the object, and A_C is the characteristic reference area of the object. A_C is commonly defined as the frontal projected area for rigid objects. For flexible plants, various definitions of A_C have been applied, including the frontal projected area under air flow (e.g., Rudnicki et al. 2004; Vollsinger et al. 2005) or under water flow (Schoneboom 2011; Wunder et al. 2011), the frontal projected area in still air (e.g., Koizumi et al. 2010; Whittaker et al. 2015), the total wetted area (e.g., Vogel 1989; Sand-Jensen et al. 2008), and the lateral projected area (Statzner et al. 2006). For rigid objects, A_C does not depend on the flow velocity, and C_D

is a function of the shape, surface roughness and Reynolds number of the object (Re=$u_C l_C/\nu$, where l_C is the characteristic length of the object). Values of C_D for simple-shaped rigid objects are well known and constant under a large range of Reynolds numbers (e.g., Vogel 1994). For a stand of rigid cylinders characterized by a complex wake flow structure, the bulk drag coefficient is additionally affected by the spacing (e.g., Tanino and Nepf 2008; Kothyari et al. 2009b) and pattern of the elements (e.g., Schoneboom 2011; Dittrich et al. 2012).

For flexible, reconfiguring plants, the drag coefficient is difficult to predict a-priori because it varies as a function of the flow velocity even if the reconfiguration-induced changes in the frontal projected area are taken into account (e.g., Rudnicki et al. 2004; Vollsinger et al. 2005; Statzner et al. 2006; Wunder et al. 2011). This explains the well-established observation that the drag forces of foliated woody plants do not increase with the square of the flow velocity (as postulated by Eq. 2), but at a lower rate (e.g., Oplatka 1998; Freeman et al. 2000; Wilson et al. 2008). Leafless woody vegetation has been generally concluded to perform similarly as rigid cylinders based on the investigations by e.g. Järvelä (2002a, 2002b) and Armanini et al. (2005). However, recent detailed studies reveal that the relationship between F and u_C may deviate from squared for leafless woody saplings (e.g., Dittrich et al. 2012; Whittaker et al. 2013; Jalonen and Järvelä 2014). Thus, it is important to parameterize the reconfiguration of woody plant parts in flow resistance prediction.

The share of the total flow resistance generated by vegetation can be determined based on the linear superposition of the associated stresses (e.g., Yen 2002). In flows where vegetation fills the entire wetted cross-section,

$$\tau = \tau' + \tau'' \tag{3}$$

where τ is the total stress (the total drag force per unit bed area), τ' is the bed shear stress (the drag force generated by the channel bed per unit bed area), and τ'' is the vegetative stress (vegetative drag force per unit bed area). It follows that the total friction factor is a linear sum of the friction factors of the bed (f') and vegetation (f''_{tot}):

$$f = f' + f''_{tot} \tag{4}$$

f''_{tot} can be derived using Eq. 2 (e.g., Aberle and Järvelä 2013):

$$f''_{tot} = 4\frac{A_C}{A_B}C_D \tag{5}$$

where A_B is the unit bed area. For grassy or aquatic vegetation, A_C/A_B is often parameterized as the frontal area index aH, where a is the frontal projected area of the vegetation per unit volume. a can be expressed as mD_S where m is the number of plants per unit bed area and D_S is the stem diameter (e.g., Luhar et al. 2008; Nepf 2012b). C_Da and C_DaH are in this thesis called the drag–

density parameter and the drag–area parameter, respectively. Similar to Eq. 2, Eq. 5 as such considers plants to be rigid.

1.3.1 Models for natural riparian plants

Five models parameterizing the reconfiguration have been proposed for foliated woody plants. The models of Whittaker et al. (2013, 2015) and Jalonen and Järvelä (2014) estimate the drag forces of single specimens while the models of Kouwen and Fathi-Moghadam (2000) and Järvelä (2004) estimate the friction factors of fully vegetated flows where emergent or just submerged plants cover the entire wetted cross-section. In these five models, vegetation density is parameterized by the leaf area index (the total one-sided leaf area per unit bed area; Kouwen and Fathi-Moghadam 2000; Järvelä 2004), the total plant area (Jalonen and Järvelä 2014), the frontal projected area in still air (Whittaker et al. 2015), or by using the total plant volume instead of a reference area (Whittaker et al. 2013).

The existing five models treat woody plants as bulk, i.e., without considering the foliage and the stem separately (Kouwen and Fathi-Moghadam 2000; Järvelä 2004; Whittaker et al. 2013, 2015; Jalonen and Järvelä 2014). Thus, these models cannot take into account the fact that the shares of the stem drag and foliage drag on the total drag are variable. The stem has been found to contribute 25–75% of the total drag for 1–4.5 m tall specimens belonging to the deciduous genera *Alnus*, *Populus*, and *Salix* (Armanini et al. 2005; Xavier 2009; Dittrich et al. 2012). Neither can the five models consider the notable differences in the reconfiguration and biomechanical properties between the foliage and the stem (e.g., Wilson et al. 2008; Dittrich et al. 2012). Taking aquatic species as an example, the flexural rigidity of the stem can be three orders of magnitude greater than that of the leaves (Albayrak et al. 2014). The investigation by Tanaka et al. (2011) suggests that the plant-scale drag is related to the abundance of the foliage in relation to the stem. Thus, it should be investigated whether a separate parameterization of the foliage and stem is advantageous compared to the representation of foliated plants by plant-scale bulk parameters that lump the effects of the foliage and stem. One example for separately modeling the drag of the foliage and woody components is provided by Schnauder and Moggridge (2009) who used Eq. 2 and leaf-scale C_D values obtained by Vogel (1989).

Partly vegetated flows where vegetation does not cover the entire wetted cross-section of the channel are more complex than fully vegetated flows because the flow differs between the vegetated regions and open water (see Sections 1.2.3 and 1.4.3). In simple cross-sections with submerged plants covering the entire channel bed, the flow resistance depends primarily on the relative submergence of the plants (e.g., Kouwen and Unny 1973; Wu et al. 1999). Based on this notion, Kouwen (1992) summarizes a procedure for estimating the total flow resistance of grassed channels using the deflected height of the vegetation. He introduced an empirical regression equation to derive the deflected height of flexible plastic elements from the total boundary shear stress and the product of the flexural rigidity and stem density of the plants. For nat-

ural grasses, Kouwen (1992) states that this product can be represented as a simple function of the vegetation height separately for green and dormant states. Empirical equations have been proposed for estimating the total flow resistance in natural channels with flexible aquatic plants. These equations parameterize vegetation with simple bulk properties, such as the spatially-averaged cross-sectional vegetative blockage factor (e.g., Green 2006; Nikora et al. 2008) or dry mass (e.g., De Doncker et al. 2009). However, it would be good to replace empirical equations by straightforward but physically-based ones.

In hydraulic models and simulation tools, plants are commonly parameterized as rigid elements using Eq. 2 although Section 1.2.1 indicated that such a simplification is often not justified for flexible natural species. For submerged aquatic stands, hydraulic models with separate layers for the vegetation and overflow have been developed (e.g., Huthoff et al. 2007; Konings et al. 2012; Luhar and Nepf 2013). Various hydraulic models, both analytical (e.g., Huai et al. 2009; Knight et al. 2010) and numerical (e.g., Kang and Choi 2006), have been proposed also for compound channels with floodplain vegetation. An exception to the modeling of plants as rigid elements is the parameterization by Luhar and Nepf (2013) that considers the reconfiguration of flexible blade-like vegetation elements using their biomechanical properties, including the flexural rigidity. The parameterization of vegetation for sediment transport analyses is reviewed in next section.

1.4 Erosion, deposition and sediment transport in vegetated flows

One of the first groups expressing interest into erosion and deposition in vegetated flows were U.S. engineers designing drainage and irrigations channels with grass linings. To aid in the design, maximum permissible flow velocities under which no notable erosion takes place were provided for various grassy species by USDA (1954). One of the first physically-based models allowing the computation of the sediment transport rate within emergent rigid cylindrical stems was developed by Li and Shen (1973). Temple et al. (1987) improved the design procedure of USDA (1954) by incorporating the vegetative cover factor, soil erodibility relations, and the $n–u_mR$ design curves into the analyses. Samani and Kouwen (2002) developed an analytical 1D formulation to predict erosion using the deflected height of grass, but also their formulation incorporates several empirical parameters and relationships. Despite the advances made by these early studies, the prediction of sediment processes in vegetated flows has remained challenging, particularly in complex channel geometries.

1.4.1 Suspended sediment processes

Physical sediment processes depend on the characteristics of the flow and sediment (e.g., Le Roux 2005), both of which are modified by the presence of vegetation. The processes of cohesive sediment are complicated by the electrochemical forces acting on the surfaces and interiors of the individual particles

(e.g., Partheniades 2009). Because of these surface forces, colliding individual cohesive particles can aggregate into larger flocs (e.g., McAnally and Mehta 2002; Nikora et al. 2004). Flocs can also disaggregate through particle collisions or flow-induced shear stresses (e.g., McAnally and Mehta 2002). Aggregation is stronger in saline water and little studied in freshwater. Thus, there is need for clarifying the role of aggregation in the fluvial context, where the binding of primary particles by bacterial polymeric fibrils or other biological processes can be important (e.g., Droppo et al. 1997; Phillips and Walling 1999).

Cohesive sediment is typically transported in suspension as the shear velocity exceeds the settling velocity of the particles (e.g., Le Roux 2005). Suspended particles settle downwards according to their settling velocity but also move in lateral, longitudinal and upward directions along with the mean flow and turbulent fluctuations. Settling can be characterized as free settling below the suspended sediment concentration (SSC) of approximately 0.1 kg/m^3, flocculation settling at SSC of ~0.1 kg/m^3 to ~10 kg/m^3, and as hindered settling above SSC of ~10 kg/m^3 (Mehta and McAnally 2008). The settling velocity increases with the increasing concentration in the flocculation settling regime because of aggregation while it decreases with the increasing concentration in the hindered settling regime. However, aggregation increases the porosity of flocs and decreases their density (e.g., Droppo et al. 1997). The effect of such dynamically varying floc structure on the settling velocity and deposition can be expressed e.g. through the fractal dimension of the flocs (e.g., Klassen et al. 2011).

For suspended particles to permanently deposit on the bed, the bed shear stress must be lower than a certain critical value that depends mainly on the strength of the bonding between the particles (e.g., Mehta and McAnally 2008). Flume deposition studies with natural flocculating sediment above the initial concentration of ~1 kg/m^3 show that the ratio between the final equilibrium SSC and the initial SSC is constant, decreasing as the bed shear stress decreases (Partheniades 2009). Field studies have revealed that flocs of cohesive clay and silt can readily deposit on floodplains (e.g., Nicholas and Walling 1996; Thonon et al. 2005). Thus, more focus should be put on investigating what proportion of the transported cohesive sediment can be deposited in natural and constructed channels, and how this mass balance can be influenced by vegetation. Once deposited, cohesive sediment undergoes consolidation, which decreases the bed level by increasing the density of the deposits at time scales of months (e.g., Berlamont et al. 1993).

Sediment is entrained from channel boundaries when the shear stress exceeds the particles' critical shear stress for erosion (e.g., García 2008b). The erosion of cohesive sediment is generally considered to be a linear function of the excess shear stress as opposed to the non-linear erosion of non-cohesive sediment. However, recent research suggests that the erosion of cohesive sediment increases at a faster rate than the excess shear stress (Walder 2015). For cohesive sediment, critical shear stress and erodibility are difficult to estimate a-priori (e.g., Clark and Wynn 2007) as they depend on sediment characteris-

tics, such as the dry bulk density, wet bulk density, water content, organic content, and the percent of clay, silt, and sand (e.g., Aberle et al. 2004; Mostafa et al. 2008; Thoman and Niezgoda 2008), as well as on sub-aerial processes, including freeze–thaw cycles (e.g., Wynn et al. 2008). In addition, the presence of vegetation decreases the erodibility and increases the critical shear stress (Wynn and Mostaghimi 2006a). Wynn and Mostaghimi (2006a, 2006b) have found that large roots (> 2 mm in diameter) reinforce the soil against erosion and that both herbaceous and woody plants decrease the number of freeze–thaw cycles, which in turn reduces erodibility.

1.4.2 Effects of vegetation on sediment transport

The presence of aquatic and riparian vegetation should be taken into account when analyzing the sediment transport in channel networks. For instance, increasing vegetative flow resistance on the floodplain has been observed to systematically reduce the bed-load transport in the main channel (Tang and Knight 2006). The flow–vegetation interaction also controls the mechanisms and amount of suspended sediment supplied to a vegetated floodplain. SS can be supplied to plant stands via longitudinal advection parallel to the main flow direction (e.g., Zong and Nepf 2010, 2011), vertical diffusion from the overflow (e.g., Nepf et al. 2007; Luhar et al. 2008), lateral turbulent diffusion normal to the main flow direction (e.g., Sharpe and James 2006), and via lateral advection (e.g., Asselman and Wijngaarden 2002). Vegetation modifies sediment transport through particle capture on plant stems (e.g., Elliott 2000) and through seasonal in-channel sediment storage and release within aquatic macrophytes (e.g., Wharton et al. 2006; Heppell et al. 2009; Asaeda et al. 2010) and riparian stands (e.g., Osterkamp and Hupp 2010). Most field studies (e.g., Zabaleta et al. 2007; López-Tarazón et al. 2009: Oeurng et al. 2010; Gay et al. 2014) have analyzed the temporal pattern of sediment transport at a spatial scale that does not provide details about the in-channel storage and release processes. Thus, new field studies are needed to determine the extent to which aquatic and riparian vegetation can influence the amount and timing of fluvial sediment loads. SSC at a given discharge is often higher during the rising limb of the hydrograph, a phenomenon called clock-wise hysteresis (e.g. Asselman 1999). Clock-wise hysteresis is typically associated with the deposited matter being re-suspended from the channel bed rapidly after the discharge increases (e.g., Oeurng et al. 2010) and with the subsequent depletion in the sediment available for transport (e.g., Williams 1989).

Stands of natural plants can undergo both erosion and deposition (e.g., Abt et al. 1994; Cotton et al. 2006; Wharton et al. 2006; Heppell et al. 2009). The spatial patterns of erosion and deposition are highly complex in plant patches with edge effects (e.g., Cotton et al. 2006; Bouma et al. 2007) and within stands of randomly distributed specimens (e.g., Rodrigues et al. 2007; Bouma et al. 2009). In the study with intertidal macrophytes by Bouma et al. (2009), net erosion took place within sparse plant stands and net deposition within dense stands. For dense patches and stands, deposition starts to occur shortly downstream of the stand frontline and is at its highest at the end of the diverg-

ing flow region where the flow within the stand is fully developed (Bouma et al. 2009; Zong and Nepf 2010). Deposition can continue some distance downstream of the patch end (e.g., Cotton et al. 2006; Bennett et al. 2008), particularly when the vegetation is emergent (Ortiz et al. 2013). Erosion is typically observed at the sides of the patches and stands as flow is deflected there (e.g., Bennett et al. 2008; Bouma et al. 2009).

Estimating sediment transport and geomorphological processes in flows with natural vegetation requires that flexible foliated plants are suitably parameterized. In the fluvial environment, annual net deposition has been observed to increase with the increasing vegetation biovolume, defined as the maximum inundated vegetation height multiplied by the areal coverage of the plants (Corenblit et al. 2009). In a flume study by Thornton et al. (1997), net deposition within natural grassy vegetation increased with the increasing number of plants per unit bed area. Bos et al. (2007) report similar findings for the seasonal net deposition in intertidal sea grass beds. Gacia et al. (1999) found that net deposition within a seagrass bed at the temporal scale of approximately one week was more related to the leaf area index (A_L/A_B) than to the vegetation biomass or height. They observed that net deposition increased up to $A_L/A_B=4$, and suggested that the bending of the plants and particle capture on the plant surfaces may hinder the free settling of suspended matter at higher vegetation densities. Mudd et al. (2010) modeled the particle capture and settling within intertidal marsh grasses. According to their model, net deposition increased with the increasing vegetation biomass, which was used to estimate the frontal projected plant area per unit volume. Regarding bed load, the flume study by Manners et al. (2015) suggested that the transport rate decreases with the increasing frontal projected area for woody stands.

Sediment transport formulas for unvegetated flows (reviewed e.g. by García 2008b; Mehta and McAnally 2008) are sometimes applied to vegetated flows by determining the mean bed shear stress from the vegetative and total stresses according to Eq. 3. The mean bed shear stress has been found to control the bed-load transport within emergent rigid cylindrical stems (Jordanova and James 2003; Kothyari 2009a). Considering these experimental data, Vargas-Luna et al. (2015) concluded that sediment transport formulas based on bed shear stress are capable of predicting the transport rate within rigid cylinders. However, considering that the hydraulic behavior of many natural plant species notably differs from rigid cylinders (see Sections 1.2.1 and 1.3), the caution expressed by Nepf (2012b) is warranted. She states that it is not clear how well transport formulas based on mean bed shear stress work for vegetated flows, where turbulence is not related to the bed shear stress but to the vegetative drag. For a stand of rigid cylinders, Liu and Shen (2008) found that a 3D turbulence model was capable of simulating the suspended sediment transport and deposition. The important role of turbulence is supported by the flume study of Ortiz et al. (2013) who observed that deposition occurred downstream of a vegetation patch only if the local turbulent kinetic energy was low enough. Thus, deposition was not directly related to the mean flow velocity and mean bed shear stress.

1.4.3 Turbulent flow structure within plant stands and effects on transport processes

Both the mean and turbulent flow structure are very complex in vegetated channels because of multi-scale flow patterns (e.g., Nepf 2012a; Aberle and Järvelä 2015). There may be large-scale turbulence that scales with the water depth (pattern no. 1 in Figure 3) and that can be modified by vegetation (e.g., Nikora et al. 2012). Turbulence is primarily governed by vegetation density, so that the flow structure has been found to notably differ between sparse and dense submerged stands for both rigid cylinders (e.g., Luhar et al. 2008) and flexible natural plants (Sukhodolov and Sukhodolova 2012; Sukhodolova and Sukhodolov 2012). Nepf (2012a) and Sukhodolov and Sukhodolova (2012) concluded that the flow structure resembles that of turbulent boundary layers in sparse stands and that of mixing layers in dense stands. Consequently, dense stands have an inflection point in the vertical profile of the streamwise mean flow velocity $u_m(Z)$ at the top of the vegetation (see the right profile in Figure 3). The difference in the mean flow velocity below and above the top of the plants generates shear-layer vortices (pattern no 3 in Figure 3) that dominate the turbulence in dense stands (e.g., Nepf 2012a). In accordance, turbulent shear stresses have been reported to reach the maximum values near the top of the vegetation for fully developed flow in dense flexible natural stands (e.g., Sukhodolova and Sukhodolov 2012). In sparse stands, the vertical profile of the mean flow velocity $u_m(Z)$ is logarithmic (see the left profile in Figure 3) and turbulence is dominated by the vortices generated by the individual plants (pattern no 2 in Figure 3, Nepf 2012a). These vortices result from the stem-scale wake turbulence and scale with the stem diameter and spacing for rigid cylinders (e.g., Luhar et al. 2008). Complex natural plants are additionally hypothesized to generate turbulence through leaf-scale mixing and boundary layers (Nikora 2010).

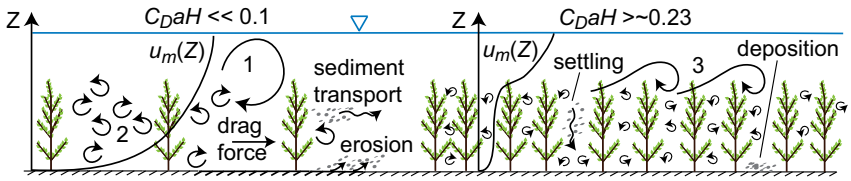

Figure 3. Key hydrodynamics and expected dominant sediment processes within sparse plant stands (on the left) and dense plant stands (on the right). $u_m(Z)$ refers to the vertical profile of the streamwise mean flow velocity. The patterns #1–#3 relate to turbulence generated by depth-scale shear (#1), individual plants (#2), and stand-scale shear-layers (#3). Modified from Nikora (2010) and Nepf (2012a).

The rare theoretical frameworks for describing the effects of turbulence on erosion and deposition processes in vegetated flows have seldom been tested under natural conditions. One of the few theories is that developed for stands of submerged rigid stems (for which C_D=1) by Luhar et al. (2008) and further elaborated e.g. by Nepf (2012a). Their theory focuses on the vertical penetration of turbulence to the stand by determining the conditions under which the above described boundary and mixing layer analogies apply. Nepf (2012a) dis-

tinguishes three hydraulic regimes with differing vegetation densities. The boundary layer analogy applies to very sparse plant stands with the drag–area parameter C_DaH<<0.1 while the mixing layer analogy applies to transitional (~0.1<C_DaH<~0.23) and dense (C_DaH>~0.23) stands. For sparse and transitional stands, turbulence levels are elevated near the bed, which can cause erosion or re-suspension of sediment or at least ensure that the incoming sediment is transported downstream, as illustrated in Figure 3. By contrast, the near-bed turbulence is low in dense stands because the momentum transferred into the stand by the shear-layer vortices is dissipated by the high vegetative drag. Thus, the theory of Luhar et al. (2008) implies that plant stands with C_DaH>~0.23 can promote settling and deposition (see Figure 3). Because of the low level of turbulence, the rate of deposition within dense stands has been linked to the mean flow velocity (Zong and Nepf 2010). Investigations with sparse and dense stands indicate that turbulence can be predicted from the C_Da parameter also for flexible aquatic plants (Sukhodolov and Sukhodolova 2012, Sukhodolova and Sukhodolov 2012). However, only few datasets allow testing the transport theory of Luhar et al. (2008) and Nepf (2012a) for natural vegetation, which motivates collecting data on C_DaH and the associated net erosion and deposition in real plant stands.

For improving the understanding of the physical sediment processes in natural flows, high temporal and spatial resolution of data is desirable (e.g., Lawler 2008). Suspended sediment transport and weather conditions can be accurately determined with adequately maintained sensors and sensor networks (e.g., Kotamäki et al. 2009; Marttila and Kløve 2012). For monitoring fluvial erosion and deposition, the capabilities of repeated cross-sectional surveys are proven (e.g., Lawler 1993). Although sophisticated methods, such as terrestrial laser scanning, can be combined with other surveying methods to determine the cross-sectional geometry of vegetated cohesive channels (e.g., Jalonen et al. 2014), there are still problems in monitoring the cross-sectional change because of the low volume of deposition.

1.5 Objectives

The literature review indicated that important gaps in knowledge exist regarding the interactions between flow, riparian plants, and cohesive sediment from the foliage and stem scale to the catchment scale. This thesis set to generate sufficient data to allow filling selected knowledge gaps highlighted in Sections 1.2–1.4. Within the research field (Figures 2 and 3), the main objective is to enhance the parameterization of natural woody and grassy riparian vegetation for flow resistance and sediment transport analyses in compound channels. A holistic approach was selected, with the thesis consisting of experimental field and flume research and of the application of existing and new models. For the field investigation, a man-made agricultural two-stage channel was chosen with the intention of advancing process understanding while providing knowledge for the practical application of environmental hydraulics. The flume analyses focused on the foliage and stem, plant, and plant stand scales

while the field experiment was targeted at the sub-reach, reach, and catchment scales (Papers I–IV are numbered from the smallest to the largest examined scale). The detailed objectives of this thesis are

1) to quantify the drag and reconfiguration of natural woody vegetation and their dependence on the leaf-area-to-stem-area-ratio A_L/A_S (I, II)
2) to develop a flow resistance model for natural woody vegetation using a physically-based parameterization for both the foliage and the stem, and to collect a dataset for testing the model (I, II)
3) to examine how the flow hydraulics in the two-stage channel depend on the properties of the floodplain vegetation, and to evaluate the suitability of a straightforward process-based flow resistance model in the two-stage geometry (III)
4) to explore how the flow–vegetation interaction explains the net deposition and erosion of cohesive sediment on the excavated bank and floodplain of the two-stage channel (III)
5) to investigate the cohesive sediment transport at the catchment scale in order to provide knowledge for the application of the two-stage approach in agricultural channels (III, IV).

The field site had spatially uniform sediment characteristics, and therefore measurements of the erosion or deposition properties of the sediment were not necessary for the research objectives. Consideration of aquatic plants and bed-load transport was also out of the scope. In the investigations, the mean flow properties were used. Referring to the literature review (e.g., Figure 3), turbulence within dense natural plant stands was expected to be generally low and therefore the turbulent flow structure was considered only theoretically to the extent relevant for explaining the findings.

2. Materials and methods

Figure 4 summarizes the main measurements, analyses, and modeling conducted in the thesis at the different examined scales. The arrows show 1) the primary pieces of measurement data on which each analysis is based on, 2) the data used to apply existing models, and 3) the data and analyses that supported the development of the new flow resistance model. More details are presented in Sections 2.1–2.2 for the measurements, Section 2.3 for the vegetation properties, and Section 2.4 for the computations and existing models.

2.1 Flume investigation with natural woody vegetation (I, II)

The flume experiments were conducted with five woody species: *Populus nigra* (Black Poplar), *Salix viminalis* (Common Osier), *Salix x rubens* (hybrid Crack Willow), *Alnus glutinosa* (Common Alder) and *Betula pendula* (Silver Birch) (Figures 5 and 6). The tested specimens were 23 cm tall tips of branches, referred to as twigs. All the experiments related to Papers I–II were carried out at the Leichtweiß-Institut für Wasserbau, Technische Universität Braunschweig, Germany. Various experiments were designed in order to investigate the effects of the relative submergence, vegetation density and foliation level on the drag and reconfiguration, and to obtain validation data for the developed model. For a summary of the data and analyses, refer to Figure 4.

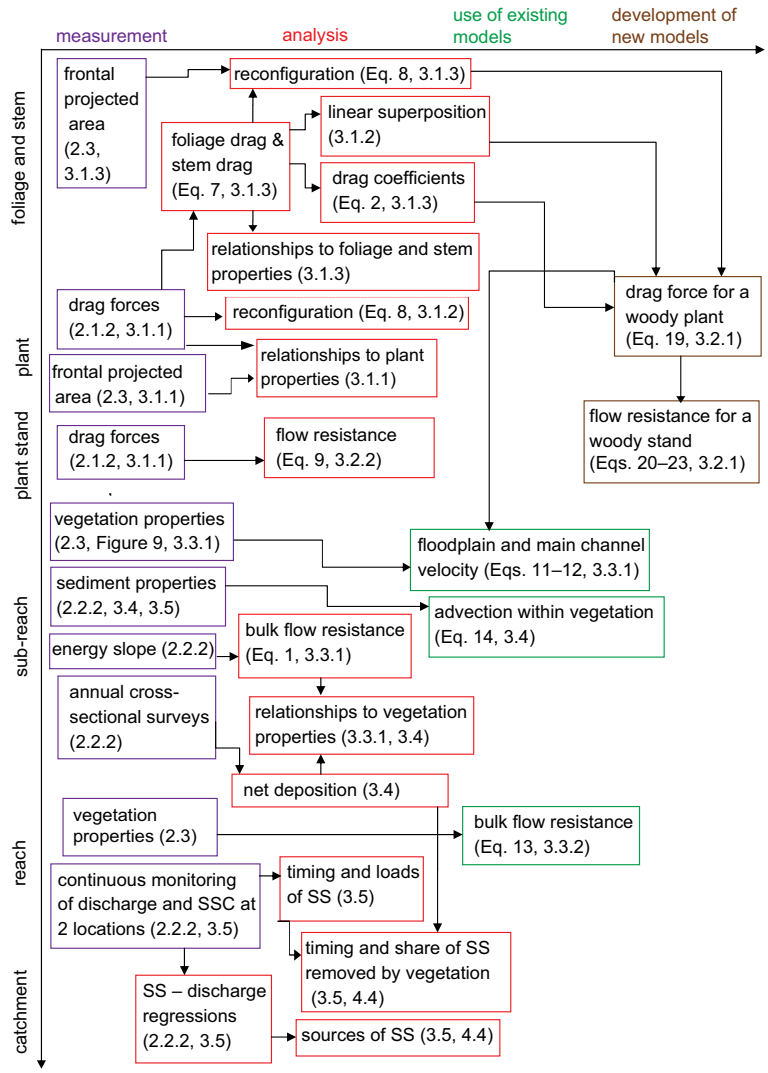

Figure 4. Main measurements, analyses, and the application of existing and new models (the color codes of the boxes correspond to those on the x-axis) at the different scales shown on the y-axis. The associated equations and the sections where the topic is handled in the thesis are shown in parentheses. SS and SSC signify suspended sediment and suspended sediment concentration, respectively.

Figure 5. Representative specimens of the examined *Salix viminalis* (Common Osier) (a), *Salix x rubens* (hybrid Crack Willow) (b), *Alnus glutinosa* (Common Alder) (c), and *Betula pendula* (Silver Birch) (d). (Paper I)

Figure 6. Representative specimen of *Populus nigra* (Black Poplar) (a), a *P. nigra* plant stand under flow (b), and determination of the frontal projected area under flow (c). (Paper II)

2.1.1 The laboratory flume and drag force sensors

The experiments (Papers I and II) were performed in a 32 m long and 0.6 m wide tilting laboratory flume at the Technische Universität Braunschweig using the flume setup and measurement system developed by Schoneboom et al. (2008) and Schoneboom (2011). The bed roughness of the flume consisted of a rubber mat with 3 mm high pyramidal-shaped elements. The water depth and water surface slope were determined using piezometers while the discharge was measured by an inductive flow meter. The water depth (ranging at 8–30 cm) was adjusted by a tailgate according to the bending of the plants to obtain the desired level of relative submergence. The cross-sectional mean flow velocity was determined with the continuity equation neglecting the vegetation volume. The experiments were carried out under steady uniform flow.

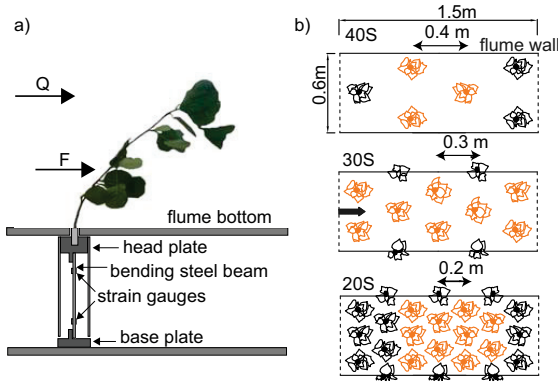

Figure 7. A schematic picture of a 23 cm tall plant attached to the approximately 20 cm high drag force sensor (a), and the three spacings (densities) at which the plant stands were examined, with orange color showing the instrumented plants (b). (Paper II)

According to the descriptions in Papers I and II, the vegetative drag forces were measured with the drag force sensor system described by Schoneboom et al. (2008) and Schoneboom (2011). Each sensor consisted of two Wheatstone full bridge configurations formed by four strain gauges (Figure 7a). The drag forces were obtained by transforming the compression strains to bending moments. The drag force sensors were located under the bottom of the flume in

the 1.5 m long measurement area 16 m downstream of the flume inlet. The time-averaged values of three 60 s long measurement periods at 200 Hz were used in the analyses. The maximum errors of the calibrated sensors were ±0.01 N for F=0–0.5 N and ±0.02 N for F=0.5–2.0 N (Schoneboom 2011).

2.1.2 Hydraulic experiments with single plants and plant stands

Investigations were conducted with two configurations: single plants and plant stands (Papers I and II). Table 1 documents the experimental conditions for the four series of experiments (A–D). All experiments investigated the plants in the foliated condition while the experiments A and C involved measuring the drag of the same specimens in the leafless condition as well. The examined twigs were collected from saplings and mature trees growing in Braunschweig, Germany. The specimens were randomly sampled among those twigs that had a reasonably straight main stem, and included both single-stemmed and branched structures. New specimens were collected for each experimental series as well as for the different plant densities examined in B. The experiments at the relative submergences (h/H) of 0.3 and 0.7 (B) were carried out with the same specimens. The plants were stored in water before the investigations. The measurements were conducted at the mean flow velocities of 0.03–0.9 m/s (Table 1) which capture the reconfiguration of foliated woody vegetation (e.g., Xavier 2009; Dittrich et al. 2012) and are typical for natural floodplain flows.

Table 1. Experimental conditions for the experiments A–D of natural woody species. All the experiments were conducted with foliated specimens, and experiments A and C additionally with the leafless stems. For the datasets B and D, the A_L/A_S value range and N refer to stand averages. Rel. sub = relative submergence, AG = *Alnus glutinosa*, BP = *Betula pendula*, PN = *Populus nigra*, SV = *Salix viminalis*, SxR = *Salix x rubens*. For more details, see Papers I and II.

Data-set & paper	Species	Config-uration	Rel. sub. (-)	No of plants per unit bed area (m^{-2})	Foliation level (%)	Stem drag measured	A_L/A_S (-)	mean velocity (m/s)	N
A, II	PN	single	1.0	-	100	yes	43–68	0.10–0.87	3
B, II	PN	stand	0.3, 0.7, 1.0	6, 11, 25	100	no	43–72	0.03–0.61	3–8
C, I	AG, BP, SV, SxR	single	1.0	-	25, 50, 75, 100	yes	6–33	0.20, 0.50, 0.80	4
D, I	AG, BP, SV, SxR	stand	1.0	11	100	no	28–40	0.05–0.84	6–8

In the experiments with the single twigs (Papers I and II), the plants were investigated either one at a time (dataset A) or four at a time (dataset C) to optimize both the time efficiency and control of the experimental conditions. As described in Paper I, the plants in the experiments C were positioned in a rectangular arrangement using the maximum possible longitudinal (1.2 m) and transverse (0.3 m) distances, which minimized the effect of the wake flows and ensured that the adjacent plants did not interfere with each other. The experi-

ments C consisted of measuring the drag forces of the foliated specimens (F_{tot}) at four foliation levels (25%–100%, see Table 1). Foliation level is defined as the share of the one-sided leaf area to that of the same specimen in the fully foliated condition, and the target foliation levels were achieved by successively removing the required number of leaves. To minimize the changes in the physical plant properties, the experiments with the foliated single specimens were accomplished within the day of the plant collection (experiments C) or by the end of the second day (A). For C, preliminary tests showed that the constant exposure to repeated cycles of increasing flow velocity decreased the drag of the specimens by an average of 4% within the measurement day. Within a day or two after finishing the experiments with the foliated plants, the specimens were tested in the defoliated condition to obtain the stem drag F_S (A and C).

In the experiments with the plant stands (B and D, Papers I and II), the drag forces were simultaneously measured for typically 6–8 specimens in each stand. However, only 3 specimens could be instrumented for the lowest plant density (6 plants/m^2). The plant stands were formed by positioning individual foliated specimens in a staggered pattern with the transverse and longitudinal spacing of either 0.2 m, 0.3 m, or 0.4 m (see Figure 7b). As explained in Papers I and II, the drag force measurement area was located in the middle of the 5 m long plant stand. To ensure a fully developed flow, the stands were preceded and followed by 6 m long vegetated areas consisting of flexible artificial plants. Each stand was examined at 4–9 mean flow velocities. The plant stand experiments were accomplished during the day of the plant collection (D), by the end of the second day (experiments with h/H=1.0 of B), or by the end of the third day (experiments with h/H=0.3 and 0.7 of B).

2.2 Field experiments in an environmental two-stage channel (III, IV)

2.2.1 The field site with differently vegetated sub-reaches

The investigated two-stage channel, Ritobäcken Brook, is located in Sipoo, Southern Finland (Figure 8, Papers III and IV). The Ritobäcken was channelized in the past to improve the drainage of the surrounding agricultural fields. The channel had since then lost some of its conveyance capacity, and the fields were frequently flooded. As an environmentally preferable alternative for enhancing the conveyance during high flows (see Section 1.2.3), a two-stage profile was designed by the Jami Aho engineering consultancy. The design and construction is documented in detail in Paper IV. The construction in February 2010 included excavating an 850 m long floodplain at the level of the estimated mean discharge. Figures 8a–b illustrate a cross-section that is representative of the 190 m long test reach on which the investigations focused. The cross-sections are comprised of the excavated bank, 2.6–3.4 m wide inner floodplain, 1.2 m wide floodplain–main channel interface, ~2 m wide main channel, and the unexcavated bank (hereafter the term floodplain includes both the inner floodplain and the interface). The longitudinal bed slope is 0.001–0.002, and the annual mean discharge at the downstream end of the

test reach was 0.12 m³/s. Agricultural fields comprise 13% of the 10 km² catchment area while the remainder is mainly forests and mires. The fields, channel margins and the transported suspended sediment are mainly composed of clay and silt.

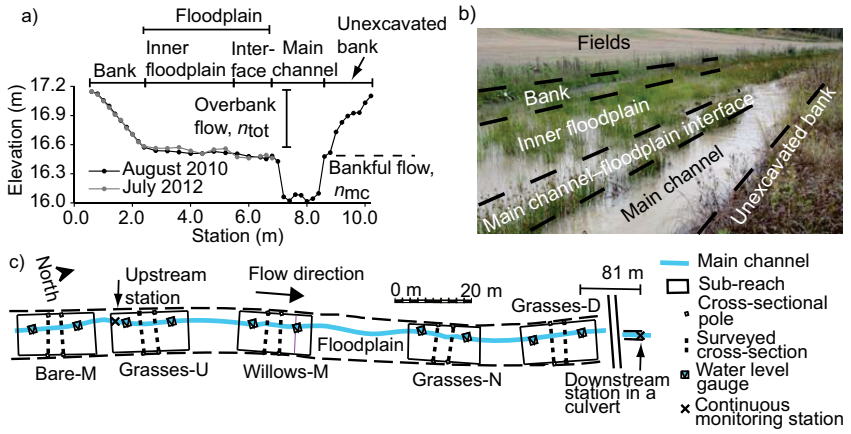

Figure 8. A representative two-stage cross-section with the surveyed geometry in 2010 and 2012 (a); the test reach at a low floodplain water depth (b); the field site with the monitoring infrastructure (c). (Paper III)

Five 20 m long sub-reaches differing in floodplain vegetation type were established within the 190 m long test reach in spring 2010 (Figure 8c). According to the description in Paper III, the sub-reaches Grasses-D and -U were sown with pasture grasses (mainly *Lolium perenne*), Grasses-N grew naturally established grasses, and Bare-M was intended to have bare soil. Willows-M was planted with cuttings of Common Osier (*Salix viminalis*) at 0.5 m x 0.5 m spacing. Willows-M and Bare-M also had sparse ~0.05 m high stubble of grass although the grassy floodplain and bank vegetation of these two sub-reaches was cut before the seasons when overbank flows occurred.

2.2.2 Monitoring of the flow, water levels and sediment processes

Monitoring was carried out both at the sub-reach and reach scales, as schematized in Figure 4. The sub-reach-scale investigations included manual water level readings, annual cross-sectional surveys, and grain size analyses, as detailed below and in Paper III, as well as the determination of the vegetation properties (see Section 2.3). Figure 9 conceptualizes the framework for the investigation of the vegetative flow resistance. Despite its empirical nature, the Manning coefficient (n) is still used in many practical applications, which warrants analyzing its dependence on the vegetative properties. The values of n were calculated (Eq. 1) from the energy slopes that were obtained at different flows from the manually gauged water levels at the upstream and downstream ends of each sub-reach (Paper III). The analyses included computing the Manning coefficient of the main channel at bankful flow (n_{mc}, Figure 8a), the bulk coefficient of the vegetated two-stage channel at overbank flows (n_{tot}), and the

coefficient of the two-stage channel when the floodplain was still completely bare (n_{base}). The resistance generated by the floodplain vegetation (n_{veg}) was determined following Eq. 3, with the corresponding formula shown in Figure 9. The floodplain vegetation strongly dominated the total flow resistance (Figure 9, Paper III), and thus the focus was on the estimation of n_{tot}. The mean errors in n were estimated to be 3% and 14% for the test reach and the sub-reaches, respectively.

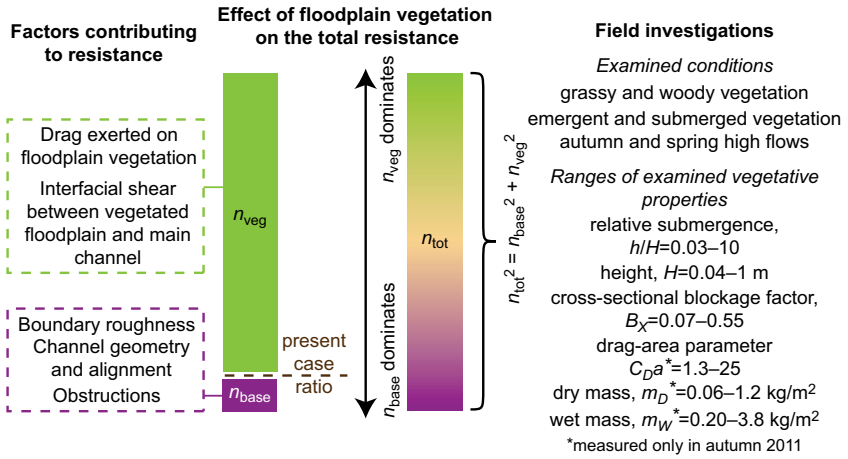

Figure 9. Conceptualization of the factors contributing to the total flow resistance (n_{tot}), and the vegetative study conditions. n_{veg} includes the factors related to floodplain vegetation while n_{base} lumps the remaining factors. In the present investigation, n_{veg} formed on average 89% of n_{tot}. (Paper III)

The cross-sectional surveys were carried out using a custom-built framework that allowed measuring the vertical distance from a reference level to the ground surface with a point gauge (Paper III). The cross-sectional geometry of the bank, inner floodplain and interface regions (see Figure 8a) was determined at 0.2–0.4 m horizontal intervals in two cross-sections located in the middle of each sub-reach (Figure 8c). The surveys were conducted in late summer when the soil was at its driest to minimize the impact of soil swelling on the ground elevation. The mean error in the reference level of a single cross-sectional measurement was approximately ± 6 mm.

As detailed in Paper III, the dispersed particle size distributions were determined with a laser-based analyzer for the top 5 cm of the bed sediment of the main channel and for the top 1 cm of the floodplain sediment from samples collected from the sub-reaches. The dispersed particle size distribution of the suspended sediment was analyzed from eight water samples with turbidities of 120–520 NTU. All samples were dispersed by exposing them to ultrasound for 5 minutes. Suspended sediment was analyzed also in the flocculated form without the ultrasound pre-treatment. Dispersed suspended sediment contained on average 40% of clay (<2 μm) and 60% of silt (2–60 μm). The top 5 cm of the bed sediment contained 11–14% of clay, and 83–97% was comprised of particles finer than 57 μm.

At the reach scale, the water level and turbidity were monitored at 5–15 min

intervals at two stations located at the upstream and downstream ends of the 190 m long test reach (Figure 8c, Papers III and IV). In addition, a weather station was established within the test reach to record meteorological variables, including rainfall. The continuous monitoring began in the autumn before the floodplain excavation, and the thesis uses the sensor data up to summer 2012. Following the description in Papers III and IV, the cross-sectional representativeness of the turbidity measurements was optimized by keeping the sensors at approximately mid-depth and by positioning them at locations where the flow was most efficiently laterally mixed: the upstream sensor was located in the main channel after the sub-reach with the bare floodplain while the downstream sensor was located in a culvert. As justified in Paper III, comparing the turbidity between the two stations allowed determining the timing of reach-scale net deposition and erosion events because the sediment was expected to be transported in suspended form.

The sensor turbidities and water levels were transformed into suspended sediment concentration (SSC) and discharge (Q), respectively, using rating curves (Papers III and IV). The stage–discharge curve was based on manual discharge measurements conducted in the culvert where the downstream station was located. The turbidity–SSC rating curves were constructed by analyzing SSC (g/m^3, EN 872:2005) from water samples collected at sensor turbidities T=20–700 NTU. Separate curves were fitted for GF-52 glass microfibre filters (nominal pore size 1.2 µm, SSC = 0.53T – 3; squared correlation coefficient r^2=0.92, probability p<0.001) and for Nuclepore track-etched polycarbonate membranes (0.4 µm, SSC = 0.59 T + *14*; r^2=0.92, p<0.001). SS loads (Q_S) were computed by multiplying SSC by the respective Q. Papers III and IV report the details on the handling of the sensor data. For analyzing the catchment-scale sediment transport (Paper IV), the seasonal loads were determined and sediment rating curves were fitted between Q and SSC or Q_S, and between the 3-hour changes in Q and the 3-hour changes in Q_S. The sediment rating curves were constructed separately for the autumn and snowmelt periods and for the rising and falling stages using power-type regressions (as reported in Paper IV) and linear regressions.

2.3 Examined vegetation properties (I–IV)

The vegetation properties used in the analyses illustrated in Figure 4 are summarized for the field investigation (see Section 2.2) in Figure 9. For the flume investigation (see Section 2.1), the properties compiled to Table 2 for the single plants at the foliation level of 100% (datasets A and C, Table 1) are representative of the properties of the plants in the stands, too. The flume plant stands (datasets B and D) exhibited foliage and stem reference areas per unit bed area of A_L/A_B=0.23–3.25 and A_S/A_B=0.008–0.056, respectively.

In the field investigation, the plant properties were determined by sampling the vegetation on the bank, inner floodplain, and interface (Figure 8a) annually in late summer, as detailed in Paper III. In the flume investigation, the properties were determined after the hydraulic experiments for those speci-

mens for which the drag forces had been measured (Papers I and II). For the twigs of the dataset C (Table 1), the properties were determined for each of the four foliation levels. For the partly submerged plants (dataset B), the areas below the plant height of 8 cm and 16 cm were considered for h/H=0.3 and h/H=0.7, respectively, which corresponded to the average water levels during these experiments.

Table 2. Foliage and stem properties of the 0.23 m tall single twigs of the datasets A and C (see Table 1) at the foliation level of 100% (standard deviation in parentheses, number of specimens *N* was three or four). AG = *Alnus glutinosa*, BP = *Betula pendula*, PN = *Populus nigra*, SV = *Salix viminalis*, SxR = *Salix x rubens*.

Species	A_L (cm^2)	$m_{F,D}$ (g)	$m_{F,W}$ (g)	$A_L/m_{F,D}$ (cm^2/g)	D_S (mm)	A_S (cm^2)	$A_{S,lat}$ (cm^2)
AG	345 (82)	1.2 (0.3)	5.3 (1.2)	288 (12)	4.6 (0.4)	10.5 (1.0)	11.2 (1.8)
BP	203 (32)	1.5 (0.2)	4.2 (0.6)	140 (6.7)	3.2 (0.8)	7.4 (1.8)	8.1 (1.3)
SV	370 (107)	2.7 (0.8)	9.9 (2.9)	135 (2.3)	5.2 (0.6)	11.9 (1.3)	10.6 (1.7)
SxR	323 (122)	2.3 (0.9)	8.5 (3.4)	139 (7.7)	5.5 (1.0)	12.6 (2.4)	13.6 (2.4)
PN	1190 (121)	-	-	117 (9.1)	7.3 (0.5)	16.7 (1.2)	20.2 (3.0)

The wet mass of grassy vegetation per unit bed area (m_W) and the foliage wet masses of woody plants ($m_{F,W}$) were measured after removing the excess water from plant surfaces. The dry mass of grassy vegetation per unit bed area (m_D) and the foliage dry masses of woody plants ($m_{F,D}$) were measured after drying the samples in an oven. In the flume investigation, the stem wet masses ($m_{S,W}$) and dry masses ($m_{S,D}$) of woody plants were obtained by weighing the entire specimen. In the field investigation, $m_{S,W}$ and $m_{S,D}$ were estimated by multiplying the stem volumes computed from measured stem diameters and heights by the bulk density determined from small stem samples.

The frontal projected stem areas (A_S) and lateral projected stem areas ($A_{S,lat}$) of woody plants were obtained by photographing the leafless stems or by computing the areas from the measured diameters and heights. The mean errors in A_S and $A_{S,\mathrm{lat}}$ were estimated to be approximately 10% for the flume investigation and somewhat higher for the field investigation. The leaf areas (A_L) of woody plants were determined from the scanned images of the leaves with an image analysis software. Additionally, the leaf-area-to-stem-area-ratio (A_L/A_S) and the dry specific leaf area ($A_L/m_{F,D}$) were computed. For grassy vegetation, the frontal area index aH was obtained from m_D using a fitted linear regression equation without intercept (Paper III):

$$aH = 6.3 m_D \tag{6}$$

where m_D has the units m²/kg (r^2=0.86). For literature comparisons, $C_D aH$ values were computed for the field data. For the grasses, C_D=1.0 was used as in e.g. Luhar et al. (2008) and Luhar and Nepf (2013) for similar plant morphology. This was justified because the grasses performed rather rigidly as the mean flow velocities within the stands were lower than ~0.05 m/s. For the

willows, $C_D aH$ was parameterized using Eq. 20 of the developed drag force model (see Section 3.2.1), with the parameter values for *S. viminalis* available from the flume investigation (see Table 3 in Section 3.2.2).

As explained in Papers I and II, the frontal projected areas of the foliated plants in still air ($A_{o,\mathrm{tot}}$) and under flow ($A_{P,\mathrm{tot}}$) were determined for three specimens in each examined stand of the flume dataset B. The frontal projected areas of the foliage under the flow ($A_{P,F}$) were determined for the datasets B and C at the foliation level of 100%. For this, each specimen was separately photographed from the downstream direction with a submersible camera, after which the areas were obtained with an image analysis software from the manually delineated contours of the plants. The mean errors in $A_{P,\mathrm{tot}}$ and $A_{P,F}$ resulting from inaccuracies in the estimation of the mass center were estimated to be approximately 10% while the error was higher for $A_{o,\mathrm{tot}}$ (see Paper II). The additional uncertainty caused by the movement of the plants under the flow action was assumed to have a minor effect on the mean intra-specific values used in the analyses.

Paper III provides additional details related to the field investigation, justifies the seasonal representativeness of the vegetation properties, and describes the estimation of the vegetation heights in the spring. In the hydraulic analyses of the field data, the spatially-averaged vegetation properties of each sub-reach and of the 190 m long test reach were used. For the sub-reaches, the cross-sectional vegetative blockage factor B_X (cf., Green 2006; Nikora et al. 2008) was computed for different water levels as $B_X = A_V/A_W$, where A_V is the wetted cross-sectional area covered by vegetation (see Figure 10). For the analysis of the mean annual deposition, the maximum inundated vegetation height, dry mass and $C_D aH$ were computed as a mean of the two-year data, assuming that the floodplain water depth of 0.5 m was representative of the maximum water levels.

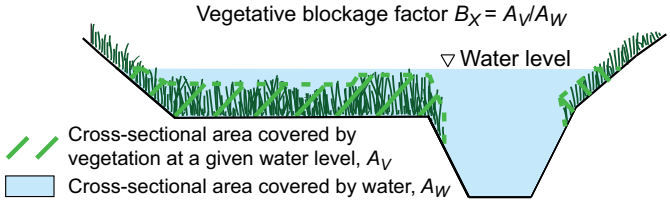

Figure 10. Determination of the cross-sectional vegetative blockage factor (B_X).

2.4 Computations and modeling (I–IV)

This section presents the equations and models that are used to describe how vegetation affects the drag, flow resistance, flow hydraulics and suspended sediment transport from the foliage and stem scale to the reach scale (Papers I–IV). The variables determined separately for the foliage and stem are denoted with the subscripts *F* and *S*, respectively, in this section and elsewhere in the thesis. The subscript tot refers to bulk analyses at the plant, sub-reach and reach scales. The data used in the analyses and modeling is illustrated in Fig-

ure 4. In the hydraulic analyses, the flow velocity was used as the independent variable because it is not solved how the Reynolds number should be determined for foliated plants (see e.g. Statzner et al. 2006).

The foliage drag (F_F) was determined from the directly measured drag forces of the foliated plant (F_{tot}) and defoliated stem (F_S) as

$$F_F = F_{tot} - F_S \tag{7}$$

Reconfiguration was quantified with the reconfiguration parameter χ (Vogel 1994; de Langre 2008) at the plant, foliage and stem scales as

$$F \propto u_m^{2+\chi} \tag{8}$$

For the emergent stands, the vegetative friction factor was computed from the spatially-averaged vegetative drag force (<F>) as (e.g., Aberle and Järvelä 2013)

$$f''_{tot} = \frac{8\langle F \rangle}{\rho u_m^2 A_B} \tag{9}$$

The plant-scale drag equation (Eq. 2) and the stand-scale flow resistance model for flexible foliated emergent vegetation (Eq. 10 below, Järvelä 2004) were used as the basis for developing the new flow resistance model (see Section 3.2).

$$f''_{tot} = 4\frac{A_L}{A_B} C_{D\chi,tot} \left(\frac{u_m}{u_\chi} \right)^{\chi_{tot}} \tag{10}$$

In Eq. 10, reconfiguration is expressed through the reconfiguration term $(u_m/u_\chi)^{\chi tot}$, where u_χ is the lowest velocity used in determining χ_{tot} (χ is equal to that in Eq. 8). $C_{D\chi,tot}$ is a drag coefficient that has a constant value at the considered velocity range (Järvelä 2004).

As described in Paper III, the dimensionless mean flow velocities within the floodplain vegetation (u^*_v) and in the unvegetated segment of the compound cross-section (u^*_o) were simulated at the sub-reach scale with an analytical two-layer model that was originally developed for patchy aquatic vegetation (Luhar and Nepf 2013):

$$u_0^* = \frac{u_0}{(gSH)^{1/2}} = \left[\frac{2P(1-B_X)}{C_f L_b + C_v L_v} \right]^{1/2} \tag{11}$$

$$u_v^* = \frac{u_v}{(gSH)^{1/2}} = \left[\frac{2PB_X + C_v L_v (u_0^*)^2}{C_D aPhB_X} \right]^{1/2} \tag{12}$$

where C_f and C_v are the drag coefficients describing the bed stress and the

shear stress at the interface between the vegetation and open water, respectively. L_b and L_v are the total lengths of the interfaces between the bed and unvegetated flow, and between the vegetation and open water, respectively. The shares of the discharge within the vegetation and in the unvegetated segment were obtained as $u^*_v B_X$ and $u^*_o(1-B_X)$, respectively. Following Luhar and Nepf (2013), it was assumed that for practical applications $C_f=C_v=C^*$, because Luhar and Nepf (2013) found similar ranges for C_f ($0.015 \leq C_f \leq 0.19$) and C_v ($0.005 \leq C_v \leq 0.21$) from literature data. C^* is thus a drag coefficient that lumps the bed and interfacial shear. For the compound channel geometry, C^* incorporates also the distinct roughness elements of the main channel.

C^* was obtained by calibrating a simplified momentum balance (Eq. 13 below; Luhar and Nepf 2013) against the experimentally determined reach-scale n_{tot}. The C^* value was derived at the lowest vegetative blockage factor separately for autumn (C^*=0.079, B_X=0.24) and spring (C^*=0.034, B_X=0.13) conditions. As justified in Paper III, Eq. 13 was applicable because the assumption of $L_b+L_v \approx P$ (Luhar and Nepf 2013) holds for the present two-stage geometry. Eq. 13 neglects the flow within the vegetation, which Luhar and Nepf (2013) justified for dense aquatic vegetation ($a \approx 100$ m^{-1}) up to $B_X \approx 0.7$, when u^*_v is an order of magnitude lower than u^*_o.

$$n_{tot}\left(\frac{g^{1/2}}{R^{1/6}}\right)=\left(\frac{C^*}{2}\right)^{1/2}\left(1-B_X\right)^{-3/2} \tag{13}$$

It follows that the general prerequisite for the validity of Eq. 13 is that $u^*_o(1-B_X) > \sim 0.8$. The test reach fulfilled this prerequisite in the spatially-averaged sense (see Section 3.3.1). The applicability of Eq. 13 for predicting the flow resistance was examined at the reach scale. The aim was to investigate how reliably n_{tot} values at larger blockages can be extrapolated from the known B_X and the seasonal C^* calibrated at the lowest B_X.

For the grassy sub-reaches, advection length scales (x_a) were computed with Eq. 14 (Zong and Nepf 2011) for sediment flocs of the measured size distribution (see Section 2.2.2) to determine whether the sub-reaches experienced limitations in the advective sediment supply:

$$x_a = u_v h / w_s \tag{14}$$

where w_s is the particle settling velocity. w_s was estimated from the relationship derived for cohesive suspended flocs of approximately similar size distribution as the present SS by Thonon et al. (2005): $w_s=2.7\times10^{-7}D^{1.57}$, where D is the floc diameter in µm and w_s has the unit m/s.

Statistical analyses were conducted at all scales, as detailed in Papers I–IV, using mainly SPSS Statistics 20.0.0–21.0.0 and Statistix 9.0. The goodness-of-fit was quantified using the root mean square error (RMSE), mean relative error, Nash–Sutcliffe efficiency (Nash and Sutcliffe 1970), correlation coefficient r, or the squared correlation coefficient r^2. The probability $p<0.05$ was considered as statistically significant.

3. Results

3.1 Flow resistance of natural woody plants (I, II)

3.1.1 Drag forces and frontal projected areas at the plant scale (II)

The flume datasets A–D (Table 1; Papers I and II) revealed how individual foliated plants interact with the flow. The processes and general trends were approximately similar for the five investigated woody species, and data of *P. nigra* (dataset B) is used in this sub-section as an overall illustration of the plant-scale drag and reconfiguration. Figure 11 shows the simultaneously measured drag forces of the individual specimens in the five experimental plant stands, i.e., at three relative submergences (h/H=0.3–1.0) and three spacings (0.2–0.4 m). The drag forces (F_{tot}) increased as a function of the mean flow velocity (u_m), but the drag differed between the individual twigs both within and between the stands. Generally, the drag forces increased with the increasing relative submergence and were the highest for the just submerged plants.

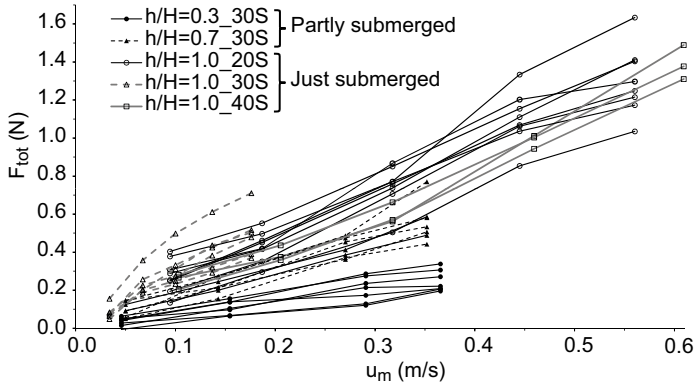

Figure 11. The simultaneously measured drag forces (F_{tot}) as a function of the mean flow velocity (u_m) for the individual *P. nigra* specimens examined in plant stands (dataset B, Table 1). In the legend, *h*/*H* refers to the level of the relative submergence and 20S–40S to the plant spacing of 0.2–0.4 m. See Paper II for a detailed description of the stands. (Paper II)

The frontal projected areas under flow ($A_{P,tot}$) strongly decreased with the increasing mean flow velocity (Figure 12). For instance, the frontal projected areas were on average 75% lower at u_m=0.6 m/s in comparison to the values

obtained in still air. The $A_{P,\mathrm{tot}}$ values exhibited intra-specific variability that was notable e.g. between the examined levels of relative submergence. Intra-specific variability was observed also in the slopes of the lines connecting the measured points (u_m, F_{tot}) in Figure 11, which indicated that each plant reconfigured in a unique pattern with respect to the mean velocity (the approach velocities of the individual specimens were not determined). On average, the reconfiguration parameter (exponent χ of Eq. 8) was -1.03 for the just submerged individuals (h/H=1.0) and -1.01 for the partly submerged individuals (h/H<1.0), revealing that the foliated plants experienced notable reconfiguration that was similar both in the emergent and just submerged conditions.

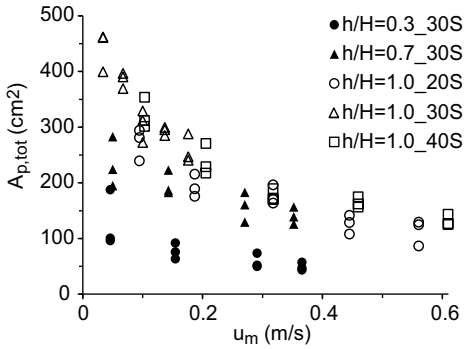

Figure 12. Measured frontal projected areas under flow ($A_{P,\mathrm{tot}}$) as a function of the mean flow velocity (u_m) for the foliated *P. nigra* twigs examined in plant stands. (Paper II)

Next, the focus is on examining whether the variability in the plant-scale drag force and frontal projected area could be explained by the four reference area definitions: the one-sided leaf area (A_L), still-air frontal projected area ($A_{o,\mathrm{tot}}$), frontal projected area under flow ($A_{P,\mathrm{tot}}$) and the leaf-area-to-stem-area ratio (A_L/A_S). As an example, Figure 13 shows the data normalized with A_L, revealing that the differences in the normalized values were low both between the three spacings (as shown by the low error bars for h/H=1.0 that lumps together the data at the three spacings) and the three levels of relative submergence. Normalizations with $A_{P,\mathrm{tot}}$ and $A_{o,\mathrm{tot}}$ as well as a more detailed description of the data are provided in Paper II (Figures 6 and 7 in Paper II). According to Welch's *t*-test for independent samples, $F_{\mathrm{tot}}/A_{P,\mathrm{tot}}$, F_{tot}/A_L and $A_{P,\mathrm{tot}}/A_L$ were mostly similar both for the two partly submerged conditions (h/H=0.3 and h/H=0.7) and for the partly submerged and just submerged conditions (see the statistically significant differences in Figure 13). Statistical tests were not conducted for normalizations with $A_{o,\mathrm{tot}}$ because $A_{o,\mathrm{tot}}$ values of three partly submerged specimens with a longitudinally bent stature were negatively biased as a result of problems in image scaling (see Paper II). Overall, normalizing drag with A_L, $A_{P,\mathrm{tot}}$ and $A_{o,\mathrm{tot}}$, and the frontal projected area with A_L and $A_{o,\mathrm{tot}}$, explained most of the observed variability in the measured values.

The reference area definitions $A_{P,\mathrm{tot}}$ and $A_{o,\mathrm{tot}}$ take into account both the foliage and stem while A_L considers only the foliage. Linear regression analyses between F_{tot}/A_L and A_L/A_S revealed that neglecting the stem had a notable im-

pact on the total drag when estimated with A_L only (Paper II). The regression equations obtained separately for the partly submerged and just submerged plant stands at each examined mean velocity had negative slopes, of which five out of nine were statistically significant (see Figure 8 in Paper II). On average, the F_{tot}/A_L values decreased by 30% at the investigated range of A_L/A_S (A_L/A_S=47–75 for the just submerged plants and A_L/A_S=28–70 for the partly submerged plants). The following sections analyze the detailed effect of A_L/A_S on the drag and reconfiguration (Section 3.1.2) and investigate the suitability of selected plant properties for the separate parameterization of the foliage and stem drag (Section 3.1.3).

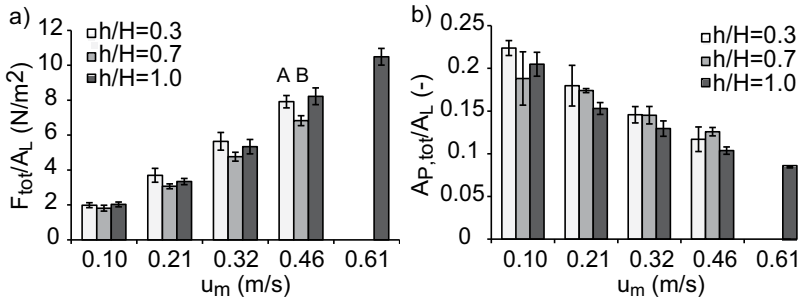

Figure 13. Drag forces F_{tot} (a) and frontal projected areas $A_{P,tot}$ (b) of the foliated *P. nigra* twigs normalized with the leaf area (A_L) at the mean flow velocities u_m=0.10–0.61 m/s. Error bars are ± 1 standard error. Letters A and B mark statistically significant differences (p<0.05) between the two partly submerged conditions (relative submergence h/H of 0.3 and 0.7); no differences were found between the partly and just submerged conditions. (Paper II)

3.1.2 Effect of the leaf-area-to-stem-area ratio (A_L/A_S) on the plant-scale drag and reconfiguration (I)

The flume dataset C (Table 1) obtained by systematically varying the foliation level of twigs of four natural woody species (see Section 2.1.2) allowed investigating how the leaf-area-to-stem-area ratio affected the plant-scale drag and reconfiguration (Paper I). The relative importance between the foliage drag (F_F) and stem drag (F_S) was described using the foliage–stem drag ratio (F_F/F_S). Linear regression analyses conducted separately for the four species at the three mean flow velocities revealed that F_F/F_S increased at an approximately similar rate as A_L/A_S. As an example, the marked increase in the foliage–stem drag ratio as a function of the leaf-area-to-stem-area ratio is illustrated in Figure 14a for u_m=0.5 m/s. The correlation between A_L/A_S and F_F/F_S was statistically significant for all three velocities and four species (r>0.66 and p<0.005) except for *Salix x rubens* at 0.2 m/s (for which r=0.44 and p=0.09). For all species, the foliage–stem drag ratio notably decreased with the increasing velocity (see Figure 5 in Paper I).

The effect of the foliage on the plant-scale reconfiguration is illustrated in Figure 14b. The reconfiguration parameter χ_{tot} (Eq. 8) decreased approximately linearly with the increasing A_L/A_S, and the correlation was statistically significant for each species (r=0.72–0.81 and p<0.003). The effect of A_L/A_S on χ_{tot} was 0.36–0.42 while the maximum inter-specific differences in χ_{tot} were

0.21.

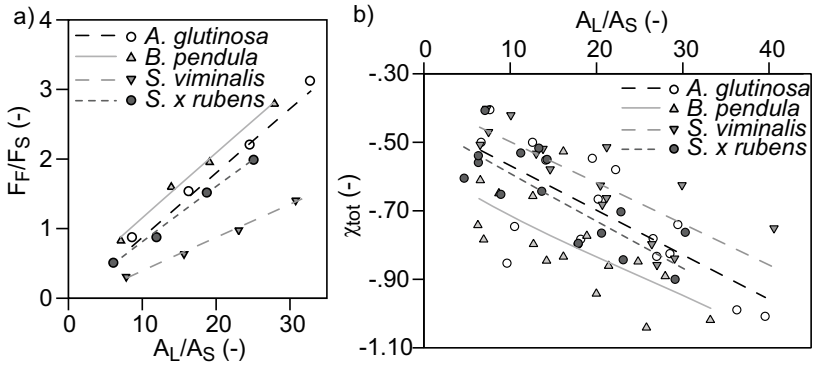

Figure 14. Linear regression between the mean leaf-area-to-stem-area ratio (A_L/A_S) and the mean foliage–stem drag ratio (F_F/F_S) at the mean flow velocity of 0.5 m/s (a), and between the leaf-area-to-stem-area ratio and the reconfiguration parameter χ_{tot} (b). (Paper I)

Next, the linear additivity of the foliage drag and stem drag is assessed to determine whether the total drag can be estimated using a linear superposition approach. Because the foliage drag was calculated with Eq. 7, the foliage drag and stem drag are linearly additive if F_F/A_L is similar at different foliation levels. Figure 15 shows F_F/A_L as a function of the foliation level for the four species of the dataset C. The mean (and maximum) deviations from the foliation-level-averaged F_F/A_L were 4% (maximum 9%) for *Alnus glutinosa*, 8% (18%) for *Betula pendula*, 3% (7%) for *Salix x rubens* and 16% (33%) for *Salix viminalis*. Linear regression analyses did not reveal any significant correlations between F_F/A_L and the foliation level for the four species and three velocities. According to the repeated measures analysis of variance (two-way ANOVA with the effects of the foliation level and velocity, followed by one-way ANOVA if significant interaction effects were detected) conducted separately for each species, F_F/A_L significantly differed between the foliation levels only for *B. pendula* at u_m=0.80 m/s (Figure 15b). These analyses indicated that the foliage drag and stem drag can be assumed to be approximately additive through linear superposition. This concept of linear superposition was used as a basis for the developed flow resistance model described in Section 3.2.

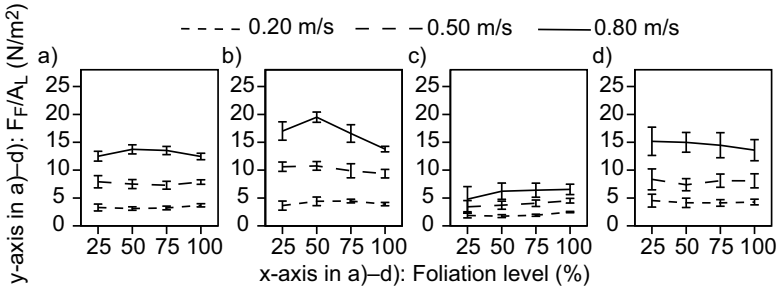

Figure 15. Foliage drag per leaf area (F_F/A_L) as a function of the foliation level at the mean flow velocities of 0.20 m/s, 0.50 m/s and 0.80 m/s for *A. glutinosa* (a), *B. pendula* (b), *S. viminalis* (c), and *S. x rubens* (d). Bars represent ± 1 standard error (N=4). (Paper I)

3.1.3 Drag and reconfiguration of the foliage and stem: plant properties for the parameterization (I, II)

The flume datasets A and C (Table 1) were used to analyze the drag and reconfiguration separately for the foliage and stem, and to examine the suitability of three foliage properties and two stem properties for estimating the drag. The accuracy and physical soundness of the plant properties as drag predictors were determined based on intra- and inter-specific coefficients of variation (c_v, standard deviation divided by the mean). The still-air frontal projected stem areas (A_S) produced on average 9% lower intra-specific c_v and 14% lower inter-specific c_v for the stem drag coefficient $C_{D,S}$ (computed with Eq. 2) as compared to the lateral projected stem areas ($A_{S,\mathrm{lat}}$). The foliage drag normalizations with the leaf area (A_L), foliage dry mass ($m_{F,D}$) and foliage wet mass ($m_{F,W}$) resulted in equal intra-specific c_v. However, the normalization with the leaf area resulted in 16% and 24% lower inter-specific c_v than the foliage wet mass and foliage dry mass, respectively. Thus, the plant properties most directly related to the foliage drag and stem drag were A_L and A_S, respectively, which were selected to be used in the subsequent analyses and in the developed flow resistance model (see Section 3.2).

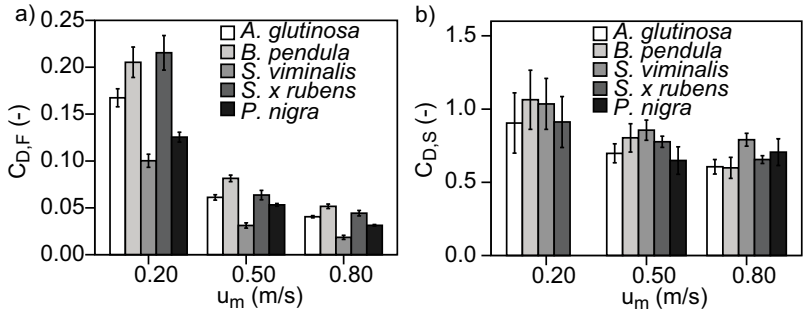

Figure 16. Foliage drag coefficients ($C_{D,F}$) computed using the leaf area as the reference area (a) and stem drag coefficients ($C_{D,S}$) computed using the still-air frontal projected stem area as the reference area (b) for the mean flow velocities u_m=0.20–0.80 m/s. (Paper I)

Examining the drag coefficients of the foliage ($C_{D,F}$, computed with Eq. 2 using A_L as the reference area) and stem as a function of the mean flow velocity revealed that both plant parts exhibited notable reconfiguration (Figure 16). Because of the reconfiguration, the stem drag coefficients reduced by an average of 32% and the foliage drag coefficients by an average of 77% between the velocities u_m=0.2 m/s and u_m=0.8 m/s. Similarly, the mean frontal projected areas of the foliage at u_m=0.8 m/s were 79–88% lower than the still-air values. At u_m=0.2 m/s, the frontal projected area of the foliage normalized with the leaf area ($A_{P,F}/A_L$) was 0.25 for *A. glutinosa*, 0.27 for *B. pendula*, 0.17 for *S. viminalis*, 0.24 for *Salix x rubens*, and 0.16 for *P. nigra*. The mean reconfiguration parameters of the foliage and stem (Eq. 8) ranged from -1.21 to -0.97 and from -0.32 to -0.20, respectively, for the five species (see Table 3 in Section 3.2.2). The marked differences in the drag coefficients (Figure 16) and reconfiguration parameters between the two plant parts implied that it is advantageous to separately consider the foliage and stem in hydraulic analyses.

3.2 Flow resistance model for woody vegetation based on the linear superposition of the foliage and stem drag (I, II)

3.2.1 Model structure (I)

The model is based on the assumption that the foliage drag (F_F) and stem drag (F_S) are linearly additive, which is justified by Figure 15 and the associated analyses in Section 3.1.2. A linear superposition approach has been used also by Yue et al. (2007) for corn and by Schnauder and Moggridge (2009) for deciduous woody species. In analogy to Eq. 4, the friction factor of an emergent stand of woody vegetation (f''_{tot}) can be expressed as a sum of the friction due to the foliage (f''_F) and the stem (f''_S):

$$f''_{tot} = f''_F + f''_S. \tag{15}$$

Modeling F_F and F_S, or f''_F and f''_S, requires taking into account the reconfiguration, which was found to importantly affect the drag coefficients of both the foliage and stem when constant, velocity-independent reference areas were used (Section 3.1.3). The reconfiguration is considered using a similar conceptual approach as in Eq. 10, i.e., through a reconfiguration term of the form of $(u_C/u_\chi)^\chi$, as detailed below. As opposed to using plant-scale bulk parameters of the foliated vegetation as in Eq. 10, the new model considers all the parameters separately for the foliage and stem (denoted with the subscripts F and S). With the reconfiguration term, the foliage and stem drag coefficients of Eq. 2 can be obtained for a given approach velocity u_C as

$$C_{D,F} = C_{D\chi,F}\left(\frac{u_C}{u_{\chi,F}}\right)^{\chi_F} \tag{16}$$

$$C_{D,S} = C_{D\chi,S}\left(\frac{u_C}{u_{\chi,S}}\right)^{\chi_S} \tag{17}$$

where $C_{D\chi,F}$ and $C_{D\chi,S}$ are coefficients that are constant at the whole examined velocity range (thus the subscript χ). $C_{D\chi,F}$ and $C_{D\chi,S}$ equal to $C_{D,F}$ and $C_{D,S}$ obtained with Eqs. 2 or 5 at the reference velocities $u_{\chi,F}$ and $u_{\chi,S}$, respectively. The reconfiguration parameters of the foliage and stem, χ_F and χ_S, describe the effect of the reconfiguration at u_C in relation to $u_{\chi,F}$ and $u_{\chi,S}$. $u_{\chi,F}$ and $u_{\chi,S}$ are thus scaling parameters that also serve to non-dimensionalize Eqs. 16–17. $u_{\chi,F}$ and $u_{\chi,S}$ should be low enough (of the order of 0.1–0.2 m/s) to adequately represent the effect of the reconfiguration on the drag coefficients. The values of the parameters χ_F, χ_S, $C_{D\chi,F}$ and $C_{D\chi,S}$ depend on the selected values of $u_{\chi,F}$ and $u_{\chi,S}$, and therefore values of all these six parameters need to be reported. The direct comparability of the values of $C_{D\chi,F}$, $C_{D\chi,S}$, χ_F, and χ_S requires $u_{\chi,F}$ and $u_{\chi,S}$ to be equal between the datasets (in this thesis, $u_{\chi,F}$=$u_{\chi,S}$=0.2 m/s).

The abundance of the foliage and stem are parameterized with the one-sided

leaf area (A_L) and the frontal projected stem area (A_S), respectively, as these were found to be the most suitable plant properties (see Section 3.1.3). Inserting Eqs. 16–17 into Eq. 2, the drag forces of a leafless plant and foliated plant can be expressed as

$$F_S = \frac{1}{2}\rho C_{D\chi,S}\left(\frac{u_C}{u_{\chi,S}}\right)^{\chi_S} A_S {u_C}^2 \tag{18}$$

$$F_{tot} = \frac{1}{2}\rho\left[C_{D\chi,F}\left(\frac{u_C}{u_{\chi,F}}\right)^{\chi_F} A_L + C_{D\chi,S}\left(\frac{u_C}{u_{\chi,S}}\right)^{\chi_S} A_S\right]{u_C}^2 \tag{19}$$

This is a conceptionally similar formulation for the drag force as that derived by Jalonen and Järvelä (2014) based on Paper I of this thesis. For a vertical layer having a thickness z, a leaf area density A_L/A_B, and a stem area density A_S/A_B, the drag–density parameter of woody vegetation can be written as

$$C_D a = \frac{A_L}{A_B z} C_{D\chi,F}\left(\frac{u_C}{u_{\chi,F}}\right)^{\chi_F} + \frac{A_S}{A_B z} C_{D\chi,S}\left(\frac{u_C}{u_{\chi,S}}\right)^{\chi_S} \tag{20}$$

For woody vegetation of the height H, the drag–area parameter is

$$C_D aH = \frac{A_L}{A_B} C_{D\chi,F}\left(\frac{u_C}{u_{\chi,F}}\right)^{\chi_F} + \frac{A_S}{A_B} C_{D\chi,S}\left(\frac{u_C}{u_{\chi,S}}\right)^{\chi_S} \tag{21}$$

Following Eq. 5, the friction factors of a leafless plant stand (f''_S) and foliated plant stand (f''_{tot}) can be expressed using the $C_D aH$ formulation of Eq. 21:

$$f''_S = 4\frac{A_S}{A_B} C_{D\chi,S}\left(\frac{u_C}{u_{\chi,S}}\right)^{\chi_S} \tag{22}$$

$$f''_{tot} = \frac{4}{A_B}\left[A_L C_{D\chi,F}\left(\frac{u_C}{u_{\chi,F}}\right)^{\chi_F} + A_S C_{D\chi,S}\left(\frac{u_C}{u_{\chi,S}}\right)^{\chi_S}\right] \tag{23}$$

The model (Eqs. 18–23) is primarily targeted for u_C of the order of 0.05–1 m/s, which are typical velocities for floodplains and river banks. When u_C approaches zero, the predicted values of F or f'' may have large errors because of the asymptotic nature of the reconfiguration term. Eqs. 18–19 can be applied to individual specimens in plant stands with $h/H \leq 1.0$ and to single plants using the depth-averaged mean flow velocity as u_C. Eqs. 22–23 can be directly used under emergent or just submerged conditions when vegetation fills the entire wetted area of the channel cross-section, in which case the cross-

sectional mean flow velocity can be used as u_C. In addition, the drag parameterizations (Eqs. 18–21) can be incorporated into hydraulic models simulating partly vegetated flows (see Section 4.4 for examples). The model applies to both leafless and foliated woody vegetation: for leafless vegetation, A_L=0 and the foliage drag component disappears from the equations. The model is applicable to both rigid and flexible leafless vegetation because it allows setting the desired value for the reconfiguration parameter of the stem. By setting χ_S=0, the reconfiguration term of the stem becomes 1, so that the formulations for the stem drag and resistance reduce to Eqs. 2 and 5, respectively. Section 3.2.2 shows that Eqs. 22–23 are valid for vegetation densities of A_L/A_B<3.2 and A_S/A_B<0.16 and for foliation levels of A_L/A_S<72.

In order to use the model for predicting the drag or flow resistance, the values of the foliage and stem drag parameters (χ_F, χ_S, $C_{D\chi,F}$ and $C_{D\chi,S}$ as well as the associated $u_{\chi,F}$ and $u_{\chi,S}$) need to be known. If no published parameter values exist for a given species, they can be either estimated based on values reported for similar species or derived from flume or field data, as described below and in Paper I. Deriving the values requires data on f'_S (or F_S) in leafless conditions and data on f'_{tot} (or F_{tot}) in foliated conditions at a few relevant values of u_C (the lowest values of u_C are used as $u_{\chi,F}$ and $u_{\chi,S}$). The associated A_L/A_B and A_S/A_B need to be measured. Recommendations for choosing u_C are provided in previous section and in Figure 25 of Section 4.4. First, the values of $C_{D\chi,S}$ and χ_S are determined by fitting Eq. 22 to the (f'_S , u_C) data points of the leafless condition. Second, the values of $C_{D\chi,F}$ and χ_F are obtained by fitting Eq. 23 to the (f'_{tot} , u_C) data points of the foliated condition using the previously determined values of $C_{D\chi,S}$ and χ_S. Alternatively, the parameter values can be derived from (F_S , u_C) and (F_{tot} , u_C) data using a similar fitting procedure with Eqs. 18–19. However, it is recommended that the drag forces of individual specimens are converted into the corresponding stand-scale friction factor with Eq. 9 for the derivation of the parameter values. When the drag coefficient and reconfiguration parameter are simultaneously derived, the parameters can be slightly inter-dependent. It is also possible to use procedures that first determine the reconfiguration parameters with Eq. (8) and then the drag coefficients. The physical factors affecting the parameter values are discussed in Section 4.2.

3.2.2 Parameter values and performance for natural plants (I, II)

In this section, the parameter values of the flow resistance model (Eqs. 18–23) are derived for the five presently examined species and the performance of the model is evaluated for twig- and sapling-sized vegetation. The parameter values were determined with SPSS Statistics from the datasets A (Table 1, N=3) and C (N=16, the single plant data from the four foliation levels were lumped together). The fitting procedure described in Section 3.2.1 was applied with u_m used as u_C and $u_{\chi,F}$=$u_{\chi,S}$=0.2 m/s. For *P. nigra*, the stem drag at u_m=0.20 m/s was estimated based on the mean $C_{D,S}$ of the other species. Table 3 reports the obtained parameter values of the model as well as those of Eq. 10 that were determined for reference.

Table 3. Parameter values for the use of Eqs. 18–23 and Eq. 10 ($u_{X,F}=u_{X,S}=u_X$=0.2 m/s).

Species	$C_{DX,F}$	X_F	$C_{DX,S}$	X_S	$C_{DX,\mathrm{tot}}$	X_{tot}
Alnus glutinosa (Common Alder)	0.18	−1.11	0.89	−0.27	0.21	−0.89
Betula pendula (Silver Birch)	0.20	−1.06	1.02	−0.32	0.26	−0.86
Populus nigra (Black Poplar)	0.13	−0.97	0.95	−0.27	0.14	−0.87
Salix viminalis (Common Osier)	0.11	−1.21	1.03	−0.20	0.15	−0.77
Salix x rubens (hybrid Crack Willow)	0.19	−1.21	0.96	−0.25	0.24	−0.90

Table 4. Key information and performance of the developed model (Eqs. 18–23) for the independent datasets at A_L/A_S=6–72.

Dataset	mean velocity (m/s)	height (m)	A_L/A_B (-)	A_S/A_B (-)	mean error in f''_S	mean error in f''_{tot}
Alnus glutinosa (dataset D)	0.05–0.84	0.23	0.78	0.021	-	10%
Betula pendula (dataset D)	0.05–0.81	0.23	0.41	0.016	-	17%
Populus nigra (dataset B)	0.03–0.61	0.23	0.46–3.25	0.011–0.056	-	17%
Salix viminalis (dataset D)	0.05–0.78	0.23	0.32	0.008	-	26%
Salix x rubens (dataset D)	0.05–0.80	0.23	0.23	0.009	-	23%
Alnus glutinosa, 3 single specimens (Xavier 2009) [a]	0.12–1.5	1.8–2.5	0.73	0.144	15%	11%
Salix caprea (Järvelä 2002a, 2002b)	0.07–0.45	0.7	3.2	0.052–0.157	30%	20%
Alnus glutinosa, 6 single specimens (Jalonen and Järvelä 2014) [b]	0.1–1.0	1.0–3.1	-	-	12%	31%
Betula pendula, 3 single specimens (Jalonen and Järvelä 2014) [b]	0.1–1.0	0.9–2.7	-	-	15%	28%

[a] Those three specimens for which A_L data existed and A_S could be estimated based on the $A_S/m_{S,D}$ value of one specimen. These three specimens were considered to form a plant stand with a spacing of 1 m.

[b] The drag forces of the individual specimens were predicted, and therefore A_L/A_B and A_S/A_B are not reported (A_L/A_S=12–33 for *A. glutinosa* and A_L/A_S=13–28 for *B. pendula*).

The model was tested against independent datasets that were available at the time of writing the compilation part of the thesis and that contained the required vegetation data (the leaf and stem areas). Table 4 shows the key information of the five datasets which include the twig stand data (datasets B and D, Table 1) and literature data on sapling-sized woody plants investigated in plant stands (Järvelä 2002a, 2002b) and as single specimens (Xavier 2009; Dittrich et al. 2012; Jalonen and Järvelä 2014). Jalonen and Järvelä (2014) tested the present model with their data, but the validation is also shown here. The drag forces and friction factors were estimated with Eqs. 19 and 23 for both the leafless and foliated conditions, using u_m as u_C and applying the independently obtained parameter values of the corresponding species from Table 3. For *Salix caprea* of Järvelä (2002a, 2002b), the parameter values of *Salix x rubens* were used because these species are of the same genus and have the most similar leaf shape. Figure 17a shows the experimentally obtained and

predicted f''_{tot} for the datasets B and D. The performance of the model for the literature data is shown in Figure 17b for those datasets for which the friction factor was predicted and in Figure 18 for those datasets for which the drag forces were predicted. The mean prediction errors in f''_S and f''_{tot} are reported in Table 4 for all the datasets.

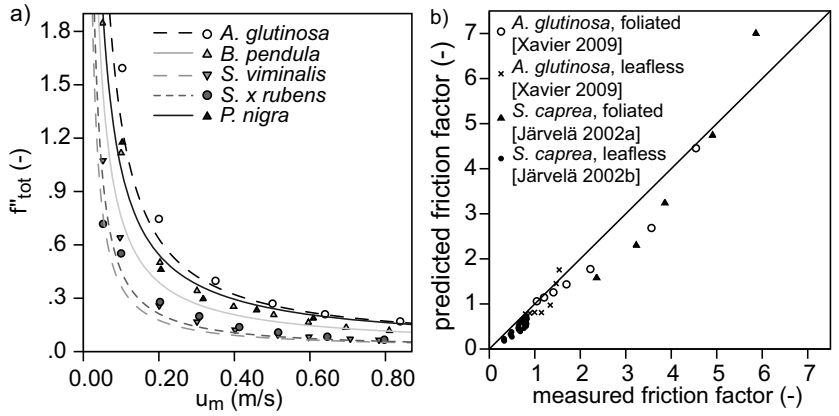

Figure 17. Performance of the model (Eq. 23) for predicting the friction factors of the twigs (a) and saplings (b). In (a), markers denote the measured friction factor (f''_{tot}) as a function of the mean flow velocity (u_m) while lines show the predicted values. See Table 3 for the parameter values used and Table 4 for the plant stand details. (Paper I)

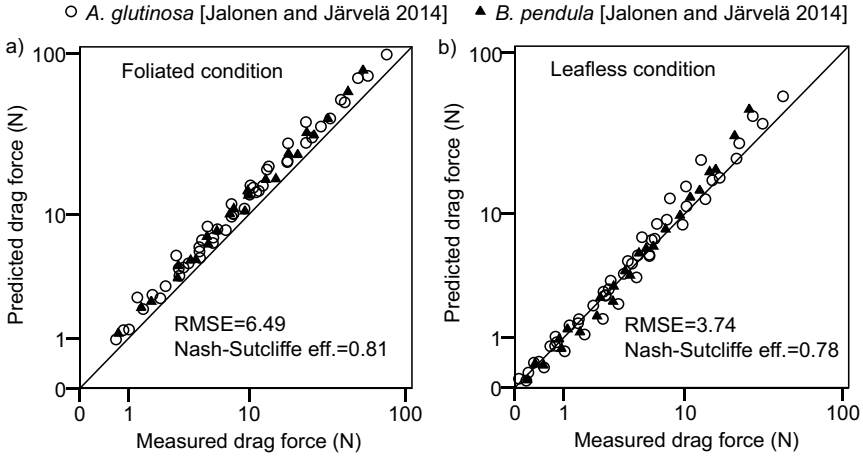

Figure 18. Performance of the model (Eq. 19) for predicting the drag forces of the saplings of Jalonen and Järvelä (2014) at u_m=0.1–1.0 m/s in the foliated condition (a) and in the leafless condition (b). See Table 3 for the parameter values used and Table 4 for the plant details.

The sensitivity of the model to the parameters can be illustrated by interspecific comparisons. Generally, the reconfiguration parameters (χ_F and χ_S) determine the shape of the f–u_C curve while the products of the drag coefficient and reference area for the foliage ($C_{D\chi,F}\,A_L/A_B$) and stem ($C_{D\chi,S}\,A_S/A_B$) determine the position of the curve on the y-axis. As an example, *S. x rubens* has a similar χ_F but a more negative χ_S than *S. viminalis* (Table 3), and there-

fore the model predicts greater total reconfiguration for *S. x rubens*. This is illustrated by *S. x rubens* having a stronger decrease in $f"_{tot}$ between u_m=0.2 m/s and u_m=0.8 m/s as compared to *S. viminalis* (Figure 17a). Further, A_L/A_B and A_S/A_B of *S. x rubens* are less than half of those of *A. glutinosa* (Table 4) while the drag coefficients of the two species are almost similar (Table 3), and thus the model predicts that the magnitude of the friction factor is considerably higher for *A. glutinosa*. This is illustrated by the fact that the f–u_C curve of *A. glutinosa* is constantly above that of *S. x rubens* in Figure 17a.

3.3 Effect of floodplain vegetation on the flow in the two-stage channel (III)

3.3.1 Dependence of flow hydraulics on vegetative properties

The field data collected from the five differently vegetated sub-reaches of the two-stage channel contained a representative range of different flow and vegetative conditions. Computed with Eq. 1, the values of the Manning resistance coefficient of the main channel (n_{mc}) were 0.035–0.154, showing variation between the seasons and sub-reaches (see Figure 3a in Paper III). The bulk Manning coefficient at overbank conditions (n_{tot}) was 0.035–0.08 in spring 2011, 0.038–0.155 in autumn 2011, and 0.027–0.115 in spring 2012. The corresponding relative submergences (h/H) on the floodplain were 0.05–0.49 for the Willows-M sub-reach and 0.03–2.8 for the grassy sub-reaches. The resistance coefficient of the unvegetated two-stage channel (n_{base}, see Figure 9) was 0.027–0.037, averaging 0.029, at conditions ranging from low to almost full submergence of the floodplain. Floodplain vegetation generated on average 89% of the total flow resistance (Paper III), and thus n_{tot} may be used instead of methods based on partitioning the cross-section. The high vegetative resistance suppressed the impacts of the relative depth (the water depth on the floodplain divided by total water depth) on the total flow resistance (e.g., Knight and Shiono 1996).

Figure 19 shows n_{tot} as a function of the three investigated vegetative properties. Excluding the lowest blockages, n_{tot} exhibited a strong increase with the cross-sectional vegetative blockage factor B_X (r=0.78, p<0.001 for B_X>0.2; Figure 19c). Exponential regressions for the different sub-reaches revealed that the increase in n_{tot} with B_X was similar for the three grassy sub-reaches but markedly lower for the leafless and foliated willows. The grasses did not exhibit notable differences in the n_{tot}–B_X relationship between the seasons or between the emergent (h/H<1.0) and submerged (h/H>1.0) conditions. By contrast, the differences in the linear regressions in Figures 19a–b revealed that the overall dependence of n_{tot} on the inundated dry vegetation mass and inundated wet vegetation mass was weaker than for B_X even though the data in Figures 19a–b represented a single season.

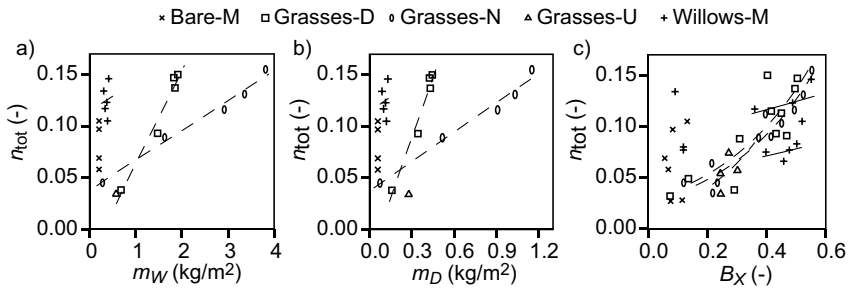

Figure 19. The Manning resistance coefficient at overbank flows (n_{tot}) as a function of inundated wet vegetation mass m_W (a), inundated dry vegetation mass m_D (b), and cross-sectional vegetative blockage factor B_X with regressions for B_X>0.2 (c). The lines denote exponential and linear regressions fitted separately for each sub-reach. In (c), the lower regression of Willows-M is for the leafless condition and the upper for the foliated condition. (Paper III)

Figure 20 presents the autumn 2011 values of the drag–density parameter (C_Da). C_Da is needed for computing the flow velocities within the vegetation and for determining whether the flow resistance of a partly vegetated channel can be modeled with Eq. 13. Figure 20 revealed that the floodplain vegetation was high and dense in the grassy sub-reaches, high but fairly sparse in Willows-M, and very low in Bare-M. With frontal area index (aH) being linearly dependent on the dry mass (Eq. 6), the differences in the C_Da values between Grasses-N and -D revealed that a certain inundated mass corresponded to different height and blockage factor in these sub-reaches, which explained the variation between their regressions in Figures 19a–b. Generally, the C_Da values of the grassy sub-reaches were an order of magnitude higher than those of Willows-M in the layers above the grassy stubble (h>0.05 m).

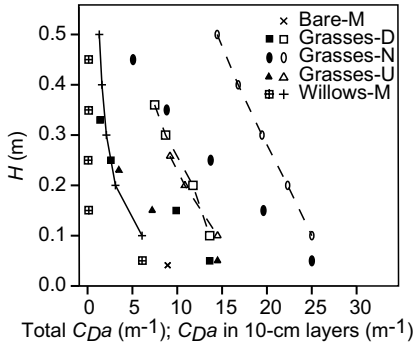

Figure 20. Total values of the drag–density parameter C_Da (markers connected with lines) and values of the C_Da in 10-cm layers (filled markers without lines) as a function of the vegetation height (H) in autumn 2011. (Paper III)

The computed mean flow velocities within the vegetation (u^*_v in Eq. 12) were an order of magnitude lower than those of the unvegetated segment of the cross-section (u^*_o in Eq. 11) for the grassy sub-reaches. By contrast, u^*_v was of the same order of magnitude as u^*_o for the willows. Thus, the sudden reduction in C_Da at the Willows-M and Bare-M sub-reaches (Figure 20) enabled diverging flows from the main channel to the floodplain, which was also visu-

ally evident during field visits. The computed share of the discharge within the vegetation was on average 8% of the total for the grassy sub-reaches and 42% for the willows during the measured conditions in autumn 2011. This difference was likely higher in the spring when the grasses were bent and the willows leafless. Thus, the grassy sub-reaches fulfilled the prerequisite for Eq. 13 which states that B_X is the only vegetation parameter needed to determine n_{tot} when $C_D a$ is high enough, i.e., when the share of the discharge within the vegetation is less than 20% of the total. By contrast, Figure 19c and the computed share of the discharge within the willows indicated that n_{tot} depended on both parameters $C_D a$ and B_X for the sparse willows. The low increase in n_{tot} with B_X for the willows (Figure 19c) was attributed to their low $C_D a$ values.

At low values of the blockage factor (B_X=0–0.2), large scatter was found in n_{tot} (Figure 19c). Because the relative errors in n_{tot} increased with the decreasing water surface slope (i.e., with the decreasing B_X), the scatter was partly caused by errors in the water level readings. In addition, the scatter reflected the differences in the main channel flow resistance between the seasons and the sub-reaches, with n_{tot} strongly depending on n_{mc} at B_X=0–0.2 (r=0.70, p =0.024).

3.3.2 Modeling the total flow resistance

Figure 21 shows the experimentally determined (Eq. 1) and modeled (Eq. 13) bulk resistance coefficient (n_{tot}) of the 190 m long test reach. In the four modeled seasons, the inundated vegetation height and cross-sectional vegetative blockage factor exhibited the spatially-averaged ranges of H=0.07–0.55 m and B_X=0.15–0.53. The water level ranged at h=0.1–0.7 m and the relative submergence reached values up to h/H=3.9. As reported in Paper III, comparing the modeled n_{tot} to the experimentally determined values resulted in the Nash–Sutcliffe efficiency coefficient of 0.71 and in the root mean squared error of 0.018. The mean relative error in the predicted n_{tot} was 17% in both autumns, 6% in spring 2011, and 15% in spring 2012. When applying Eq. 13, the values of the bulk drag coefficient (C^*) calibrated at the lowest B_X in spring 2011 (C^*=0.034) and autumn 2010 (C^*=0.079) were used in the other years, as well. The seasonal difference in C^* was mainly attributed to the seasonal variation in the main channel vegetation that was not included in the determination of B_X. In the test reach, approximately 90% of the floodplain area grew dense grassy vegetation, and the modeled share of the discharge in the unvegetated segment of the cross-section averaged 92% for the grassy sub-reaches (see Section 3.3.1). Thus, the test reach fulfilled the prerequisite of Eq. 13, i.e., the spatially-averaged discharge in the unvegetated segment was more than 80% of the total discharge.

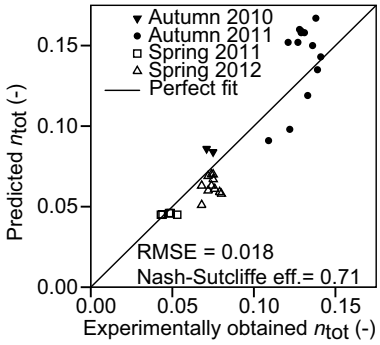

Figure 21. Manning resistance coefficient at overbank flows (n_{tot}) as experimentally obtained (Eq. 1) and as predicted with Eq. 13. (Paper III)

3.4 Effect of floodplain vegetation on the erosion and deposition of cohesive matter (III)

The cross-sectional data collected from the differently vegetated sub-reaches revealed that the mean annual net deposition exhibited a positive relationship with both the maximum inundated vegetation height and dry mass (Figure 22). The correlation was fairly strong (r=0.54–0.74, p=0.017–0.11) for the three cross-sectional parts, except for the dry mass on the inner floodplain (r=0.18, p=0.62). The mean difference in the net deposition between the two examined cross-sections of each sub-reach (7 mm/a) was expected to result mostly from measurement errors. Thus, the following analyses use the average net deposition of each sub-reach. Based on the average values, net erosion occurred in all cross-sectional parts of the sub-reach Bare-M (with the drag–area parameter having a two-year mean value of C_DaH=0.19) and deposition dominated in all parts of the grassy sub-reaches (C_DaH=1.9–4.9). Willows-M (C_DaH=0.38) experienced both net deposition and erosion. The matter deposited on the floodplain had a notable fraction of clay (17%), and 91% of the deposits consisted of particles finer than 58 μm.

The length scales of longitudinal advection calculated with Eq. 14 revealed that the increasing distance to the nearest upstream suspended sediment (SS) replenishment point (i.e., a sub-reach allowing efficient advection from the main channel to the floodplain) decreased the suspended sediment load conveyed on the inner floodplain. The sub-reaches Bare-M and Willows-M were considered as SS replenishment points, because the diverging flows from the main channel onto the floodplain (see Section 3.3.1) were assumed to replenish the SS stock on the inner floodplain. As an example, computations using the representative conditions of u_v=0.01 m/s and H=0.2 m showed that the largest 17–19% of the SS flocs conveyed by the longitudinal advection were deposited before the sub-reaches Grasses-N and -D having the distances of 39 m and 73 m, respectively, to the SS replenishment point (in Willows-M, see Figure 8c). The corresponding value was 3% for Grasses-U that had a shorter distance of 15 m to the SS replenishment point (in Bare-M). Figures 22b and e revealed that the increasing distance from the SS replenishment point resulted

in more negative deviations from the linear regression lines for the inner floodplain: the average deposition was higher than predicted by the regression equations in Grasses-U (distance of 15 m), equal in Grasses-N (39 m), and lower than predicted in Grasses-D (73 m). In Grasses-N and -D, the average annual deposition was 8 mm or 64% lower on the inner floodplain compared to the interface although the vegetation properties differed by less than 20% between these cross-sectional parts.

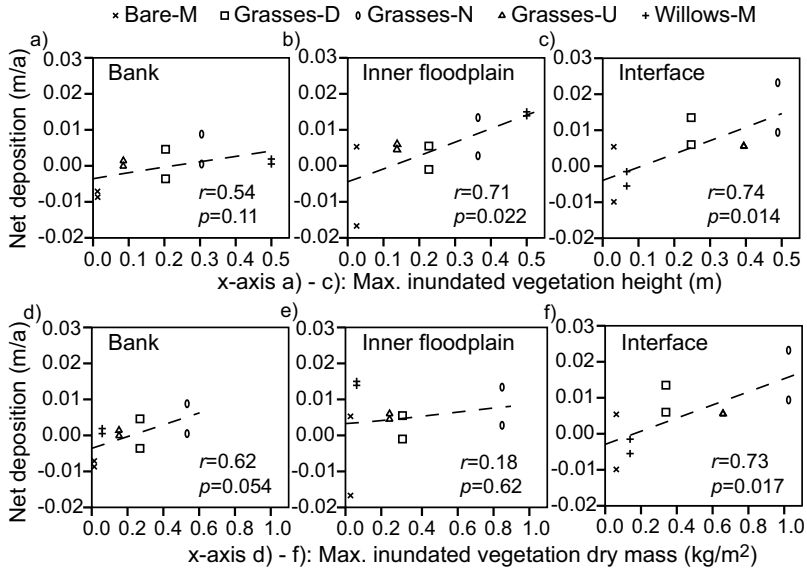

Figure 22. Two-year net deposition (negative values denote net erosion) in the five sub-reaches as a function of the maximum inundated vegetation height (a–c) and maximum inundated dry mass (d–f) for the excavated bank, inner floodplain and the main channel–floodplain interface. (Paper III)

3.5 Cohesive sediment transport in the two-stage channel: catchment-scale perspective (III, IV)

To provide a general picture of the suspended sediment transport, Figure 23 shows the discharge and suspended sediment concentration (SSC) in autumn 2009 and spring 2010 as measured at the downstream end of the test reach (see Figure 8). Although data in Figure 23 were collected before the floodplain vegetation was established, the measurements were representative of the catchment-scale processes and seasonality occurring in the following years. Between autumn 2009 and summer 2012, SSC peaked to approximately 100–500 g/m^3 (as measured with the 1.2 µm filters) during moderate to high flow events generated by rainfall, and to a maximum of ~80 g/m^3 during high discharges caused by the snowmelt. After the rain events, SSC declined to the background concentration that ranged at 5–20 g/m^3 between autumn 2009 and summer 2012.

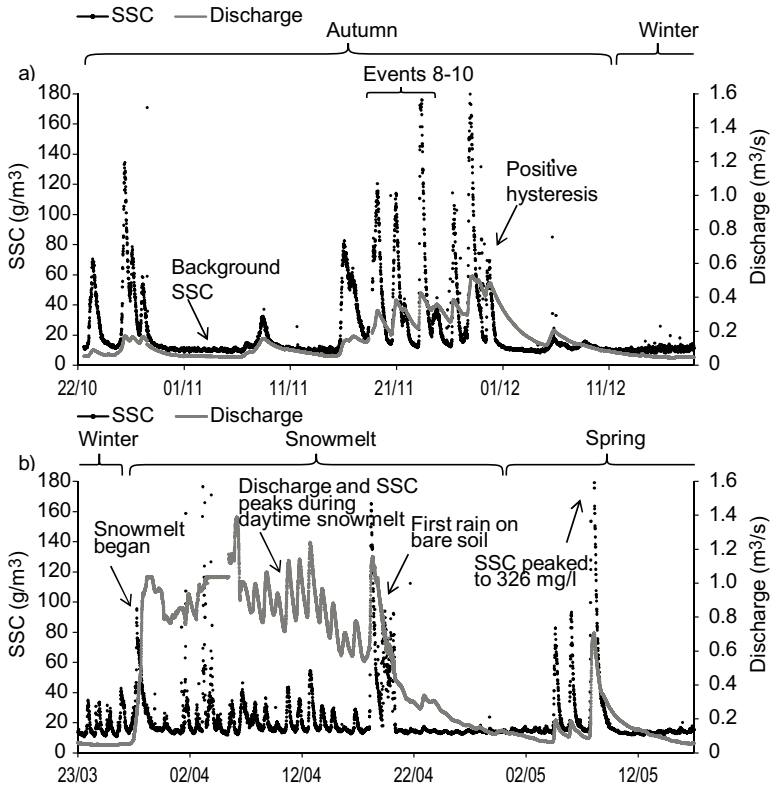

Figure 23. Suspended sediment concentration (SSC) and discharge in autumn 2009 (a) and spring 2010 (b) as measured at 5–15 min intervals at the downstream monitoring station. (Paper IV)

Analyzing the seasonal mean values of the discharge (Q), SSC, and SS load (Q_S) from autumn 2009 to the end of summer 2010 (Paper IV) revealed that the 1 month long snowmelt period produced the highest daily SS loads (0.15 t/d/km^2). The second highest daily loads were generated by the 2 months long autumn period (0.05 t/d/km^2). The differences in the seasonal mean SSC were appreciably lower, varying from 14 g/m^3 in winter to 25 g/m^3 in autumn (Table I in Paper IV). Thus, the differences in the average seasonal loads were mainly caused by the seasonal differences in discharge. When the seasonal sediment rating curves were compared between the three variable pairs (Q–SSC, Q–Q_S, and 3-hour changes in Q – 3-hour changes in Q_S), Q–SSC was found not to exhibit the strongest correlation in any case. Comparing the two other variable pairs, the highest correlation coefficients were in five out of six cases obtained for the 3-hour changes in Q – 3-hour changes in Q_S for the rising stage, while both performed best in three cases out of six for the falling stage (see Table 2 in Paper IV for the power-type curves).

SSC was observed to decline towards the background concentration after the rain events although the discharge remained high, as is evident e.g. in the data from November 2009 (Figure 23a). For a certain discharge, SSC was typically higher during the rising stages compared to the falling stages, as illustrated by Figure 24 for three consecutive rain events in November 2009 (the events 8–

10 marked in Figure 23a). During these events, SSC rapidly decreased in the falling stage but reached again higher values in the immediately following rising stage generated by the next rain event. This positive hysteresis was common in later years, as well.

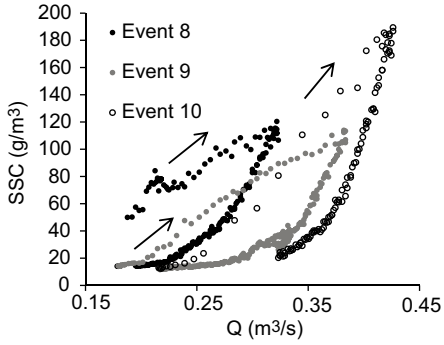

Figure 24. Suspended sediment concentration (SSC) as a function of the discharge (*Q*) during three consecutive flow events 8–10. Arrows show the direction of the hysteresis. (Paper IV)

In the first year of the monitoring of the differently vegetated sub-reaches (from summer 2010 to summer 2011), the values of the annual mean SSC were 41 g/m^3 with the 0.4 μm filter and 21 g/m^3 with the 1.2 μm filter while the annual mean *Q* was 0.08 m^3/s. In the second year, the corresponding values were 54 g/m^3 and 34 g/m^3, respectively, for the mean *Q* of 0.16 m^3/s (Paper III). Compared to the spatially-averaged net deposition of 5.4 kg/m^2/a computed from the cross-sectional measurements (Section 3.4), the 190 m long vegetated floodplain trapped 3.4–5.5% of the annual SS load depending on the considered filter. According to the particle size analyses, the D_{10}–D_{90} grain sizes of the suspended sediment were 2–5 times higher in the flocculated compared to the dispersed form.

The shares of the discharge and SS load transported during overbank flows amounted to 59% and 69–78%, respectively, of the total in the first, drier year, and to 75% and 88–92%, respectively, in the second, wetter year. Comparing SSC between the two monitoring stations showed that the two-stage test reach underwent net deposition during the two-year period. Deposition typically occurred during rainfall-induced overbank flows in the autumn and spring, mainly at SSC=100–500 g/m^3 although events with such a high concentration covered only 2% of the time.

4. Discussion

4.1 Flow–vegetation interaction of natural plants

This section presents the most important new findings of the thesis concerning the interactions between flowing water and riparian vegetation. The findings are also discussed in a wider context, pointing at how they can contribute to the general understanding of the flow–plant interactions, where the interest ranges from aquatic to riparian and terrestrial species and from water to air flows.

One of the findings of this thesis is the key role of the leaf-area-to-stem-area ratio (A_L/A_S) in governing the drag and reconfiguration of foliated woody vegetation. The reconfiguration systematically increased with the increasing A_L/A_S (Figure 14b) because reconfiguration was greater for the foliage compared to the stem (see Table 3). In addition, A_L/A_S controlled the share of the foliage to the total drag (as revealed by the foliage–stem drag ratio F_F/F_S), and thus this detailed investigation confirmed the tentative observations of Wilson et al. (2008) and Tanaka et al. (2011). The presented findings regarding A_L/A_S are expected to apply at least qualitatively also for sapling-sized vegetation because the foliage was tested at real scale and because the satisfactory results of the flow resistance modeling for the leafless saplings (Section 3.2.2) indicated that the stems of twigs and saplings behave fairly similarly. Thus, the effects of A_L/A_S may to some degree explain the marked intra-specific variability that could not be related to other plant properties in the studies of woody saplings by e.g. Rudnicki et al. (2004), Vollsinger et al. (2005), Xavier (2009), and Whittaker et al. (2013). For instance, the fact observed by Aberle and Järvelä (2013) that the *A. glutinosa* saplings of Dittrich et al. (2012) had a notably lower share of foliage drag than the present *A. glutinosa* twigs can be explained by the lower leaf-area-to-stem-area ratio of the saplings: the mean foliage–stem drag ratios of the saplings having an estimated mean A_L/A_S=6 (Table 4) were in close agreement with the values extrapolated from the relationships between A_L/A_S and F_F/F_S obtained for the twigs (Figure 14a as well as Figure 5 in Paper I).

The strong impact of the foliage on the total drag indicated that plant-scale bulk properties that are mainly controlled by the stem are not physically representative for characterizing foliated plants. As an example, the bulk Young's modulus and flexural rigidity are the key properties for governing the reconfiguration of flexible elements simpler than foliated plants (e.g., Gosselin et al.,

2010; Luhar and Nepf, 2013) and are typically used to characterize woody saplings (e.g., Xavier 2009; Stone et al. 2013; Whittaker et al. 2013). However, these plant-scale bulk parameters do not adequately reflect the effect of the foliage on the reconfiguration. This reasoning is likely one explanation for the finding of Butler et al. (2012) that the reconfiguration (which they refer to as streamlining efficacy) of foliated woody species correlates poorly with their bulk flexural rigidity and Young's modulus. This thesis showed that even at the inter-specific level, the reconfiguration of the twigs was primarily explained by A_L/A_S (see Figure 14) while the inter-specific variation in the reconfiguration parameters of the foliage and stem (χ_F and χ_S, see Table 3) was of minor importance. Thus, A_L/A_S may provide improved explanatory power for the inter-specific differences in the drag and reconfiguration reported for foliated woody plants e.g. by Vollsinger et al. (2005), Butler et al. (2012) and Whittaker et al. (2013). The new findings related to A_L/A_S can also apply to other types of bending plants (sensu Nikora et al. 2010), such as coniferous woody species or cereal crops that have parts with distinctly different biomechanical properties. In fact, the explicit parameterization of the foliage and stem improved the LES prediction of turbulence within corn stands compared to the conventional approach of horizontally uniform drag distribution (Yue et al. 2007). As even highly flexible aquatic species, such as *Ranunculus* spp, *Callitriche* spp and *Glyceria fluitans*, can have differences in the drag, reconfiguration, and biomechanical properties between the foliage and stem (e.g., Figure 2 in Bal et al. 2011; Albayrak et al. 2014), it could be advantageous to consider a parameter such as A_L/A_S in studies with tensile plants, as well.

The second important new finding relates to the possibility of using the linear superposition of the foliage drag and stem drag in the estimation of the total drag. The conducted in-depth investigation confirmed the linear additivity at the foliage scale (i.e., with the leaves naturally attached to the stem) by showing that no inter-specifically systematic differences existed in the foliage drag between foliation levels ranging from sparse (A_L/A_S=6–11) to dense (A_L/A_S=26–33, see Section 3.1.2). Differences in the drag between dense and sparse foliation have been earlier investigated at the leaf scale by Vogel (1989), who found that the drag per leaf area is typically up to half lower for leaf clusters compared to single leaves. The present twigs mainly consisted of individual leaves and had a naturally occurring range of leaf orientations (see Figure 5) whereas Vogel's (1989) experiments were conducted by positioning the leaves and clusters in a downstream orientation. The differing study conditions likely explained the different findings concerning the linear additivity. According to the current research, the potential drag-reducing mechanisms associated with an increasing foliage density (i.e., A_L/A_S), including the mutual sheltering among the foliage, the greater bending of the stem due to the drag on the foliage, and the less intense vibration of the stem, were of only minor significance for the twigs. However, the bending of the stem has been found to moderately increase with the foliation level for sapling-sized plants, so that the actual stem drag of foliated saplings can be somewhat lower than that estimated based on measurements with leafless saplings (Jalonen and Järvelä 2014). The linear

superposition approach could be applicable to other types of vegetation as well. Albayrak et al. (2014) investigated the linear superposition for the semi-aquatic species *Glyceria fluitans*, for which the sum of the foliage and stem drag was approximately 10% lower than the total drag of the same specimen in the foliated condition, but the low number of examined specimens precluded making definite conclusions.

The third advancement of the thesis is the improved understanding on the level of detail required for parameterizing floodplain vegetation for straightforward flow resistance estimation in compound channels. In the investigated sub-reaches of the two-stage channel, the cross-sectional blockage factor (B_X) was found to be the vegetative parameter that could most reliably determine the flow–vegetation interaction for dense grassy vegetation (Figure 19c). For high drag densities (C_Da=5–25), the density did not exert a notable control on the total flow resistance (n_{tot}), as illustrated by the same dependence of n_{tot} on B_X (Figure 19c) for the sub-reaches Grasses-N and -D differing in C_Da (Figure 20). These results are in accordance with the field studies by Green (2006) and Nikora et al. (2008) that demonstrate the key role of B_X for dense aquatic vegetation. By contrast, also the C_Da parameter was important for the sparser willow stand.

The data collected for the thesis allowed determining the minimum densities of woody floodplain stands allowing B_X to be used as the sole vegetative parameter in the estimation of the total flow resistance of comparable compound channels. For this, the discharge within the stand should be less than ~20% of the total (see prerequisites for Eq. 13 in Section 2.4). According to Eqs. 11–12, a *S. viminalis* stand with B_X=0.5 would require C_DaH>~1, which leads to A_L/A_B>2.3 and A_S/A_B>0.33 for the cross-sectional mean flow velocity of u_m=0.25 m/s and to A_L/A_B>6.3 and A_S/A_B>0.9 for u_m=1.25 m/s. In the above calculations, the C_DaH definition of Eq. 21 was used with the parameter values obtained from Table 3 and assuming that the leaf-area-to-stem-area ratio is equal to that of Willows-M (A_L/A_S=7). For typical deciduous woody floodplain stands, the frontal area per volume ranges at a=0.01–0.13 m^{-1} for the stems (Zinke 2011, and references therein) and the mean A_L/A_B is approximately 1–4 (Antonarakis et al. 2010; Forzieri et al. 2011). Taking into account that less than half of the foliage is typically located within the lowest few meters that are most prone to inundation (Antonarakis et al. 2010), the required minimum densities for using B_X as the sole vegetation parameter at typical flood flow velocities are at the upper range of or exceed the reported density values (Antonarakis et al. 2010; Forzieri et al. 2011; Zinke 2011). These considerations stress the need for reliably parameterizing the density, drag coefficient and reconfiguration of woody stands when modeling partly vegetated flows.

With respect to modeling partly vegetated flows, the present research verified the applicability of the simplified two-layer model (Eq. 13) of Luhar and Nepf (2013) to a new domain, namely to a two-stage geometry with predominantly grassy floodplain vegetation. Section 3.3.2 showed that Eq. 13 could predict the total flow resistance (n_{tot}) of the two-stage channel in different sea-

sons, years, water levels, and levels of relative submergence using B_X as the sole vegetative parameter. The only calibration that was involved was the seasonal value of the bulk drag coefficient (C^*) at one overbank condition to take into account the seasonal resistance changes due to sources other than the floodplain vegetation. Some of these other sources of resistance, such as boundary roughness (see Figure 9), can be estimated by standard hydraulic approaches instead of calibrating. As discussed in Paper III, the C^* values were physically reasonable as they corresponded to n=0.036–0.048 and were thus somewhat higher than the resistance coefficient of the bare two-stage channel (n_{base}=0.029) where the interfacial shear stress between vegetation and open water was absent. In addition, the C^* values fell to the ranges documented by Luhar and Nepf (2013) for the drag coefficients C_f ($0.015 \leq C_f \leq 0.19$) and C_v ($0.005 \leq C_v \leq 0.21$), and were close to the values found for simple channels with vegetated interfaces ($0.05 \leq C^* \leq 0.13$). Although Eq. 13 is intended for submerged flows characterized by interfacial shear above the vegetation, it performed approximately equally for both emergent and submerged floodplain vegetation. There was likely interfacial shear during the flows classified as emergent as well, because the C_Da values (Figure 20) indicated that the majority of the grass blades were notably lower than the determined vegetation height.

The detailed picture given by the thesis on the hydraulic behavior of woody vegetation can also be regarded from ecological viewpoint. For instance, Figure 16a reveals that woody species can have manifold differences in the foliage drag coefficient, which was strongly related to the inter-specific differences in the capability of obtaining a drag-efficient orientation of the foliage, reflected by the parameter $A_{P,F}/A_L$ (see a more detailed discussion in Section 4.2). Ultimately, such factors can be a manifestation of the inter-specific differences in the adaptation strategies that the plants use e.g. to cope with the mechanical stress imposed by the flow. For aquatic plants, the study by Puijalon et al. (2011) indicates that some species apply avoidance strategies by minimizing the drag forces while others apply tolerance strategies by maximizing their resistance to breakage, and that there appears to be an avoidance–tolerance tradeoff. In the future, there is much room for ecological considerations regarding the interactions between flow (either wind or water) and woody plants in order to reveal e.g. how the evolution of plant properties is constrained by flow (see e.g. Anten and Sterck 2012, Butler et al. 2012).

4.2 The new flow resistance model: advantages and limitations

The developed flow resistance model (Eqs. 18–23 in Section 3.2.1) explicitly parameterizes both the foliage and the stem. This was considered important because the two plant parts strongly influenced, but in different magnitudes, the total drag and reconfiguration of foliated woody plants (Section 3.1). Compared to models that lump the influence of the foliage and stem into bulk parameters (Kouwen and Fathi-Moghadam 2000; Järvelä 2004; Jalonen and Järvelä 2014; Whittaker et al. 2013; 2015), the present model is more physical-

ly-based in the sense that it acknowledges that the biomechanics of the foliage and stem differ. The independent validation data demonstrated that the model was capable of estimating the notable reconfiguration of the twigs and saplings manifested e.g. as the strong reduction in the friction factor with the increasing mean flow velocity (Figure 17a). By taking into account the reconfiguration processes and the foliage, the proposed parameterization provides a more realistic description of foliated plants compared to the "rigid cylinder analogy" (Eqs. 2 and 5) that is common in hydraulic models aimed at compound channels with floodplain vegetation (e.g., Kang and Choi 2006; Huai et al. 2009; Knight et al. 2010) or at flows with submerged vegetation (e.g., Huthoff et al. 2007; Konings et al. 2012). The hydraulic conditions and vegetation densities under which the model is valid are described in Section 3.2. The new drag–density parameterization (Eqs. 18–21) can also be incorporated into existing models simulating partly vegetated flows (see Figure 25 in Section 4.4 for details). The equations of the model are dimensionally correct.

The separate parameterization of the foliage and stem allowed using the same model and same parameter values for foliation conditions ranging from leafless (A_L/A_S=0) to sparsely and densely foliated (A_L/A_S=6–72). By contrast, for instance Järvelä's (2004) model (Eq. 10) which parameterizes only the foliage can lead to biased results depending on the value of the leaf-area-to-stem-area ratio (Paper I: Section 4.2 and Figure 10). The new model provided satisfactory predictions at a large range of friction factors and drag forces, as shown by the limited amount of available validation data for leafless and foliated vegetation of the height of 0.23–3.1 m (Figures 17 and 18). Thus, the new model potentially allows using the same parameter values for both twigs and saplings because it can take into account the fact that twigs have larger values of A_L/A_S (A_L/A_S=30–70, present study) than saplings (A_L/A_S=6–19, present study; Dittrich et al. 2012; Jalonen and Järvelä 2014). The potential transferability of the parameter values between twigs and saplings is also supported by Jalonen and Järvelä (2014) who examined the effect of plant size on drag.

The separate consideration of the foliage and stem enables the developed model to be used for exploring issues that cannot be addressed using Eqs. 2 and 5 or the models developed specifically for woody vegetation by Kouwen and Fathi-Moghadam (2000), Järvelä (2004), Whittaker et al. (2013, 2015), and Jalonen and Järvelä (2014). As an example, the model is capable of predicting how differing abundance of the foliage in relation to the stem influences the total reconfiguration of foliated vegetation or how inter-specific differences in the values of the foliage and stem parameters affect the total flow resistance.

The data available for validating the model is scarce, and therefore the model could not be tested against all the factors that can affect vegetative drag. The morphological and biomechanical properties of natural woody plants show intra- and inter-specific variability resulting from e.g. size (e.g., Niklas 1997; Sutili et al. 2012; Jalonen and Järvelä 2014) and season, as discussed in Section 1.2.2. Any model of the drag or flow resistance is practicable only if the parameter values are relatively universal for a given species or for groups of

similar species. Thus, new measurements are required to determine to what extent the parameter values can be held constant for specimens of different ages, sampling seasons, growth shapes and orientations or for plant stands of different densities. Presently, none of the other available models (Kouwen and Fathi-Moghadam 2000, Järvelä 2004, Whittaker et al. 2013, 2015; Jalonen and Järvelä 2014) have been rigorously tested for these factors. This thesis could confirm the validity of the model only to those types of plants documented in Table 4.

The limitations of the model include the fact that the reported parameter values (Table 3) may not be representative of full-sized trees because large trunks and branches likely reconfigure less than the woody parts of twigs and saplings. The parameter values are likely further affected by the scale of investigation, and they presumably differ e.g. between the leaf and foliage scales. The model does not distinguish between the plant and stand scales as it does not consider the potential effects of the spacing and pattern of the plants on the bulk drag coefficient (e.g., Tanino and Nepf 2008; Kothyari et al. 2009b; Schoneboom 2011; Dittrich et al. 2012). Regarding the hydraulic conditions, the velocity range under which the present model is valid was addressed by Jalonen and Järvelä (2014). They found that the parameter values of Table 3 notably over-estimated the drag of the saplings at mean flow velocities exceeding the recommended range of 0.05 –1.0 m/s.

The meaningfulness of using separate parameterization for the foliage and stem, and the choice of the leaf area and stem area as the density parameters, is supported by ecological considerations. Specifically for temperate woody species, Sun et al. (2006) state that the leaf and stem areas and masses at the twig scale form one of the leading dimensions of plant ecological variation. In addition, the specific leaf area ($A_L/m_{F,D}$, defined as the leaf area divided by the leaf mass) is among the ecologically most important plant properties as it is linked to ecological stress factors, such as soil nutrient status and rainfall level (e.g., Fonseca et al. 2000), and more broadly to the ecological strategies that plants use to secure their survival and reproduction (as reviewed e.g. by Westoby et al. 2002). Because basic fluid mechanics theory states that the area is the property most directly governing both the form drag and skin friction, the inter-specific differences in $A_L/m_{F,D}$ (see Table 2) likely partly explained why the foliage drag was less strongly related to the foliage mass than to the total leaf area at the inter-specific level (see Section 3.1.3). The leaf area is a more suitable drag predictor than the foliage mass also because the specific leaf area can exhibit intra-specific variation caused by factors such as shading (e.g., Westoby et al. 2002). Sophisticated measurement techniques have been developed for determining both the leaf and stem areas of foliated vegetation at the scale of several hundred square meters (e.g., Zou et al. 2009).

The values of the model parameters $C_{D\chi,S}$, $C_{D\chi,F}$, χ_F and χ_S (Eqs. 18–23) depend on several physical factors, but herein the focus is on the most important ones considering woody vegetation at scales and sizes relevant for natural flows (for a more in-depth discussion, see section 4.2 in Paper I). The stem drag coefficient ($C_{D\chi,S}$) likely depends primarily on the surface roughness of the

woody elements, with investigations of Tanaka et al. (2011) and Shields and Alonso (2012) showing that $C_{D,S}$ decreases with the declining surface roughness. The results in Section 3.1.3 indicated that the foliage drag coefficient ($C_{D\chi,F}$) is mainly affected by the orientation of the foliage at the lowest examined velocity ($u_{\chi,F}$) as species having a more drag-efficient orientation of the foliage (i.e., a lower $A_{P,F}/A_L$) had a lower $C_{D\chi,F}$ as well. Thus, the foliage-scale $C_{D\chi,F}$ is expected to be more importantly governed by the capability of achieving a drag-efficient orientation of the leaves than by leaf-scale factors, such as leaf shape and smoothness of the leaf margins (see Albayrak et al. 2012).

The reconfiguration parameters χ_F and χ_S mainly depend on the velocity-induced changes in the frontal projected area and shape of the foliage and stem. This was evident for the foliage from the marked decline in both the frontal projected area and the drag coefficient as the flow velocity increased (see Section 3.1.3 and Figure 8 in Paper I). The frontal projected area of the foliage can decrease e.g. by compaction of the foliage (e.g., Vogel 1989; Vollsinger et al. 2005), or as the individual leaves attain a closer to parallel orientation with respect to the main flow direction. The efficiency of such mechanisms is enhanced as the flexural rigidity of leaf blades decreases (Albayrak et al. 2012) and as the petiole length increases (Vogel 1989). For the stem, reduction in the frontal projected area is likely related to the flexural rigidities of the various trunk, branch, and twig elements that determine the ability of the stem to bend in the main flow direction. Generally, the values of the reconfiguration parameters also depend on the examined velocity range (e.g., Jalonen and Järvelä 2014).

In fluid mechanics, results obtained in water flows can be generally extended to flows in air or other media by ensuring the dynamic similarity (e.g., Schlichting and Gersten 2000). However, studies comparing the results of flexible plants in different flow media are rare. Kouwen and Fathi-Moghadam (2000) obtained similar values of the friction factor for trees in water and air flows when the size of the specimens was taken into account by the horizontal area they covered. Kouwen and Fathi-Moghadam (2000) transformed the air flow velocities to equivalent water flow velocities by assuming Reynolds number similarity and equal characteristic length in all cases. Applying such similarity considerations, Paper II showed that the ratio between the drag force and the velocity-dependent frontal projected area ($F_{\mathrm{tot}}/A_{P,\mathrm{tot}}$) was similar for the present *Populus nigra* twigs and the saplings of other *Populus* species tested in a wind tunnel by Vollsinger et al. (2005). These similarity considerations suggested that the developed flow resistance model and the improved process understanding can be of use when assessing the wind drag on trees. Wind drag can result in branch loss, stem breakage, or uprooting, which cause economic losses and other implications e.g. for forestry. Thus, there is a pronounced interest in predictive models for analyzing the risks and the effectiveness of different forest management options (e.g., Peltola 2006). Quantifying the drag and windthrow risk is essential also for urban tree management (e.g., Cullen 2005) and for green roofing systems growing shrubs (Cao et al. 2012). From the ecological viewpoint, windthrow can have long-lasting impacts on the spe-

cies dominance, structure, and demography of natural tree stands (e.g., Woods 2004).

4.3 Flow–plant–sediment interactions

This thesis increased the understanding regarding the dependence of erosion and deposition on measurable properties of natural vegetation. The study setting allowed minimizing the effects of other variables, such as the inundation frequency and duration (e.g., Rodrigues et al. 2007) and the particle settling velocity. The present study considered natural plant stands using physically-based properties (e.g., height and frontal area) instead of other quantitative but less hydraulically meaningful descriptors, such as the number of plants per unit bed area. The spatially-averaged deposition on the 190 m long vegetated floodplain (5.4 kg/m²/a or 0.7 cm/m²/a) fell within the ranges documented for a Danish agricultural floodplain (0–6.3 kg/m²/a, Kronvang et al. 2009) and for British floodplains (0.4–12.2 kg/m²/a, Walling 1999), but these two studies do not report the plant properties. At the Ritobäcken, the total amount of trapped sediment was likely higher than indicated by the cross-sectional surveys because settling on vegetation surfaces can up to double the removal of SS depending on the horizontal plant area and the effect of the plants on the vertical turbulent mixing (e.g., Elliott 2000; Pluntke and Kozerski 2003).

The linear regressions (Figure 22) indicated that increasing maximum inundated vegetation height (mean r = 0.66) and dry mass (mean r = 0.51) generated a greater tendency towards deposition. The finding that the height was a key vegetation property explaining the deposition agreed with the results of Corenblit et al. (2009) for a gravel-bed river. They found that the two-year accretion of silt and sand within grassy to woody riparian plant stands was significantly correlated only with the intercepted biovolume, which was defined in analogy to the maximum inundated height used herein. The results were also in agreement with those obtained in a flume study with natural grasses (Thornton et al. 1997) by revealing that deposition increased with the increasing vegetation density (understood as the dry mass per unit bed area in the present case and as the number of stems per unit bed area in Thornton et al. 1997). The present positive correlations between the deposition and the dry mass and height are explained below by considering the drag–area parameter $C_D aH$ (defined using Eq. 21 of Section 3.2.1 for the willows) because the three vegetation properties strongly depended on each other.

The change in the dominant process from net erosion for the sparse sub-reach Bare-M ($C_D aH$=0.19) to net deposition for the dense grassy sub-reaches ($C_D aH$=1.9–4.9) can be associated with the anticipated density-induced effects on the flow hydraulics. The present sub-reaches experienced both submerged and emergent flows, and vegetation density modifies the mean flow velocity and the turbulent flow structure under both conditions (e.g., Luhar et al. 2008, Nepf 2012a; Aberle and Järvelä 2015). Increasing density (a, A_L/A_B or A_S/A_B) was expected to decrease the mean flow velocities within the plant stands by linearly increasing the vegetative drag, as indicated for grassy vegetation by

Eq. 12 and for woody vegetation by the presently developed model (e.g., Eq. 23) and previous models (e.g., Eq. 10). This decrease in the flow velocity and the associated decrease in the turbulent kinetic energy, dominated by the shear-layer turbulence for dense submerged vegetation and by the plant-scale turbulence for emergent vegetation (see Figure 3; Nepf 2012a), were likely the main explanations for the observed higher deposition in the sub-reaches with denser vegetation.

The obtained C_DaH values of the present plant stands allow quantitatively analyzing whether the sediment processes within the natural vegetation followed the theory developed by Luhar et al. (2008) for rigid submerged cylinders (see Section 1.4.3 and Figure 3). As the simulated mean flow velocities within the floodplain stands were low (~0.01–0.1 m/s), the grassy and woody vegetation behaved almost rigidly. The theory states that the shear-layer turbulence formed at the top of the stand can penetrate to the bed and re-suspend sediment only if $C_DaH<0.23$ (e.g., Luhar et al. 2008; Nepf 2012a). Applying the theory to the present natural vegetation, the low frontal area index of Bare-M ($C_DaH=0.19$) led to erosion whereas the turbulent stresses were mostly not able to reach the bed in the more densely vegetated sub-reaches that thus allowed suspended sediment to deposit. Further, the notably greater spatially-averaged deposition in Willows-M ($C_DaH=0.38$) compared to Bare-M ($C_DaH=0.19$) supported the aH threshold derived by Luhar et al. (2008) from the experimental data of Moore (2004), which shows that aquatic stands having frontal area indices of $aH>\sim0.4$ can reduce suspended sediment concentration markedly more than stands having a lower aH.

For the emergent conditions, the present results can be reflected on the flume study by Bouma et al. (2009) conducted at the mean velocity of 0.3 m/s. They explained the erosion and deposition patterns within a stand of randomly spaced aquatic *Spartina anglica* by three alternative flow regimes (as reviewed e.g. by Vogel 1994). Bouma et al. (2009) reported that low vegetation densities (vegetation dry mass of 23 g/m²) caused independent flow and scouring around each stem while intermediate densities (58–97 g/m²) resulted in interactive flow with larger erosion areas because the scouring effects of the individual stems merged. Bouma et al. (2009) found that net deposition occurred only when the spatially-averaged density was higher than approximately 1500 shoots/m² (corresponding to a dry mass of ~170 g/m²). They concluded that above this density, the flow was increasingly deflected around the stem clusters, and this skimming flow (e.g., Vogel 1994) enabled net deposition within the stand. At the vegetation density of 312 g/m², deposition was observed throughout the stand. Although the present stands did not have areas so clearly devoid of plants as the stands of Bouma et al. (2009), it is plausible that during the emergent conditions, the present grassy stands were experiencing a similar skimming flow regime with the flow deflected to the areas of less dense or lower vegetation. Such differences in the density and height within the stands are evident e.g. from investigations with terrestrial laser scanning conducted at the same sub-reaches (Figure 12 in Jalonen et al. 2014; Figure 8 in Jalonen et al. 2015). The threshold densities for emergent vegetation likely

vary according to the particle properties, such as the settling velocity and critical shear stress for erosion, and according to the mean flow velocity, with decreasing velocity shifting the balance towards net deposition. Thus, the present density values and the associated net erosion or deposition cannot be directly compared to the study of Bouma et al. (2009) that was conducted with coarser sediment and higher flow velocities. However, the qualitative effects of the vegetation density on the turbulent flow structure and on the tendency towards net erosion or deposition under emergent conditions were expected to be roughly similar for the present cohesive particles.

The maximum inundated vegetation dry mass explained on average 32% and the height 45% of the deposition (Figure 22), which indicated the presence of other controlling factors. Flume measurements with real woody plants and bed load show that the effect of vegetation properties on sediment transport is dampened under conditions of limited sediment supply (Manners et al. 2015). According to the example computations with Eq. 14, the distances from the nearest upstream SS replenishment point to the sub-reaches Grasses-N and -D exceeded the advection length scales for a notable fraction of the suspended sediment (see Section 3.4). Thus, at least under emergent conditions, the supply of larger flocs to the floodplain was dominated by lateral diffusion from the main channel in these sub-reaches (see e.g. Zong and Nepf 2011). However, the interface vortices (see Figure 2) could not efficiently supply SS to the inner areas of the 5 m wide floodplain, as indicated by the 64% lower deposition on the inner floodplain compared to the interface in Grasses-N and -D. This finding revealed that the common assumption of laterally uniform deposition of fine sediment across floodplains (e.g., Walling and He 1997; Kronvang et al. 2009) cannot be routinely expected to hold for floodplains growing long, dense, often emergent plant stands. Flume experiments with rigid emergent stems (Sharpe and James 2006) show that lateral diffusion cannot effectively supply fine sand to inner floodplain areas under comparable flow velocities and depths. These considerations imply that occasional floodplain areas allowing lateral advection from the main channel notably increase the amount of sediment supplied to floodplains when vegetation has relative submergence close to or above 1. Accordingly, the diverging flows from the main channel enabled by the sudden reduction in the plant density (Figure 20, Section 3.3) likely explained to some degree the high deposition on the inner floodplain in the fairly sparsely vegetated Willows-M ($C_D aH$=0.38).

These findings on how measurable vegetation properties influenced the transport of cohesive sediment in the agricultural compound channel serve the design and management of similar channels (see next section), but the obtained process understanding can be used also in other environments where the interaction between vegetation and fine sediment is important, such as in estuarine and coastal areas (e.g., Mudd et al. 2010; Temmerman et al. 2013). The same vegetation properties are expected to control the hydraulic transport of coarser mineral sediment, organic sediment, and substances sorbed on particles, as well. For coarser suspended sediment, the effects of lateral and longitudinal supply limitations within dense plant stands are even more pro-

nounced as larger particles settle faster. The thesis can also support ecological studies on the effects of erosion and deposition on plant survival (e.g., Schnauder and Moggridge 2009; Kui et al. 2014; Pasquale et al. 2014), or on ecosystem engineering by plants (e.g., Bos et al. 2007; Schoelynck et al. 2012; Gurnell 2014).

4.4 Implications for research and engineering

This section gives some viewpoints on the wider implications that the findings of the thesis have for research and practical engineering at different scales. The focus is on the developed flow resistance model, the design and management of two-stage channels, and the potential of two-stage channels for improving agricultural water quality. The laboratory and field investigations confirmed that woody and grassy floodplain vegetation markedly influence the flow hydraulics. The reconfiguration strongly modifies the drag and flow resistance (see e.g. Figures 16 and 17a), and should therefore be suitably parameterized for instance in the research on plant–flow interactions. At the sub-reach and reach scales, floodplain vegetation can increase the total flow resistance of a compound channel by up to fourfold (Section 3.3) and thus the water surface slopes by over an order of magnitude. These findings highlight the importance of the reliable prediction of the vegetative flow resistance in the design and management of engineered channels, such as agricultural channels where adequate conveyance is crucial to ensure the performance of the sub-surface drainage.

Figure 25 illustrates how the developed flow resistance model (Eqs. 18–23) can be used for determining the hydraulic effects of woody vegetation at different scales and levels of relative submergence. At the plant scale, the drag force parameterization (Eq. 19) is applicable to both submerged and emergent flows because similar plant-scale drag was found for different levels of submergence (Section 3.1.1). The depth-averaged mean flow velocity or the mean flow velocity on the floodplain can be used as u_C in most plant-scale analyses. Eq. 23 can be directly applied for estimating the friction factor of an emergent plant stand, for which case the cross-sectional mean flow velocity (u_m) can be used as u_C. Submerged stands can be modeled by replacing the rigid, bulk-scale C_DaH parameter by the new drag–area parameter (Eq. 21) for instance in two-layer models (e.g., Huthoff et al. 2007; Luhar and Nepf 2013), in which case the mean flow velocity within the vegetation (u_V) is used as u_C. The deflected vegetation height can be determined e.g. by coupling the proposed drag force equation (Eq. 19) with the bending algorithm of Stone et al. (2013).

For reach-scale analyses, the parameterization of the vegetative friction factor (Eq. 23) can be used in 1D considerations that require determining the total flow resistance caused by different factors according to Eq. 3 (e.g., Yen 2002). In addition, the new parameterizations for C_Da and C_DaH (Eqs. 20–21) can be implemented into existing analytical and numerical hydraulic models (e.g., Kang and Choi 2006; Huai et al. 2009; Knight et al. 2010) to improve the description of woody vegetation. As an example, Eq. 20 and the derived pa-

rameter values (Table 3) were incorporated into Eq. 12 to compute the flow within the emergent floodplain willows at the examined two-stage channel (Section 3.3.1). The developed model is straightforward to use once the representative values of the parameters χ_F, χ_S, $C_{D\chi,F}$, and $C_{D\chi,S}$ are known for a given species. The one-sided leaf area (A_L) and frontal projected stem area (A_S), or A_L/A_B and A_S/A_B, are the only additional vegetation properties required for using the model.

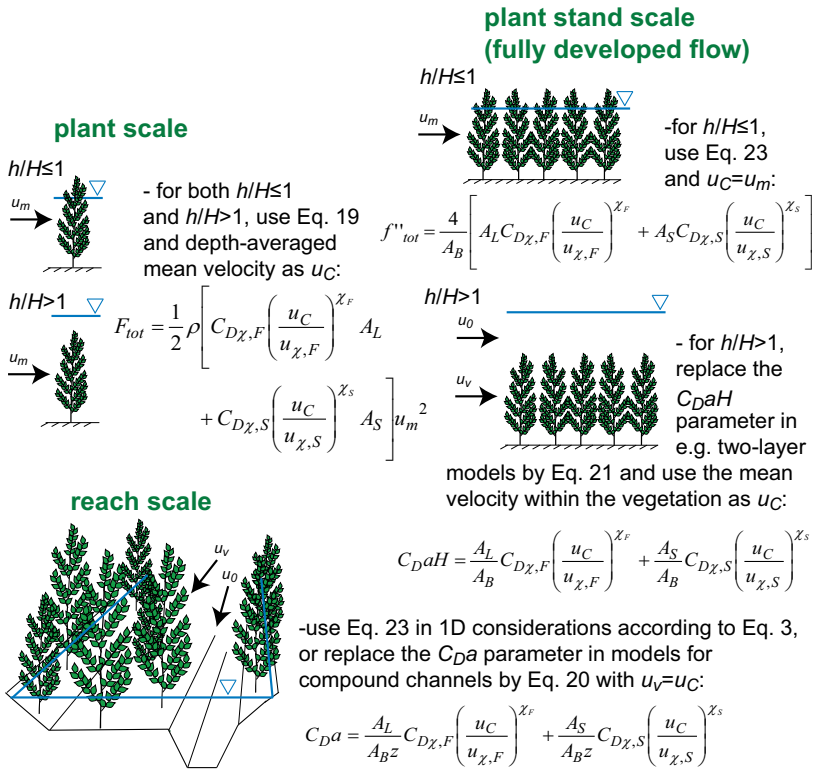

Figure 25. Usage of the new model of vegetative drag and flow resistance (Eqs. 18–23) for investigating the hydraulic effects of woody vegetation from plant to reach scales and at different levels of relative submergence (h/H). Equations are written for the drag force (F_{tot}), friction factor (f''_{tot}), drag–density parameter (C_Da), and the drag–area parameter (C_DaH) using the total leaf area (A_L), the frontal projected stem area (A_S), and the unit bed area (A_B). Values of χ_F, χ_S, $C_{D\chi,F}$, $C_{D\chi,S}$, $u_{\chi,F}$, and $u_{\chi,S}$ are reported in Table 3 for the presently investigated species.

The potential applications of the new drag parameterization (Eqs. 18–23) range from flood inundation studies to river restoration, floodplain reforestation, and channel design and management. In addition, the developed model can be of interest to the research of ecohydraulics. The model can be used to analyze how vegetation density, foliation, and reconfiguration properties affect the habitat conditions of fauna and flora through modification of the flow velocities.

The thesis provides scientific understanding for the design and management of two-stage channels, for which there is little research but a great interest e.g. in agricultural drainage (e.g., Needelman et al. 2007; Powell et al. 2007; USDA

2007; Jormola et al. 2008). For instance, the successful prediction of Manning's n in the predominantly grassy two-stage channel (Figure 21) indicated that Eq. 13 can be used in the design of comparable vegetated channels. Eq. 13 is a straightforward tool and more objective than look-up tables or reference photographs of n values. Eq. 13 can be used also in channel maintenance for determining how the vegetative blockage factor needs to be changed to reduce the water levels and flow resistance to a required level.

Concerning sediment transport, both the hysteresis analyses and sediment rating curves (Section 3.5) indicated that the high SS loads observed during the rising stages originated mainly from the sub-surface drained agricultural areas that produced rapid runoff (see Paper IV). The lower SS loads during the falling stages resulted from the mixing of the sediment-rich agricultural runoff and the sediment-poor runoff from the less effectively drained forested areas. The dominance of the catchment for producing the SS loads was supported by the fact that the 190 m long vegetated test reach, representative of the upstream two-stage reaches, did not experience notable net erosion events after a plant cover had been established. Rather, the floodplain underwent net deposition amounting to 3.4–5.5% of the annual SS load depending on the filter type used for analyzing the suspended sediment concentration (SSC). The sediment deposited on the floodplain was predominantly clay and silt. During the events of net deposition, SSC values (100–500 g/m^3) fell into the range of flocculation settling (e.g., Mehta and McAnally 2008), indicating that the deposition was enhanced by the aggregation of the cohesive primary particles. These results support the earlier observations for the important role played by aggregation for enabling fine sediment deposition in fluvial environment (e.g., Thonon et al. 2005). The findings imply that fine sediment load from the catchment should be taken into account in environmentally preferable channel designs involving abundant bank and floodplain vegetation.

The field investigation gave understanding on the vegetation properties needed to prevent erosion and convey incoming sediment, or alternatively, to generate deposition (Figure 22). The threshold between erosion and deposition was observed at $C_D aH \approx 0.2–0.4$. The variable a is more time-consuming and less accurate to obtain than e.g. dry mass and vegetation height but can be derived for comparable floodplain grasses with Eq. 6 or with terrestrial laser scanning (e.g., Jalonen et al. 2015). In practice, the regression lines (Figure 22) suggested that natural plant stands with a dry mass above approximately 200 g/m^2 or height above ~0.1 m cause deposition of cohesive sediment. However, the results showed that deposition can be supply-limited even on such narrow floodplains if the vegetation forms dense, continuous, mostly emergent stands. Under supply-limited conditions, deposition can be increased by cutting the floodplain vegetation from short, regularly-spaced sub-reaches, which allows suspended sediment to be effectively distributed from the main channel to the floodplain (Paper III). The flow velocities simulated for the sub-reaches (see Section 3.3.1) indicated that the increasing density of the floodplain vegetation likely caused flow acceleration in the main channel. Similar flow acceleration has been observed in the open water around plant patches (e.g., Bouma et al.

2007; Zong and Nepf 2010), and it has been associated with erosion outside of the vegetation (e.g., Bouma et al. 2009). Although the current study could not measure the changes in the bed level of the main channel, the reach-scale magnitude of net deposition indicated that the main channel did not experience notable erosion.

The two-stage channel was shown to have potential for improving the agricultural water quality. The floodplain at the mean water level appeared suitable for the removal of substances because overbank flows transported two thirds of the total discharge and 90% of the suspended sediment load (Section 3.5). Most of the SS was transported in autumn and spring, with the erect autumn vegetation providing better potential for deposition than the bent spring vegetation. The flow–vegetation–sediment analyses (Section 3.4) indicated that the whole two-stage channel length could function as a sediment trap if floodplain vegetation is managed suitably. According to tentative estimates, the deposited load was computed to increase almost linearly with the length of the two-stage reach under optimal supply conditions. Thus, the annual removal of SS on the present 850 m long two-stage channel could be approximately 20%.

The data demonstrated that floodplain vegetation can enhance water quality especially during high flows by reducing peak turbidities and concentrations of cohesive SS. In channels receiving such high concentrations of SS, the two-stage approach allows decreasing the loads of e.g. eutrophication-causing phosphorus, pesticides or toxic heavy metals by managing the processes of the cohesive sediment (see also Shore et al. 2014). Thus, the two-stage concept may be an important addition to field-scale agricultural water protection measures that include reduced fertilizer rates, enhanced vegetative cover in winter, reduced tillage practices, buffer strips, and organic farming (see e.g., Puustinen et al. 2007; Aakkula et al. 2012). Two-stage designs can directly treat the sub-surface drainage waters when the drainage pipes discharge on the floodplain whereas e.g. buffer strips may not be effective for sub-surface drained fields (Warsta et al. 2014). To efficiently decrease the loads of harmful substances to downstream water bodies, attempts should be targeted at coupling the process understanding from the field scale to channel network scale. Focus should be put on the sediment–nutrient processes associated with the different size classes of cohesive sediment, and on the effects of vegetation on the transport of soluble nutrients.

4.5 Future directions

Solving the many remaining gaps concerning the interactions between flow, natural riparian plants and sediment transport requires detailed investigations that recognize that vegetation is primarily a biological component. Such a notion has advanced the state of understanding of flows with aquatic vegetation (e.g., Nikora 2010; Nepf 2012a; Nikora et al. 2012; Sukhodolov and Sukhodolova 2012). The universality of the developed model could be improved by establishing linkages between the model parameters and the inher-

ent biomechanical properties of the foliage and stem. Concerning the transport processes, it should be tested whether the turbulent flow structure within foliated reconfiguring plant stands can be predicted with theories developed for rigid cylindrical elements (e.g., Luhar et al. 2008; Nepf 2012a) if the new drag parameterization is applied. An important but often missing step is the upscaling of flume results to actual channels having more heterogeneous vegetation and geometry. This includes testing the new model in a real river, and analyzing how the turbulence and the supply of matter to floodplain plant stands differs between natural vegetated compound channels and laboratory setups with simulated vegetation (e.g., Sharpe and James 2006; Zong and Nepf 2010, 2011). To reliably model sediment transport, future studies should determine which turbulent flow parameters (mean bed shear stress, Reynolds stresses, turbulent kinetic energy) can be used to predict the erosion and deposition of fine sediment within flexible plant stands.

5. Conclusions

The flume investigation and the field study in the two-stage channel showed that the processes at the foliage and stem scales affect the hydraulic behavior of plants and plant stands. These smaller-scale processes were found to have pronounced effects on the flow resistance and sediment transport at the reach and catchment scales. The thesis demonstrated that straightforward analyses and models accompanied with a physically-based parameterization of the plants can be successfully used to describe the impact of natural riparian vegetation on flow resistance and sediment deposition. The following conclusions can be drawn from the smallest to the largest examined scale:

1) Both the foliage and stem were demonstrated to be important for the flow resistance of woody plants. The densities of the two plant parts were successfully parameterized using the total one-sided leaf area for the foliage and the frontal projected woody area for the stem. At the plant scale, the drag and reconfiguration were found to be strongly controlled by the leaf-area-to-stem-area-ratio (A_L/A_S) because the drag coefficient (C_D) and reconfiguration parameter markedly differed between the foliage and stem. The analyses indicated that the separate consideration of the drag–density parameter (C_Da) for the two plant parts allows a better representation of the physical processes compared to plant-scale bulk parameters.
2) A new approach was proposed for modeling the drag forces and flow resistance of woody vegetation (Eqs. 18–23). The model is based on the demonstrated linear superposition of the foliage drag and stem drag, and it incorporates a novel formulation of C_Da to take into account the reconfiguration of both plant parts. The developed model and the derived parameter values allow estimating the drag and flow resistance exerted by natural flexible plants at twig and sapling scales, as indicated by the successful application of the model to a wide range of foliation conditions (A_L/A_S=6–72) and to leafless vegetation. Further, the developed parameterization can be implemented into hydraulic models to improve the description of woody vegetation compared to the conventionally used approach based on rigid cylindrical elements.
3) For the partly vegetated flows in the two-stage channel, the woody and grassy sub-reaches differing in the drag–density parameter were

shown to have different impact on the flow partitioning between the floodplain and the main channel, and thus on the bulk flow resistance. For the dense grassy sub-reaches, the bulk flow resistance was found to be primarily dependent on the cross-sectional vegetative blockage factor (B_X) that was computed using the spatially-averaged vegetation height. For the sparser woody sub-reach, also the C_Da value appeared important, and thus the field investigation supported the need for the newly developed parameterization of C_Da for woody plant stands. At the reach scale, the simplified two-layer model (Eq. 13) was proven capable of predicting the effect of the predominantly grassy floodplain vegetation on the bulk flow resistance.

4) The drag–density parameter (C_Da) and the vegetation height (H) that strongly controlled the drag and flow resistance also explained the net deposition of clay and silt on the constructed bank and floodplain of the compound channel. The drag–area parameter (C_DaH) was observed to characterize the tendency of the sub-reaches towards erosion or deposition, in accordance with a previous hydrodynamic theory developed with rigid cylinders. The magnitude of the annual net deposition was best explained by the maximum inundated vegetation height. The results showed that the amount of fine suspended sediment supplied by longitudinal advection and lateral diffusion can be limited in long and dense floodplain plant stands, which can decrease the net deposition of cohesive sediment on floodplains of a width as low as 5 m. The findings confirmed that the transport of cohesive sediment can be managed through appropriately maintained floodplain vegetation.
5) The amount and timing of cohesive sediment transport were governed by out-of-channel processes, with high discharges and loads originating from the agricultural catchment during rising water levels. The patterns of flow generation and cohesive sediment entrainment occurring in different catchment land use classes should be considered in the design phase to ensure optimal functioning of agricultural two-stage channels. The results showed that two-stage reaches can accomplish a net removal of the transported cohesive sediment through deposition on vegetated floodplains. The deposition was facilitated by the aggregation of the cohesive suspended particles and by the high share of the sediment transported at overbank flows. The two-stage approach appeared promising for enhancing the conveyance while providing positive impacts on the water quality in agricultural channels.

References

Aakkula, J., Kuussaari, M., Rankinen, K., Ekholm, P., Heliölä, J., Hyvönen, T., Kitti, L., and Salo, T. 2012. Follow-up study on the impacts of agri-enviromental measures in Finland. In: Evaluation of Agri-Environmental Policies: Selected Methodological Issues and Case Studies, pp. 111–128. OECD Publishing. doi:10.1787/9789264179332-en.

Aberle, J., and Järvelä, J. 2013. Flow resistance of emergent rigid and flexible vegetation. J. Hydraul. Res., 51(1), 33–45. doi:10.1080/00221686.2012.754795.

Aberle, J., and Järvelä, J. 2015. Hydrodynamics of vegetated channels. In: Rowinski, P., and Radecki-Pawlik, A. (eds.), Rivers – physical, fluvial and environmental processes, pp. 519–541. GeoPlanet: Earth and Planetary Sciences, Springer, Berlin. doi:10.1007/978-3-319-17719-9_21.

Aberle, J., Nikora, V., and Walters, R. 2004. Effects of bed material properties on cohesive sediment erosion. Mar. Geol., 207(1–4), 83–93.

Abt, S.R., Clary, W.P., and Thornton, C.I. 1994. Sediment deposition and entrapment in vegetated streambeds. J. Irrig. Drain. Eng., 120, 1098–1111.

Albayrak, I., Nikora, V., Miler, O., and O'Hare, M. 2012. Flow-plant interactions at a leaf scale: effects of leaf shape, serration, roughness and flexural rigidity. Aquat. Sci., 74(2), 267–286. doi:10.1007/s00027-011-0220-9.

Albayrak, I., Nikora, V., Miler, O., and O'Hare, M. 2014. Flow–plant interactions at leaf, stem and shoot scales: drag, turbulence, and biomechanics. Aquat. Sci., 76, 269–294. doi:10.1007/s00027-013-0335-2.

Anten, N.P.R., and Sterck, F.J. 2012. Terrestrial vs aquatic plants: how general is the drag tolerance–avoidance trade-off? New Phytol., 193, 6–8.

Antonarakis, A.S., Richards, K.S., Brasington, J., and Muller, E. 2010. Determining leaf area index and leafy tree roughness using terrestrial laser scanning. Water Resour. Res., 46, W06510. doi:10.1029/2009WR008318.

Armanini, A., Righetti, M., and Grisenti, P. 2005. Direct measurement of vegetation resistance in prototype scale. J. Hydraul. Res., 43, 481–487.

Asaeda, T., Rajapakse, L., and Kanoh, M. 2010. Fine sediment retention as affected by annual shoot collapse: Sparganium erectum as an ecosystem engineer in a lowland stream. River Res. Applic., 26, 1153–1169. doi:10.1002/rra.1322

Asselman, N.E.M. 1999. Suspended sediment dynamics in a large drainage basin: the River Rhine. Hydrol. Process., 13(10), 1437–1450.

Assselman, N.E.M, and van Wijngaarden, M. 2002. Development and application of a 1D floodplain sedimentation model for the River Rhine in The Netherlands. J. Hydrol., 268(1–4), 127–142. doi:10.1016/S0022-1694(02)00162-2.

Bal, K.D., Bouma, T.J., Buis, K., Struyf, E., Schoelynck, J., Backx, H., and Meire, P. 2011. Trade-off between drag reduction and light interception of macrophytes: comparing five aquatic plants with contrasting morphology. Funct. Ecol., 25, 1197–1205. doi:10.1111/j.1365-2435.2011.01909.x

Baptist, M.J. 2005. Modelling floodplain biogeomorphology. Doctoral thesis. Delft University of Technology. ISBN 90-407-2582-9.

Barclay, H.J., Trofymow, J.A., and Leach, R.I. 2000. Assessing bias from boles in calculating leaf area index in immature Douglas-fir with the LI-COR canopy analyzer. Agr. Forest Meteorol., 100, 255–260.

Battiato, I., and Rubol. S. 2014. Single-parameter model of vegetated aquatic flows, Water Resour. Res., 50, 6358–6369. doi:10.1002/2013WR015065.

Bennett, S.J., Wu, W., Alonso, C.V., and Wang, S.S.Y. 2008. Modeling fluvial response to in-stream woody vegetation: implications for stream corridor restoration. Earth Surf. Process. Landforms, 33, 890–909. doi:10.1002/esp.1581.

Berlamont, J., Ockenden, M., Toorman, E., and Winterwerp, J. 1993. The characterization of cohesive sediment properties. Coast. Eng., 21, 105–128.

Bertoldi, W., Gurnell, A.M., and Drake, N.A. 2011. The topographic signature of vegetation development along a braided river: Results of a combined analysis of airborne lidar, color air photographs, and ground measurements. Water Resour. Res., 47, W06525. doi:10.1029/2010WR010319.

Bilotta, G.S., and Brazier, R.E. 2008. Understanding the influence of suspended solids on water quality and aquatic biota. Water Res., 42(12), 2849–2861.

Blann, K.L., Anderson, J.L., Sands, G.R., and Vondracek. B. 2009. Effects of agricultural drainage on aquatic ecosystems: a review. Crit. Rev. Env. Sci. Tech., 39(11), 909–1001. doi:10.1080/10643380801977966.

Bociag, K., Galka, A., Lazarewicz, T., and Szmeja, J. 2009. Mechanical strength of stems in aquatic macrophytes. Acta Soc. Bot. Pol., 78(3), 181–187.

Boller, M., and Carrington, E. 2006. The hydrodynamic effects of shape and size change during reconfiguration of a flexible macroalga. J. Exp. Biol., 209, 1894–1903. doi:10.1242/jeb.02225.

Boller, M., and Carrington, E. 2007. Interspecific comparison of hydrodynamic performance and structural properties among intertidal macroalgae. J. Exp. Biol., 210, 1874–1884. doi:10.1242/jeb.02775.

Bos, A.R., Bouma, T.J., de Kort, G.L.J., van Katwijk, M.M. 2007. Ecosystem engineering by annual intertidal seagrass beds: Sediment accretion and modification. Estuar. Coast. Shelf S., 74, 344–348. doi:10.1016/j.ecss.2007.04.006.

Bouma, T.J., van Duren, L.A., Temmerman, S., Claverie, T., Blanco-Garcia, A., Ysebaert, T., and Herman P.M.J. 2007. Spatial flow and sedimentation patterns within patches of epibenthic structures: Combining field, flume and modelling experiments. Cont. Shelf Res., 27, 1020–1045. doi:10.1016/j.csr.2005.12.019.

Bouma, T.J., Friedrichs, M., van Wesenbeeck, B.K., Temmerman, S., Graf, G., and Herman, P.M.J. 2009. Density-dependent linkage of scale-dependent feedbacks: a flume study on the intertidal macrophyte *Spartina anglica*. Oikos, 188, 260–268. doi:0.1111/j.1600-0706.2008.16892.x.

Bréda, N.J.J. 2003. Ground-based measurements of leaf area index: a review of methods, instruments and current controversies. J. Exp. Bot., 54, 2403–2417. doi:10.1093/jxb/erg263.

Brinson, M.M., and Malvárez, A.I. 2002. Temperate freshwater wetlands: types, status, and threats. Environ. Conserv., 29(2): 115–133. doi:10.1017/S0376892902000085

Butler, D.W., Gleason, S.M., Davidson, I., Onoda, Y., and Westoby, M. 2012. Safety and streamlining of woody shoots in wind: an empirical study across 39 species in tropical Australia. New Phytol., 193, 137–149. doi:10.1111/j.1469-8137.2011.03887.x.

Cao, J., Tamura, Y., and Yoshida, A. 2012. Wind tunnel study on aerodynamic characteristics of shrubby specimens of three tree species. Urban Forestry and Urban Greening, 11, 465–476. doi:10.1016/j.ufug.2012.05.003

Camporeale, C., Perucca, E., Ridolfi, L., and Gurnell, A.M. 2013. Modeling the interactions between river morphodynamics and riparian vegetation. Rev. Geophys., 51(3), 379–414. doi: 10.1002/rog.20014.

Carpenter, S.R., and Lodge, D.M. 1986. Effects of submersed macrophytes on ecosystem processes. Aqua. Bot., 26, 341–370.

Chapman, J.A., Wilson, B.N., and Gulliver, J.S. 2015. Drag force parameters of rigid and flexible vegetal elements. Water Resour. Res., 51, 3292–3302. doi:10.1002/2014WR015436

Chow, V.T. 1959. Open-Channel Hydraulics. McGraw-Hill, NewYork, NY.

Clark, L.A., and Wynn, T.M. 2007. Methods for determining streambank critical shear stress and soil erodibility: implications for erosion rate predictions. Transactions of the ASABE, 50(1), 95–106.

Clarke, S.J. 2002. Vegetation growth in rivers: influences upon sediment and nutrient dynamics. Prog. Phys. Geog., 26(2), 159-–72.

Corenblit, D., Steiger, J., Gurnell, A.M., Tabacchi, E., and Roques, L. 2009. Control of sediment dynamics by vegetation as a key function driving biogeomorphic succession within fluvial corridors. Earth Surf. Process. Landforms, 34, 1790–1810. doi:10.1002/esp.1876.

Cotton, J.A., Wharton, G., Bass, J.A.B., Heppell, C.M., and Wotton, R.S. 2006. The effects of seasonal changes to in-stream vegetation cover on patterns of flow and accumulation of sediment. Geomorphology, 77(3–4), 320–334. doi:10.1016/j.geomorph.2006.01.010.

Crosato, A., and Saleh, M.S. 2011. Numerical study on the effects of floodplain vegetation on river planform style. Earth Surf. Process. Landforms 36, 711–720. doi: 10.1002/esp.2088.

Cullen, S. 2005. Trees and wind: a practical consideration of the drag equation velocity exponent for urban tree risk management. J. Arboric., 31, 101–113.

Curran, J.C., and Hession, W.C. 2013. Vegetative impacts on hydraulics and sediment processes across the fluvial system. J. Hydrol., 505, 364–376. doi:10.1016/j.jhydrol.2013.10.013

Cutini, A., Matteucci, G., and Mugnozza, G.S. 1998. Estimation of leaf area index with the Li-Cor LAI 2000 in deciduous forests. Forest Ecol. Manag., 105, 55–65.

DEFRA. 2004. Reducing uncertainty in river flood conveyance, Phase 2: Conveyance Manual. Department for Environment, Food, and Rural Affairs, Environment Agency, Bristol, UK.

De Doncker, L., Troch, P., Verhoeven, R., Bal, K., Desmet, N., and Meire, P. 2009. Relation between resistance characteristics due to aquatic weed growth and the hydraulic capacity of the river Aa. River Res. Applic., 25, 1287–1303. doi:10.1002/rra.1240.

Demars, B.O.L., Kemp, J.L., Friberg, N., Usseglio-Polatera, P., and Harper, D.M. 2012. Linking biotopes to invertebrates in rivers: Biological traits, taxonomic composition and diversity. Ecol. Ind., 23, 301–311. doi: 10.1016/j.ecolind.2012.04.011.

Dibble, E.D., Killgore, K.J., Harrel, S.L. 1997. Assessment of fish-plant interactions. Miscellaneous Paper A-97-6, U.S. Army Engineer Waterways Experiment Station, Vicksburg, MS.

Dittrich, A., Aberle, J., and Schoneboom, T. 2012. Drag forces and flow resistance of flexible riparian vegetation. In Rodi, W., and Uhlmann, M. (eds.), Environmental Fluid Mechanics: Memorial Volume in honour of Prof. Gerhard H. Jirka, pp. 195–215. IAHR Monographs, CRC Press, London.

Droppo, I.G., Leppard, G.G., Flannigan, D.T., and Liss, S.N. 1997. The freshwater floc: a functional relationship of water and organic and inorganic floc constituents affecting suspended sediment properties. Water Air Soil Poll., 99(1-4), 43–54.

Elliott, A.H. 2000. Settling of fine sediment in a channel with emergent vegetation. J. Hydraul. Eng., 126(8), 570–577.

Fonseca, C.R., Overton J. McC., Collins, B., and Westoby, M. 2000. Shifts in trait-combinations along rainfall and phosphorus gradients. J. Ecol., 88, 964–977.

Forzieri, G., Guarnieri, L., Vivoni, E.R., Castelli, F., and Preti, F. 2011. Spectral-ALS data fusion for different roughness parameterizations of forested floodplains. River Res. Applic., 27: 826–840. doi: 10.1002/rra.1398.

Franklin, P., Dunbar, M., Whitehead, P. 2008. Flow controls on lowland river macrophytes: A review. Sci. Total Environ., 400, 369–378. doi:10.1016/j.scitotenv.2008.06.018.

Freeman, G.E., Rahmeyer, W.H., and Copeland, R.R. 2000. Determination of resistance due to shrubs and woody vegetation. Technical Report ERDC/CHL TR-00-25. US Army Corps of Engineers.

Gacia, E., Granata, T.C., and Duarte, C.M. 1999. An approach to measurement of particle flux and sediment retention within seagrass (*Posidonia oceanica*) meadows. Aquat. Bot., 65, 255–268.

García, M.H. (ed.) 2008a. Sedimentation Engineering. ASCE Manuals and Reports on Engineering Practice No. 100, American Society of Civil Engineers, Reston, 1132 pp. ISBN: 978-0-7844-0814-8.

García, M.H. 2008b. Sediment transport and morphodynamics. In: García, M.H. (ed.), Sedimentation Engineering. ASCE Manuals and Reports on Engineering Practice No. 100, pp. 21–163. American Society of Civil Engineers, Reston. ISBN: 978-0-7844-0814-8.

Gay, A., Cerdan, O., Delmas, M., Desmet, M. 2014. Variability of suspended sediment yields within the Loire river basin (France). J. Hydrol., 519, 1225–1237. doi:10.1016/j.jhydrol.2014.08.045

Geerling, G.W., Kater, E., van den Brink, C., Baptist, M.J., Ragas, A.M.J., and Smits, A.J.M. 2008. Nature rehabilitation by floodplain excavation: The hydraulic effect of 16 years of sedimentation and vegetation succession along the Waal River, NL. Geomorphology, 99(1–4), 317–328.

Gorrick, S., and Rodríguez, J.F. 2012. Sediment dynamics in a sand bed stream with riparian vegetation. Water Resour. Res., 48, W02505. doi:10.1029/2011WR011030.

Gosselin, F., de Langre, E., and Machado-Almeida, B.A. 2010. Drag reduction of flexible plates by reconfiguration. J. Fluid Mech., 650, 319–341. doi:10.1017/S0022112009993673.

Green, J.C. 2005. Comparison of blockage factors in modeling the resistance of channels containing submerged macrophytes. River Res. Applic., 21, 671–686. doi:10.1002/rra.854.

Green, J.C. 2006. Effect of macrophyte spatial variability on channel resistance. Adv. Water Resour., 29, 426–438.

Gregory, S.V., Swanson, F.J., McKee, W.A., and Cummins, K.W. 1991. An ecosystem perspective of riparian zones. Bioscience, 41(8), 540–551.

Grizzle, R.E., Short, F.T., Newell, C.R., Hoven, H., and Kindblom, L. 1996. Hydrodynamically induced synchronous waving of seagrasses: 'monami' and its possible effects on larval mussel settlement. J. Exp. Mar. Biol. Ecol., 206, 165–177.

Gurnell, A. 2014. Plants as river system engineers. Earth Surf. Process. Landforms, 39, 4–25. doi:10.1002/esp.3397.

Helmiö, T., and Järvelä, J. 2004. Hydraulic aspects of environmental flood management in boreal conditions. Boreal Env. Res., 9(3), 227–241.

Heppell, C.M., Wharton, G., Cotton, J.A.C., Bass, J.A.B., and Roberts, S.E. 2009. Sediment storage in the shallow hyporheic of lowland vegetated river reaches. Hydrol. Process., 23, 2239–2251. doi:10.1002/hyp.7283.

Hey, R.D. 2009. Environmentally sensitive river engineering. In: Calow, P., and Petts, G. E. (eds.), The Rivers Handbook: Hydrological and Ecological Principles, Volume Two, pp. 337–362. Blackwell Science Ltd, Oxford, UK. doi:10.1002/9781444313871.ch18.

Hopkinson, L., and Wynn, T. 2009. Vegetation impacts on near bank flow. Ecohydrol., 2, 404–418. doi:10.1002/eco.87.

Huai, W., Gao, M., Zeng, Y., and Li, D. 2009. Two-dimensional analytical solution for compound channel flows with vegetated floodplains. Appl. Math. Mech. -Engl. Ed., 30(9), 1121–1130. doi:10.1007/s10483-009-0906-z.

Huang, H.Q., and Nanson, G.C. 1997. Vegetation and channel variation: a case study of four streams in southeastern Australia. Geomorphology, 18, 237–249.

Huthoff, F., Augustijn, D.C.M., and Hulscher, S.J.M.H. 2007. Analytical solution of the depth-averaged flow velocity in case of submerged rigid cylindrical vegetation. Water Resour. Res., 43, W06413. doi: 10.1029/2006WR005625.

Jalonen, J., and Järvelä, J. 2014. Estimation of drag forces caused by natural woody vegetation of different scales. J. Hydrodyn., 26, 608–623. doi:10.1016/S1001-6058(14)60068-8.

Jalonen, J., Järvelä, J., Koivusalo, H., and Hyyppä, H. 2014. Deriving floodplain topography and vegetation characteristics for hydraulic engineering applications by means of terrestrial laser scanning. J. Hydraul. Eng., 140(11), 04014056. doi:10.1061/(ASCE)HY.1943-7900.0000928.

Jalonen, J., Järvelä, J., Virtanen, J.-P., Vaaja, M., Kurkela, M., and Hyyppä, H. 2015. Determining characteristic vegetation areas by terrestrial laser scanning for floodplain flow modeling. Water, 7(2), 420–437. doi:10.3390/w7020420.

Jones, C.G., Lawton, J.H., and Shachak, M. 1994. Organisms as ecosystem engineers. Oikos, 69, 373–386.

Jordanova, A.A., and James, C.S. 2003. Experimental study of bed load transport through emergent vegetation. J. Hydraul. Eng., 129(6), 474–478. doi:10.1061/(ASCE)0733-9429(2003)129:6(474).

Jormola, J., L. Laitinen, and A. Sarvilinna. 2008. Environmentally friendly drainage practices. In: Proc. 10th International Drainage Workshop of ICID Working Group on Drainage, pp. 259–268. Helsinki University of Technology, Water Resources Publications, Helsinki/Tallinn.

Junk, W.J., Bayley, P.B., and Sparks, R.E. 1989. The flood pulse concept in river-floodplain systems. In: Dodge, D.P. (ed.), Proceedings of the International Large River Symposium, pp. 110–127. Can. Spec. Publ. Fish. Aquat. Sci., 106.

Järvelä, J. 2002a. Flow resistance of flexible and stiff vegetation: a flume study with natural plants. J. Hydrol., 269, 44–54.

Järvelä, J. 2002b. Determination of flow resistance of vegetated channel banks and floodplains. In: Bousmar, D., and Zech, Y. (eds.), Proceedings of the River Flow 2002 Conference, pp. 311–318. Swets & Zeilinger, Lisse, Netherlands.

Järvelä, J. 2004. Determination of flow resistance caused by non-submerged woody vegetation. Intl. J. River Basin Manag., 2(1), 61–70.

Kang, H., and Choi, S-U. 2006. Turbulence modeling of compound open-channel flows with and without vegetation on the floodplain using the Reynolds stress model. Adv. Water Res., 29, 1650–1664.
Kemp, J.L., Harper, D.M., and Crosa, G.A. 2000. The habitat-scale ecohydraulics of rivers. Ecol. Eng., 16, 17–29.
Kemp, P., Sear, D., Collins, A., Naden, P., and Jones, I. 2011. The impacts of fine sediment on riverine fish. Hydrol. Process., 25, 1800–1821. doi:10.1002/hyp.7940.
Kirby, J.T., Durrans, S.R., Pitt, R., and Johnson, P.D. Hydraulic resistance in grass swales designed for small flow conveyance. J. Hydraul. Eng., 131(5), 65–68. doi:10.1061/(ASCE)0733-9429(2005)131:1(65).
Klassen, I., Hillebrand, G., Olsen, NR., Vollmer, S., Lehmann, B., and Nestmann, F. 2011. Modeling fine sediment aggregation processes considering varying fractal dimensions. In: Proc. of the 7th IAHR Symposium on River, Coastal and Estuarine Morphodynamics, 6 –8 September 2011, Beijing, China.
Knight, D.W., and Shiono, K. 1996. River channel and floodplain hydraulics. In: Anderson, M.G., Walling, D.E., and Bates, P.D. (eds.), Floodplain processes, pp. 139–181. Wiley, Chichester. ISBN 0-471-96679-7.
Knight, D. W., Tang, X., Sterling, M., Shiono, K., and McGahey., C. 2010. Solving open channel flow problems with a simple lateral distribution model. In: Dittrich, A., Koll, Ka., Aberle, J., and Geisenhainer, P. (eds.), River Flow 2010, pp. 41–48. Bundesanstalt für Wasserbau, Karlsruhe. ISBN 978-3-939230-00-7.
Koizumi, A., Motoyama, J. Sawata, K., Sasaki, Y. and Hirai, T., 2010. Evaluation of drag coefficients of poplar-tree crowns by a field test method. J. Wood Sci., 56, 189–193.
Konings, A.G., Katul, G.G., and Thompson, S.E. 2012. A phenomenological model for the flow resistance over submerged vegetation. Water Resour. Res., 48, W02522. doi:10.1029/2011WR011000.
Kotamäki, N., Thessler, S., Koskiaho, J., Hannukkala, A.O., Huitu, H., Huttula, T., Havento, J., and Järvenpää, M. 2009. Wireless in-situ sensor network for agriculture and water monitoring on a river basin scale in Southern Finland: evaluation from a data user's perspective. Sensors, 9, 2862–2883. doi:10.3390/s90402862.
Kothyari, U.C., Hashimoto, H., and Hayashi, K. 2009a. Effect of tall vegetation on sediment transport by channel flows. J. Hydrau. Res., 47(6), 700–710. doi:10.3826/jhr.2009.3317.
Kothyari, U.C., Hayashi, K., and Hashimoto, H. 2009b. Drag coefficient of unsubmerged rigid vegetation stems in open channel flows. J. Hydraul. Res., 47(6), 691–699. doi:10.3826/jhr.2009.3283.
Kouwen, N. 1992. Modern approach to design of grassed channels. J. Irrig. Drain. Eng., 118(5), 733–743.
Kouwen, N., and Fathi-Moghadam, M. 2000. Friction factors for coniferous trees along rivers. J. Hydraul. Eng., 126, 732–740.
Kouwen, N., and Unny, T. E. 1973. Flexible roughness in open channels. Journal of the Hydraulics Division, 99(5), 713–728.
Kronvang, B., Hoffmann, C.C., and Dröge, R. 2009. Sediment deposition and net phosphorus retention in a hydraulically restored lowland river floodplain in Denmark: combining field and laboratory experiments. Mar. Freshwater Res., 60, 638–646.
Kui, L., Stella, J.C., Lightbody, A., and Wilcox, A.C. 2014. Ecogeomorphic feedbacks and flood loss of riparian tree seedlings in meandering channel experiments. Water Resour. Res., 50(12), 9366–9384. doi:10.1002/2014WR015719.

de Langre, E. 2008. Effects of wind on plants. Annu. Rev. Fluid Mech., 40, 141–168.
Larsen, S., Vaughan, I.P., and Ormerod, S.J. 2009. Scale-dependent effects of fine sediments on temperate headwater invertebrates. Freshwater Biol., 54, 203–219.
Lawler, D.M. 1993. The measurement of river bank erosion and lateral channel change: a review. Earth Surf. Process. Landforms, 18, 777–821.
Lawler, D.M. 2008. Advances in the continuous monitoring of erosion and deposition dynamics: Developments and applications of the new PEEP-3T system. Geomorphology, 93, 17–39.
Le Roux, J.P. 2005. Grains in motion: a review. Sediment. Geol., 178, 285–313. doi:10.1016/j.sedgeo.2005.05.009.
Li, R.-M., and Shen, H.W. 1973. Effect of tall vegetations on flow and sediment. Journal of the Hydraulics Division, 99(5), 793–814.
Liu, C., and Shen, Y-M. 2008. Flow structure and sediment transport with impacts of aquatic vegetation. J. Hydrodyn., 20(4), 461–468.
López-Tarazón, J.A., Batalla, R.J., Vericat, D., and Francke, T. 2009. Suspended sediment transport in a highly erodible catchment: the River Isábena (Southern Pyrenees). Geomorphology, 109 (3–4), 210–221. doi:10.1016/j.geomorph.2009.03.003.
Luhar, M., and Nepf, H. 2011. Flow-induced reconfiguration of buoyant and flexible aquatic vegetation. Limnol. Oceanogr., 56(6), 2003–2017. doi:10.4319/lo.2011.56.6.2003.Luhar, M., and Nepf, H. 2013. From the blade scale to the reach scale: A characterization of aquatic vegetative drag. Adv. Water Resour., 51, 305–316. doi:10.1016/j.advwatres.2012.02.002.
Luhar, M., Rominger, J., and Nepf, H. 2008. Interaction between flow, transport and vegetation spatial structure. Environ. Fluid Mech., 8, 423–439.
Manners, R., Wilcox, A.C., Kui, L., Lightbody, A., Stella, J., and Sklar, L. 2015. When do plants modify fluvial processes? Plant-hydraulic interactions under variable flow and sediment supply rates. Water Resour. Res., 120(2), 325–345. doi:10.1002/2014JF003265.
Marion, A., Nikora, V., Puijalon, S., Bouma, T., Koll, K., Ballio, F., Tait, S., Zaramella, M., Sukhodolov, A., O'Hare, M., Wharton, G., Aberle, J., Tregnaghi, M., Davies, P., Nepf, H., Parker, G., and Statzner, B. 2014. Aquatic interfaces: a hydrodynamic and ecological perspective. J. Hydraul. Res., 52(6), 744–758. doi:10.1080/00221686.2014.968887.
Marjoribanks, T.I., Hardy, R.J., Lane, S.N., and Parsons, D.R. 2014a. High-resolution numerical modelling of flow–vegetation interactions. J. Hydraul. Res., 52(6), 775–793. doi:10.1080/00221686.2014.948502.
Marjoribanks, T.I., Hardy, R.J., Lane, S.N. 2014b. The hydraulic description of vegetated river channels: the weaknesses of existing formulations and emerging alternatives. WIREs Water, 1, 549–560. doi:10.1002/wat2.1044.
Marttila, H., and Kløve, B. 2012. Use of turbidity measurements to estinmate suspended solids and nutrient loads from peatland forestry drainage. J. Irrig. Drain. Eng., 138(12), 1088–1096. doi:10.1061/(ASCE)IR.1943-4774.0000509.
McAnally, W.H., and A.J. Mehta. 2002. Signifigance of aggregation of fine sediment particles in their deposition. Estuar. Coast. Shelf S., 54(4), 643–653.
McBride, M., Hession, W.C., and Rizzo, D.M. 2010. Riparian reforestation and channel change: How long does it take? Geomorphology, 116, 330–340. doi:10.1016/j.geomorph.2009.11.014.

McBride, M., Hession, W.C., Rizzo, D.M., and Thompson, D.M. 2007. The influence of riparian vegetation on near-bank turbulence: a flume experiment. Earth Surf. Process. Landforms, 32(13), 2019–2037. doi:10.1002/esp.1513.

Mehta, A.J., and McAnally, W.H. 2008. Fine-grained sediment transport. In García, M.H. (ed.), Sedimentation Engineering. ASCE Manuals and Reports on Engineering Practice No. 100, pp. 253–306. American Society of Civil Engineers, Reston. ISBN: 978-0-7844-0814-8.

Miler, O., Albayrak, I., Nikora, V., and O'Hare, M. 2012. Biomechanical properties of aquatic plants and their effects on plant–flow interactions in streams and rivers. Aquat. Sci., 74, 31–44. doi:10.1007/s00027-011-0188-5.

Miler, O., Albayrak, I., Nikora, V., and O'Hare, M. 2014. Biomechanical properties and morphological characteristics of lake and river plants: implications for adaptations to flow conditions. Aquat. Sci., 76, 465–481. doi:10.1007/s00027-014-0347-6.

Moore, K.A. 2004. Influence of seagrasses on water quality in shallow regions of the lower Chesapeake Bay. J. Coast. Res., 20, 162–178.

Mostafa, T.S., Imran, J., Chaudhry, M.H., and Kahn, I.B. 2008. Erosion resistance of cohesive soils. J. Hydraul. Res., 46(6), 777–787.

Mudd, S.M., D'Alpaos, A.D., and Morris, J.T. 2010. How does vegetation affect sedimentation on tidal marshes? Investigating particle capture and hydrodynamic controls on biologically mediated sedimentation. J. Geophys. Res., 115, F03029. doi:10.1029/2009JF001566.

Myers, W.R., and Lyness, J.F. 1994. Hydraulic study of a two-stage channel. Regul. River., 9, 225–235.

Naiman, R.J., and Décamps, H. 1997. The ecology of interfaces: Riparian zones. Annu. Rev. Ecol. Syst., 28, 621–658.

Naiman, R.J., Décamps, H., McClain, M.E., and Likens, G.E. 2005. Riparia – Energy, conservation, and management of streamside communities. Academic Press, Burlington. ISBN 9780126633153.

Naiman, R.J., Décamps, H., and Pollock, M. 1993. The role of riparian corridors in maintaining regional biodiversity. Ecol. Applic., 3(2), 209–212.

Nash, J.E., and Sutcliffe, J.V. 1970. River flow forecasting through conceptual models, Part I – A discussion of principles. J. Hydrol., 10, 282–290.

Needelman, B.A., Kleinman, P.J.A., Strock, J.S., and Allen, A.L. 2007. Improved management of agricultural drainage ditches for water quality protection: an overview. J. Soil Water Conserv., 62(4), 171–178.

Nepf, H. 2012a. Flow and transport in regions with aquatic vegetation. Annu. Rev. Fluid Mech., 44, 123–142, doi:10.1146/annurev-fluid-120710-101048.

Nepf, H. 2012b. Hydrodynamics of vegetated channels. J. Hydraul. Res., 50(3), 262–279. doi:10.1080/00221686.2012.696559.

Nepf, H., Ghisalberti, M., White, B., and Murphy, E. 2007. Retention time and dispersion associated with submerged aquatic canopies. Water Resour. Res., 43, W04422. doi:10.1029/2006WR005362.

Nicholas, A.P. 2013. Modelling the continuum of river channel patterns. Earth Surf. Process. Landforms, 38, 1187–1196. doi: 10.1002/esp.3431.

Nicholas, A.P., and Walling, D.E. 1996. The significance of particle aggregation in the overbank deposition of suspended sediment on river floodplains. J. Hydrol., 186, 275–293.

Niklas, K.J. 1997. Size- and age-dependent variation in the properties of sap- and heartwood in Black Locust (*Robinia pseudoacacia* L.). Annals of Bot., 79, 473–478.

Niklas, K.J. 1999. Research review: a mechanical perspective on foliage leaf form and function. New Phytol., 143, 19–31.

Nikora, N., Nikora, V., and O'Donoghue, T. 2013. Velocity profiles in vegetated open-channels flows: combined effects of multiple mechanisms. J. Hydraul. Eng., 139, 1021–1032. doi:10.1061/(ASCE)HY.1943-7900.0000779.

Nikora, V. 2010. Hydrodynamics of aquatic systems: An interface between ecology, biomechanics and environmental fluid mechanics. River Res. Appl., 26, 367–384. doi:10.1002/rra.1291.

Nikora, V., Aberle, J., and Green, M. 2004. Sediment flocs: settling velocity, flocculation factor, and optical backscatter. J. Hydraul. Eng., 130(10), 1043–1047. doi:10.1061/(ASCE)0733-9429(2004)130:10(1043).

Nikora, V., Larned, S., Nikora, N., Debnath, K., Cooper, G., and Reid, M. 2008. Hydraulic resistance due to aquatic vegetation in small streams: field study. J. Hydraul. Eng., 134(9), 1326–1332.

Nikora, V., Cameron, S., Albayrak, I., Miler, O., Nikora, N., Siniscalchi, F., Stewart, M., and O'Hare, M. 2012. Flow-biota interactions in aquatic systems: scales, mechanisms, and challenges. In: Rodi, W., and M Uhlmann, M. (eds), Environmental Fluid Mechanics: Memorial Volume in honour of Prof. Gerhard H. Jirka. IAHR Monographs, CRC Press/Balkema, pp. 217–235.

Oeurng, C., Sauvage, S., and Sánchez-Pérez, J.-M. 2010. Dynamics of suspended sediment transport and yield in a large agricultural catchment, southwest France. Earth Surf. Process. Landforms, 35(11), 1289–1301.

Oplatka, M. 1998. Stabilität von Weidenverbauungen an Flussufern. Mitteilungen 156. Versuchsanstalt für Wasserbau, Hydrologie und Glaziologie, ETH Zürich.

Ortiz, A.C., Ashton, A., and Nepf, H. 2013. Mean and turbulent velocity fields near rigid and flexible plants and the implications for deposition. J. Geophys. Res., 118, 2585–2599. doi:10.1002/2013JF002858.

Osterkamp, W.R., and Hupp, C.R. 2010. Fluvial processes and vegetation — Glimpses of the past, the present, and perhaps the future. Geomorphology, 118, 274–285. doi:10.1016/j.geomorph.2009.11.018.

Osterkamp, W.R., Hupp, C.R., and Stoffel, M. 2012. The interactions between vegetation and erosion: new directions for research at the interface of ecology and geomorphology. Earth Surf. Process. Landforms, 37, 23–36. doi:10.1002/esp.2173

Owens, P.N., Batalla, R.J., Collins, A.J., Gomez, B., Hicks, D.M., Horowitz, A.J., Kondolf, G.M., Marden, M., Page, M.J., Peacock, D.H., Petticrew, E.L., Salomons, W., and Trustrum, N.A. 2005. Fine-grained sediment in river systems: environmental significance and management issues. River Res. Applic., 21, 693–717. doi: 10.1002/rra.878.

Pajula, H., and Järvenpää, L. (eds.) 2007. Maankuivatuksen ja kastelun suunnittelu - työryhmän mietintö [Making plans for agricultural drainage and irrigation - Working group report]. Suomen ympäristökeskuksen raportteja 23/2007. Finnish Environment Institute, Helsinki, Finland. (In Finnish)

Partheniades, E. 2009. Cohesive sediments in open channels. Butterworth-Heinemann, Burlington, USA. 358 pp. ISBN 978-1-85617-556-2.

Pasche, E., and Rouvé, G. 1985. Overbank flow with vegetatively roughened flood plains. J. Hydraul. Eng., 111(9), 1262–1278.

Pasquale, N., Perona, P., Francis, R., and Burlando, P. 2014. Above-ground and below-ground *Salix* dynamics in response to river processes. Hydrol. Process., 28, 5189–5203. doi:10.1002/hyp.9993.

Peltola, H.M. 2006. Mechanical stability of trees under static loads. Am. J. Bot., 93(10), 1501–1511.

Petryk, S., and Bosmajian, G. 1975. Analysis of flow through vegetation. Journal of the Hydraulics Division, 101(7), 871–884.
Phillips, J.M., and Walling D.E. 1999. The particle size characteristics of fine-grained channel deposits in the River Exe Basin, Devon, UK. Hydrol. Process., 13(1–19).
Pizzuto, J., O'Neal, M., and Stotts, S. 2010. On the retreat of forested, cohesive riverbanks. Geomorphology, 116, 341–352. doi:10.1016/j.geomorph.2009.11.008.
Pluntke, T., and Kozerski, H.-P. 2003. Particle trapping on leaves and on the bottom in simulated submerged plant stands. Hydrobiologia, 506–509, 575–581.
Powell, G.E., Ward, A.D., Mecklenburg, D.E., Draper, J., and Word, W. 2007. Two-stage channel systems: Part 2, case studies. J. Soil Water Conserv., 62(4), 286–296.
Puijalon, S., Bouma, T.J., Douady, C.J., van Groenendael, J., Anten, N.P.R., Martel, E., and Bornette, G. 2011. Plant resistance to mechanical stress: evidence of an avoidance–tolerance trade-off. New Phytol., 191, 1141–1149. doi:10.1111/j.1469-8137.2011.03763.x
Puustinen, M., Tattari, S., Koskiaho, J., and Linjama, J. 2007. Influence of seasonal and annual hydrological variations on erosion and phosphorus transport from arable areas in Finland. Soil. Till. Res., 93, 44–55. doi:10.1016/j.still.2006.03.011.
Rameshwaran, P., Naden, P., Wilson, C.A.M.E., Malki, R., Shukla, D.R., and Shiono, K. 2013. Inter-comparison and validation of computational fluid dynamics codes in two-stage meandering channel flows. Appl. Math. Model., 37, 8652–8672. doi:10.1016/j.apm.2013.07.016
Rantala, M.J., Ilmonen, J., Koskimäki, J., Suhonen, J., and Tynkkynen, K. 2004. The macrophyte, *Stratiotes aloides*, protects larvae of dragonfly *Aeshna viridis* against fish predation. Aquatic Ecol., 38(1), 77–82. doi:10.1023/B:AECO.0000021005.22624.16.
Rhee D.S., Woo H., Kwon B.A., and Ahn, H.K. 2008. Hydraulic resistance of some selected vegetation in open channel flows. River Res. Appl., 24, 673–687. doi:10.1002/rra.1143.
Ricardo, A.M., Koll, K., Franca, M.J., Schleiss, A.J., and Ferreira, R.M.L. 2014. The terms of turbulent kinetic energy budget within random arrays of emergent cylinders. Water Resour. Res., 50, 4131–4148. doi:10.1002/2013WR014596.
Righetti, M. 2008. Flow analysis in a channel with flexible vegetation using double-averaging method. Acta Geophys., 56(3), 801–823. doi:10.2478/s11600-008-0032-z.
Rodrigues, S., Bréhéret, J.-G., Macaire, J.-J. Greulich, S., and Villar, M. 2007. In-channel woody vegetation controls on sedimentary processes and the sedimentary record within alluvial environments: a modern example of an anabranch of the River Loire, France. Sedimentology, 54, 223–242. doi:10.1111/j.1365-3091.2006.00832.x.
Rominger, J.T., Lightbody, A.F., and Nepf, H. 2010. Effects of added vegetation on sand bar stability and stream hydrodynamics. J. Hydraul. Eng., 136(12), 994–1002. doi:10.1061/(ASCE)HY.1943-7900.0000215.
Rudnicki, M., Mitchell, S.J., and Novak, M.D., 2004. Wind tunnel measurements of crown streamlining and drag relationships for three conifer species. Can. J. For. Res., 34: 666–676.
Samani, J.M.V., and Kouwen, N. 2002. Stability and erosion in grassed channels. J. Hydraul. Eng., 128(1), 40– 45. doi:10.1061/(ASCE)0733-9429(2002)128:1(40).

Sand-Jensen, K., and Pedersen, M.L. 2008. Streamlining of plant patches in streams. Freshwater Biol., 53, 714–726. doi:10.1111/j.1365-2427.2007.01928.x.

Schlichting, H., and Gersten, K. 2000. Boundary Layer Theory, 8th edition. Springer Verlag, Berlin. ISBN 3-540-66270-7.

Schnauder, I., and Moggridge, H.L. 2009. Vegetation and hydraulic-morphological interactions at the individual plant, patch and channel scale. Aquat. Sci., 71, 318–330. doi:10.1007/s00027-009-9202-6.

Schoelynck, J., De Groote, T., Bal, K., Vandenbruwaene, W., Meire,P., and Temmerman, S. 2012. Self-organised patchiness and scale-dependent bio-geomorphic feedbacks in aquatic river vegetation. Ecography, 35, 760–768. doi:10.1111/j.1600-0587.2011.07177.x.

Schoneboom, T. 2011. Widerstand flexibler Vegetation und Sohlenwiderstand in durchströmten Bewuchsfeldern. Mitt. Leichtweiß-Institut für Wasserbau No. 157. Technische Universität Braunschweig, Braunschweig, Germany. (In German)

Schoneboom, T., Aberle, J., Wilson, C.A.M.E, and Dittrich, A. 2008. Drag force measurements of vegetation elements. In: Proc. of 8th International Conference on Hydroscience & Engineering, 8–12 September, Nagoya, Japan.

Sellin, R.H.J. 1964. A laboratory investigation into the interaction between the flow in the channel of a river and that over its flood plain. La Houille Blanche, 7, 793–801.

Sellin, R.H.J., Giles, A., and van Beesten, D.P. 1990. Post-implementation appraisal of a two-stage channel in the River Roding, Essex. Water and Env. J., 4, 119–130. doi:10.1111/j.1747-6593.1990.tb01567.x.

Sharpe, R.G., and James, C.S. 2006. Deposition of sediment from suspension in emergent vegetation. Water SA, 32(2), 211–218.

Shields, F.D., Jr. 2009. Do we know enough about controlling sediment to mitigate damage to stream ecosystems? Ecol. Eng., 35, 1727–1733. doi:10.1016/j.ecoleng.2009.07.004.

Shields, F.D., Jr., and Alonso, C.V. 2012. Assessment of flow forces on large wood in rivers. Water Resour. Res., 48, W04516. doi:10.1029/2011WR011547.

Shields, F.D., Jr., Copeland, R.R., Klingeman, P.C., Doyle, M.W., and Simon, A. 2003. Design for stream restoration. J. Hydraul. Eng., 129(8), 575–584.

Shiono, K., and Knight, D.W. 1991. Turbulent open channel flows with variable depth across the channel. J. Fluid Mech., 222, 617–646.

Shiono, K., and Muto, Y. 1998. Complex flow mechanisms in compound meandering channels with overbank flow. J. Fluid Mech., 376, 221–261.

Shore, M., Jordan, P., Mellander, P.-E., Kelly-Quinn, M., and Melland, A.R. 2014. An agricultural drainage channel classification system for phosphorus management. Agriculture, Ecosystems and Environment, 199, 207–215. doi:10.1016/j.agee.2014.09.003.

Siniscalchi, F., and Nikora, V.I. 2013. Dynamic reconfiguration of aquatic plants and its interrelations with upstream turbulence and drag forces. J. Hydraul. Res., 51(1), 46–55. doi: 10.1080/00221686.2012.743486.

Siniscalchi, F., Nikora, V.I., and Aberle, J. 2012. Plant patch hydrodynamics in streams: Mean flow, turbulence, and drag forces. Water Resour. Res., 48, W01513. doi:10.1029/2011WR011050.

Solari, L., van Oorschot, M., Belletti, B., Hendriks, D., Rinaldi, M., and Vargas-Luna, A. 2015. Advances on modeling riparian vegetation–hydromorphology interactions. River Res. Applic., doi:10.1002/rra.2910.

Statzner, B., Lamoroux, N., Nikora, V., and Sagnes, P. 2006. The debate about drag and reconfiguration of freshwater macrophytes: Comparing results obtained by three recently discussed approaches. Freshwat. Biol., 51, 2173–2183.

Stephan, U., and Gutknecht, D. 2002. Hydraulic resistance of submerged flexible vegetation. J. Hydrol., 269, 27–43.Stoesser,T., Kim, S.J., Diplas, P. 2010.Turbulent flow through idealized emergent vegetation. J. Hydraul. Eng., 136(12), 1003–1017. doi:10.1061/ASCEHY.1943-7900.0000153.

Stoesser, T., Palau-Salvador, G., and Rodi, W. 2009. Large eddy simulation of turbulent flow through submerged vegetation. Transport Porous Med., 78(3), 347–365. doi:10.1007/s11242-009-9371-8.

Stone, M.C., Chen, L., McKay, S.K., Goreham, J., Acharya, K., Fischenich, C., and Stone, A.B. 2013. Bending of submerged woody riparian vegetation as a function of hydraulic flow conditions. River Res. Applic., 29(2), 195–205. doi:10.1002/rra.1592.

Sukhodolov, A.N. 2015. Field-based research in fluvial hydraulics: potential, paradigms and challenges. J. Hydraul. Res., 53(1), 1–19. doi:10.1080/00221686.2015.1012126.

Sukhodolov, A.N., and Sukhodolova, T.A. 2010. Case study: effect of submerged aquatic plants on turbulence structure in a lowland river. J. Hydraul. Eng., 136(7), 434–446. doi: 10.1061/(ASCE)HY.1943-7900.0000195.

Sukhodolov, A.N., and Sukhodolova, T.A. 2012. Vegetated mixing layer around a finite-size patch of submerged plants: Part 2. Turbulence statistics and structures. Water Resour. Res., 48, W12506. doi:10.1029/2011WR011805.

Sukhodolova, T.A., and Sukhodolov, A.N. 2012. Vegetated mixing layer around a finite-size patch of submerged plants: 1. Theory and field experiments. Water Resour. Res., 48, W10533. doi:10.1029/2011WR011804.

Sun, S., Jin, D., and Shi, P. 2006. The leaf size–twig size spectrum of temperate woody species along an altitudinal gradient: an invariant allometric scaling relationship. Ann. Bot., 97, 97–107. doi:10.1093/aob/mcj004 .

Sutili, F.J., Denardia, L., Durlob, M.A. , Rauch, H.P., and Weissteiner, C. 2012. Flexural behaviour of selected riparian plants under static load. Ecol. Eng., 43, 85–90. doi:10.1016/j.ecoleng.2012.02.012.

Tabacchi, E., Correll, D.L., Hauer, R., Pinay, G., Planty-Tabacchi, A.-M., and Wissmar, R.C. 1998. Development, maintenance and role of riparian vegetation in the river landscape. Freshwater Biol., 40, 497–516.

Tal, M., and Paola, C. 2007. Dynamic single-thread channels maintained by the interaction of flow and vegetation. Geology, 35(4), 347–350. doi: 10.1130/G23260A.1

Tanaka, N., Takenaka, H., Yagisawa, J., and Morinaga, T. 2011. Estimation of drag coefficient of a real tree considering the vertical stand structure of trunk, branches, and leaves. Intl. J. River Basin Manag., 9, 221–230. doi:10.1080/15715124.2011.606427.

Tang, X., and Knight, D.W. Sediment transport in river models with overbank flows. J. Hydraul. Eng., 132(1), 77–86. doi:10.1061/(ASCE)0733-9429(2006)132:1(77).

Tanino, Y., and Nepf, H.M. 2008. Laboratory investigation of mean drag in a random array of rigid, emergent cylinders. J. Hydraul. Eng., 134(1), 34–41. doi:10.1061/(ASCE)0733-9429(2008)134:1(34).

Temmerman, S., Bouma, T.J., Van de Koppel, J., Van der Wal, D., De Vries, M.B., and Herman, P.M.J. 2007. Vegetation causes channel erosion in a tidal landscape. Geology, 35(7), 631–634. doi: 10.1130/G23502A.1.

Temmerman, S., Meire, P., Bouma, T.J., Herman, P.M.J., Ysebaert, T., and De Vriend, H.J. 2013. Ecosystem-based coastal defence in the face of global change. Nature, 504, 79–83. doi:10.1038/nature12859 .

Temple, D.M., Robinson, K.M., Ahring, R.M., and Davis, A.G. 1987. Stability design of grass-lined open channels. Agriculture Handbook Number 667. United States Department of Agriculture, Washington, D.C.

Thoman, R.W., and Niezgoda, S.L. 2008. Determining erodibility, critical shear stress, and allowable discharge estimates for cohesive channels: Case study in the Powder River Basin of Wyoming. J. Hydraul. Eng., 134(12), 1677–1687.

Thonon, I., Roberti, J.R., Middelkoop, H., van der Perk, M., and Burrough, P.A. 2005. In situ measurements of sediment settling characteristics in floodplains using a LISST-ST. Earth Surf. Process. Landforms, 30, 1327–1343. doi:10.1002/esp.1239.

Thornton, C.I., Abt, S.R., and Clary, W.P. 1997. Vegetation influence on small stream siltation. J. Am. Water Resour. As., 33(6), 1279–1288.

Tockner, K., Malard, F., and Ward, J.V. 2000. An extensionof the flood pulse concept. Hydrol. Process., 14, 2861–2883.

Tockner, K., and Stanford, J.A. 2002. Riverine flood plains: present state and future trends. Environ. Conserv., 29(3), 308–330. doi:10.1017/S037689290200022X.

USDA. 1954. Handbook of channel design for soil and water conservation. SCS-TP-61. United States Department of Agriculture, Washington, D.C. Revised in June 1954.

USDA, 2007. Two-Stage Channel Design. In: National Engineering Handbook, Part 654, Stream Restoration Design. United States Department of Agriculture, Natural Resources Conservation Service.

Usherwood, J.R., Ennos, A.R., and Ball, D.J. 1997. Mechanical and anatomical adaptations in terrestrial and aquatic buttercups to their respective environments. J. Exp. Bot., 48(312), 1469–1475.

Vandenbruwaene, W., Bouma, T.J., Meire, P., and Temmerman, S. 2013. Biogeomorphic effects on tidal channel evolution: impact of vegetation establishment and tidal prism change. Earth Surf. Process. Landforms, 38, 122–132. doi:10.1002/esp.3265.

Vargas-Luna, A., Crosato, A., and Uijttewaal, W.S.J. 2015. Effects of vegetation on flow and sediment transport: comparative analyses and validation of predicting models. Earth Surf. Process. Landforms, 40, 157–176. doi:10.1002/esp.3633.

Vogel, S. 1989. Drag and reconfiguration of broad leaves in high winds. J. Exp. Bot., 40, 941–948.

Vogel, S. 1994. Life in moving fluids – The physical biology of flow. Second edition. Princeton University Press, Princeton, UK.

Vollsinger, S., Mitchell, S.J., Byrne, K.E., Novak, M.D., and Rudnicki, M. 2005. Wind tunnel measurements of crown streamlining and drag relationships for several hardwood species. Can. J. For. Res., 35, 1238–1249.

de Vriend, H.J., van Koningsveld, M., Aarninkhof, S.G.J., de Vries, M.B., and Baptist, M.J. 2014. Sustainable hydraulic engineering through building with nature. J. Hydro-Environ. Res., 9(2), 159–171. doi:10.1016/j.jher.2014.06.004.

Walder, J.S. 2015. Dimensionless erosion laws for cohesive sediment. J. Hydraul. Eng., 10.1061/(ASCE)HY.1943-7900.0001068, 04015047.

Walling, D.E. 1999. Linking land use, erosion and sediment yields in river basins. Hydrobiologia, 410, 223–240.

Walling, D.E., and He, Q. 1997. Investigating spatial patterns of overbank sedimentation on river floodplains. Water Air Soil Poll., 99, 9–20.Warsta, L., Taskinen, A.,

Paasonen-Kivekäs, M., Karvonen, T., and Koivusalo, H. 2014. Spatially distributed simulation of water balance and sediment transport in an agricultural field. Soil. Till. Res., 143, 26–37. doi:10.1016/j.still.2014.05.008.
Weissteiner, C., Jalonen, J., Järvelä, J., and Rauch, H.-P. 2015. Spatial-structural properties of woody riparian vegetation with a view to reconfiguration under hydrodynamic loading. Ecol. Eng., 85, 85–94.
Westoby, M., Falster, D.S., Moles, A.T., Vesk, P.A., and Wright, I.J. 2002. Plant ecological strategies: Some leading dimensions of variation between species. Annu. Rev. Ecol. Syst., 33, 125–159. doi:10.1146/annurev.ecolsys.33.010802.150452.
Wharton, G., Cotton, J.A., Wotton, R.S., Bass, J.A.B., Heppell, C.M., Trimmer, M., Sanders, I.A., and Warren, L.L. 2006. Macrophytes and suspension-feeding invertebrates modify flows and fine sediments in the Frome and Piddle catchments, Dorset (UK). J. Hydrol., 330, 171–184. doi:10.1016/j.jhydrol.2006.04.034.
Whittaker, P., Wilson, C., Aberle, J., Rauch, H.P., and Xavier, P. 2013. A drag force model to incorporate the reconfiguration of full-scale riparian trees under hydrodynamic loading. J. Hydraul. Res., 51(5), 569–580. doi:10.1080/00221686.2013.822936.
Whittaker, P., Wilson, C., and Aberle, J., 2015. An improved Cauchy number approach for predicting the drag and reconfiguration of flexible vegetation. Adv. Water Res., 83, 28–35. doi: 10.1016/j.advwatres.2015.05.005.
Williams, G.P. 1989. Sediment concentration versus water discharge during single hydrologic events in rivers. J. Hydrol., 111(1–4): 89–106.
Wilson, C.A.M.E., and Horritt, M.S. 2002. Measuring the flow resistance of submerged grass. Hydrol. Process., 16, 2589–2598. doi: 10.1002/hyp.1049.
Wilson, C.A.M.E., Hoyt, J., and Schnauder, I. 2008. Impact of foliage on the drag force of vegetation in aquatic flows. J. Hydraul. Eng., 134(7), 885–891.
Wood, P.J., and Armitage, P.D. 1997. Biological effects of fine sediment in the lotic environment. Environ. Manage., 21(2), 203–217.
Woods, K.D. 2004. Intermediate disturbance in a late-successional hemlock-northern hardwood forest. J. Ecol., 92, 464–476.
Wu, F., Shen, H., and Chou, Y. 1999. Variation of roughness coefficients for unsubmerged and submerged vegetation. J. Hydraul. Eng., 125(9), 934–942.
Wunder, S., Lehmann, B., and F. Nestmann, F. 2011. Determination of the drag coefficients of emergent and just submerged willows. Intl. J. River Basin Manag., 9, 231–236.
Wynn, T.M., Henderson, M.B., and Vaughan, D.H. 2008. Changes in streambank erodibility and critical shear stress due to subaerial processes along a headwater stream, southwestern Virginia, USA. Geomorphology, 97(3–4), 260–273.
Wynn, T., and Mostaghimi, S. 2006a. The effects of vegetation and soil type on streambank erosion, Southwestern Virginia, USA. J. Am. Water Resour. As., 42(1), 69–82.
Wynn, T., and Mostaghimi, S. 2006b. Effects of riparian vegetation on stream bank subaerial processes in southwestern Virginia, USA. Earth Surf. Process. Landforms, 31(4), 399–413. doi:10.1002/esp.1252.
Xavier, P. 2009. Floodplain woodland hydrodynamics, Doctoral thesis, Cardiff School of Engineering, Cardiff University, Cardiff, UK.
Yang, K., Liu, X., Cao, S., and Huang, E. 2014. Stage-discharge prediction in compound channels. J. Hydraul. Eng., 140(4), 06014001. doi:10.1061/(ASCE)HY.1943-7900.0000834.

Yang, K., Cao, S., and Knight, D.W. 2007. Flow patterns in compound channels with vegetated floodplains. J. Hydraul. Eng., 133(2), 148–159. 10.1061/(ASCE)0733-9429(2007)133:2(148).

Yang, X.-D., Yan, E.-R., Chang, S.X., Da, L.-J., and Wang, X.-H. 2015. Tree architecture varies with forest succession in evergreen broad-leaved forests in Eastern China. Trees, 29, 43–57. doi:10.1007/s00468-014-1054-6

Yen, B.C. 2002. Open channel flow resistance. J. Hydraul. Eng., 128, 20–39.

Yue, W., Parlange, M.B., Meneveau, C., Zhu, W., van Hout, R., and Katz, J. 2007. Large-eddy simulation of plant canopy flows using plant-scale representation. Boundary-Layer Meteorol., 124, 183–203. doi:10.1007/s10546-007-9173-x.

Zabaleta, A., Martínez, M., Uriarte, J.A., and Antigüedad, I. 2007. Factors controlling suspended sediment yield during runoff events in small headwater catchments of the Basque Country. Catena, 71 (1), 179–190. doi:10.1016/j.catena.2006.06.007.

Zinke, P. 2011. Modelling of flow and levee depositions in a freshwater delta with natural vegetation. Doctoral thesis. Faculty of Civil Engineering, Norwegian University of Science and Technology.

Zinke, P., Olsen, N.R.B., and Bogen, J. 2011. Three-dimensional numerical modelling of levee depositions in a Scandinavian freshwater delta. Geomorphology, 129, 320–333. doi:10.1016/j.geomorph.2011.02.027.

Zong, L., and Nepf, H. 2010. Flow and deposition in and around a finite patch of vegetation. Geomorphology, 116, 363–372. doi:10.1016/j.geomorph.2009.11.020.

Zong, L., and Nepf, H. 2011. Spatial distribution of deposition within a patch of vegetation. Water Resour. Res., 47, W03516. doi:10.1029/2010WR009516.

Zou, J., Yan, G., Zhu, L., and Zhang, W. 2009. Woody-to-total area ratio determination with a multispectral canopy imager. Tree Physiol., 29, 1069–1080. doi:10.1093/treephys/tpp042.

Aalto-DD 220/2015

ISBN 978-952-60-6598-4 (printed)
ISBN 978-952-60-6597-7 (pdf)
ISSN-L 1799-4934
ISSN 1799-4934 (printed)
ISSN 1799-4942 (pdf)

Aalto University
School of Engineering
Department of Civil and Environmental Engineering
www.aalto.fi

BUSINESS +
ECONOMY

ART +
DESIGN +
ARCHITECTURE

SCIENCE +
TECHNOLOGY

CROSSOVER

DOCTORAL
DISSERTATIONS